Toward Better Understanding of Molecular Magnetic Properties with *ab initio* Simulation Methods

Shichao Sun

A dissertation
submitted in partial fulfillment of the
requirements for the degree of

Doctor of Philosophy

University of Washington

2020

Reading Committee:

Xiaosong Li, Chair

Daniel Gamelin

Ting Cao

Program Authorized to Offer Degree:
Chemistry

University of Washington

Abstract

Toward Better Understanding of Molecular Magnetic Properties with *ab initio* Simulation Methods

Shichao Sun

Chair of the Supervisory Committee:
Prof. Xiaosong Li
Department of Chemistry

Simulating and understanding magnetic properties are essential for developing new magnetic materials. In this dissertation, some advances in *ab initio* methodologies for simulating magnetic properties based on the variational treatment of magnetic fields are presented. The new methodologies are applied for properties such as noncollinear spin and magnetic circular dichroism (MCD), and bring further insights into these phenomena. In Chapter 1, we give a general introduction of the interaction between matter and electromagnetic fields. In Chapter 2, the generalized Hartree-Fock formalism with variational magnetic field is outlined and applied for simulating the non-collinear spin in molecular systems induced by external magnetic field. We show that the two component formalism is a natural choice for accommodating the spin collinearity in strong magnetic field. Chapters 3 and 4 present a new simulation method for magnetic circular dichroism based on linear response with variational treatment of magnetic fields. This variational treatment is advantageous in both calculation efficiency and the ability of approaching strong magnetic field compared with the traditional perturbation theory. We also include spin-orbit coupling variationally, which enables the simulation of temperature dependence of MCD for open-shell systems. The non-collinear density functional theory (DFT) and time-dependent density funcrional theory (TDDFT) are implemented with finite field gauge including atomic orbital (GIAO) to mitigate the

gauge origin dependence problem in simulating magnetic properties. In Chapter 5, the MCD simulation method by real time electronic dynamics with variational treatment of magnetic fields is outlined. We showed the relationship between the MCD signal and the magnetically perturbed electric dipole-dipole response function.

TABLE OF CONTENTS

LIST OF FIGURES

LIST OF TABLES

GLOSSARY

2C: Two component formalism

4C: Four component formalism

B3LYP: Becke 3-parameter hybrid exchange functional with Lee-Yang-Parr correlation

BDFT: Magnetic field density functional theory

CDFT: Current density functional theory

CSDFT: Current-spin density functional theory

DFT: Density functional theory

DHF: Dirac-Hartree-Fock

ECD: Electronic circular dichroism

ED: Dlectric dipole

GHF: Generalized Haree-Fock

GKS: Generalized Kohn-Sham

HF: Hartree-Fock

HFP: Head-Gordon-Pople algorithm

MCD: Magnetic circular dichroism

MMUT: modified-midpoint unitary transformation propagation algorithm

NC: Non-collinear

RHF: Restricted Hartree-Fock

RKS: Restricted Kohn-Sham

RT: Real time

SCF: Self-consistent field

TDDFT: Time-dependent density functional theory

TDHF: Time-dependent Hartree-Fock

UHF: Unrestricted Hartree-Fock

UKS: Unrestricted Kohn-Sham

X2C: Exact two component

ACKNOWLEDGMENTS

First, I wish to express my deepest gratitude to my advisor, Professor Xiaosong Li, for his generous support and help, his guidance in scientific research and being so considerable in the past five years. His optimism helped me going through the tough times when I have difficulty in my research. My success in research would not have been achieved without his inspiring ideas and invaluable experience.

I also want to thank University of Washington for giving me the chance for pursuing my PhD and providing great academic environment.

I want to express my deep gratitude to my committee, Professor Xiaodong Xu, Professor Daniel Gamelin, Professor Ting Cao, Professor Munira Khalil for their helpful suggestion and constructive criticism for my research and dissertation. I also want to extend my deep gratitude to Professor Stefan Stoll, who cannot be in my committee due to his sabbatical leave.

I am deeply indebted to Dr. Alessio Petrone, Dr. David Williams-Young, Dr. Hongbin Liu, Dr. David Lingerfelt and Dr. Bo Peng for both their guidance in my research and life. They helped me through the beginning of my research. I also want to thank Dr. Joshua Goings, Dr. Patrick Lestrange, Dr. Franco Egidi, Dr. Chad Hoyer and Dr. Andrew Jenkins for helping me with their unparalleled expertise in my research. Lots of thanks to Ethan Vo for writing integral code with me. I will never forget the interesting discussions with Dr, Luning Zhao and Dr. Tianyuan Zhang about their experience. And it is a great pleasure to work together with other members in the group Dr. Greta Donati, Dr. Andrew Valentine, Joe Kasper, Joseph Radler, Torin Stetina, Andrew Wildman, Mr. Ryan Beck, Hang Hu, Lauren Koulias, Kara Gallo, Alexis Mills, Lixin Lu, Xiaolin Liu, Laurence Giordano.

I want to express my special gratitude to my family, especially my parents for their understanding in the past five years. Though pursuing PhD has no immediate pay back, they have always been supportive and encouraged me. Thank you so much!

DEDICATION

to my dear parents, Yesen and Aijuan

PREFACE

This dissertation focuses on the recent development in the ab initio simulation of molecular magnetic properties, especially the spin phase transition in the magnetic fields and magnetic circular dichroism. The non-perturbative treatment of the magnetic fields is highlighted. It enables the simulation of spin-noncollinearity caused by the magnetic fields, simplify the calculation and understanding of the magnetic properties and open up a door to the strong field realm. My contributions and the contributions of the others' to the development of these methods will be outlined in the following chapters.

Chapter 1 provides the preliminaries to understand the phenomena in the magnetic fields. The magnetic fields are introduced in the Hamiltonian in the form of vector fields. The gauge transformation and gauge origin dependence problem is discussed in detail, which explain the advantages of using gauge including atomic orbital in the non-perturbative treatment of magnetic fields. The light-matter interaction is briefly discussed to provide the basic notions for studying magnetic circular dichroism in the following chapters.

Chapter 2 present the development of non-relativistic generalized Hartree-Fock formalism for simulating molecules with a variational treatment of the magnetic fields. It is known to us that without periodic boundary condition, the magnetic field is the only thing to break time reversal symmetry, which can cause the spin-non-collinearity in the molecular systems. Thus, the generalized Hartree-Fock, or two-component formalism is vital for simulating the magnetic properties and spin-phase transitions. However, for closed shell molecules, when the magnetic field is not strong, restricted Hartree-Fock is still a valid formalism. Appendix A outlines the Obara-Saika algorithm for calculating the gauge including atomic orbital integrals, which is important in the ab initio simulation. A relativistic two-component formalism

for the non-perturbative treatment of magnetic fields is presented in Chapter 4. Without magnetic field, the spin-orbit coupling induce the spin-anisotropy while conserving the time-reversal symmetry.

Chapter 3 and Chapter 4 present the development of using linear response method to simulate and analyze the magnetic circular dichroism. In Chapter 3, the linear response TDHF is developed and used for simulating closed shell molecules. The non-perturbative treatment simplifies the explanation and simulation of $\mathscr{B}$ term in MCD. The $\mathscr{A}$ term caused by Zeeman effect and peak broadening is discussed in Appendix B Chapter 4 present the simulation of closed shell and open shell with transition metal compounds. The spin-orbit coupling and magnetic fields are treated non-perturbatively in the exact two-component formalism. The excitation energy and transition moments are simulated by non-collinear TDDFT in the linear response formalism. The temperature dependence of the open shell systems is a big challenge. With non-perturbative treatment of magnetic field, this can be simulated by the transition from different microstates weighted by a temperature dependent Boltzmann factor.

Chapter 5 provide a method of simulating MCD with real-time electronic dynamics. It is shown that the MCD spectrum can be related to the frequency dependent electric dipole-electric dipole response function. This response function can be related to the time evolution of the expectation value of electric dipole perturbed by an electric field. Such relation can be generalized to the absorption spectra and electronic circular dichroism spectra.

Chapter 6 is about the unfinished work of four component relativistic formalism in GIAO orbitals.

Chapter 1

INTRODUCTION

In order to study the magnetic properties with ab initio simulations, we need to introduce the magnetic fields in molecular quantum mechanics. We are interested in the interaction between the magnetic fields and the molecule as well as the plane wave and the electrons. In this work, we limit our discussion of these interactions to semi-classical treatment of electromagnetic fields. We believe that in the experimental condition, when the intensity of the field is not too strong, and the frequency of the plane wave is not too high, the semi-classical approximation is valid.

First, we introduce the magnetic fields in both Schrödinger's equation and Dirac's equation in the Coulomb gauge. Next, we will brifly go through the light-matter interaction in the semi-classical treatment.

One difficulty for molecular ab initio simulation of the magnetic properties is the gauge origin problem. In principle, gauge transformation does not change the physics. However, in the presence of magnetic fields, with localized atomic orbitals, the simulated energy as well as other properties will become gauge origin dependent. We will give an explanation and introduce gauge including atomic orbital to mitigate this unphysical dependence of magnetic properties upon gauge origin choice.

1.1 Introducing Magnetic Fields in the non-relativistic Hamiltonian

Generally, vector potential and magnetic fields always have the relation

$$\mathbf{B} = \nabla \times \mathbf{A} \tag{1.1}$$

Define scalar potential as ϕ, then the electric field is

$$\mathbf{E} = -\nabla\phi - \frac{\partial}{\partial t}\mathbf{A} \tag{1.2}$$

The gauge transformation can be defined with an arbitrary scalar field of space and time $f(\mathbf{r}, t)$,

$$\mathbf{A} \to \mathbf{A}' = \mathbf{A} + \nabla f \tag{1.3}$$

$$\phi \to \phi' = \phi - \frac{\partial}{\partial t} f \tag{1.4}$$

and the electromagnetic fields are unchanged after the transformation.

Next, we will introduce the fields in the Schrödinger's and Dirac's equation. It can be proofed that the scalar fields is not involved in the Hamiltonian, thus we only consider the vector potential in the Hamiltonian.

We choose Coulomb gauge (also known as the radiation gauge) throughout the whole thesis,

$$\nabla \cdot \mathbf{A} = 0 \tag{1.5}$$

In the free particle Schrödinger's equation

$$i\frac{\partial \psi(\mathbf{r}, t)}{\partial t} = \frac{\mathbf{p}^2}{2m} \tag{1.6}$$

In the Pauli equation, we introduce spin by replacing $\mathbf{p}$ with $\boldsymbol{\sigma} \cdot \mathbf{p}$, and the Hamiltonian without external fields is the same as Eq. (1.6).

We introduce the vector potential with minimal coupling, i.e., by relplacing $\mathbf{p}$ with $\mathbf{p} - q\mathbf{A}$. For electrons, $q = -e = -1$ in the atomic units. Then the spin-free Schrödinger's Hamiltonian of free electron becomes

$$H = -\frac{\nabla^2}{2} - i\mathbf{A} \cdot \nabla + \frac{\mathbf{A}^2}{2} \tag{1.7}$$

and by using the Dirac identity

$$(\boldsymbol{\sigma}\cdot\mathbf{u})(\boldsymbol{\sigma}\cdot\mathbf{v}) = (\mathbf{u}\cdot\mathbf{v})\mathbf{I}_2 + i\boldsymbol{\sigma}\cdot\mathbf{u}\times\mathbf{v} \tag{1.8}$$

we can show that the spin dependent non-relativistic Pauli's Hamiltonian becomes

$$H = -\frac{\nabla^2}{2} - i\mathbf{A}\cdot\nabla + \frac{\mathbf{A}^2}{2} + \mu_B\boldsymbol{\sigma}\cdot\mathbf{B} \tag{1.9}$$

The last term in Eq. (1.9) is the spin Zeeman term, where $\boldsymbol{\sigma} = 2\mathbf{s}$ and μ_B is Bohr magneton, which is $\frac{1}{2}$ in atomic units.

By introducing the minimal coupling in the Dirac's Hamiltonian, we have

$$H_D = c\boldsymbol{\alpha}\cdot(-i\nabla + \mathbf{A}) + \beta mc^2 \tag{1.10}$$

1.2 Gauge Transformation of Many Electron Systems

Now we want to show that the N electron system is invariant under gauge transformation of vector potential Eq. (1.3). After the gauge transformation, the many electron Hamiltonian transform from $H = \sum_i^N[\boldsymbol{\sigma}\cdot(\mathbf{p}_i + \mathbf{A})]^2$ to $H = \sum_i^N[\boldsymbol{\sigma}\cdot(\mathbf{p}_i + \mathbf{A} + \nabla f)]^2$, or from $H_D = \sum_i^N c\boldsymbol{\alpha}\cdot(p+\mathbf{A})+\beta mc^2$ to $H_D = \sum_i^N c\boldsymbol{\alpha}\cdot(p+\mathbf{A}+\nabla f)+\beta mc^2$. The transformed Hamiltonian can be written as

$$H(\mathbf{A}') = \exp(-iF)H(\mathbf{A})\exp(iF) \tag{1.11}$$

where $F = \sum_{i=1}^N f(\mathbf{r}_i)$. The unitary transformation of Hamiltonian can be proofed by showing that

$$(-i\nabla_i + \mathbf{A})\exp[if(\mathbf{r}_i)] = \exp[if(\mathbf{r}_i)](-i\nabla_i + A + \nabla f(\mathbf{r}_i)) = \exp[if(\mathbf{r}_i)](-i\nabla_i + A') \tag{1.12}$$

The transformation of other operators, such as nuclear attraction operator, electron-electron repulsion operators, are trivial.

Corresponding to the change in the Hamiltonian, the wave function is also transformed

$$\Psi' = \exp(-iF)\Psi \tag{1.13}$$

with this transformation, the energy is invariant to the gauge transformation, and there is a connection between the original wave function and transformed wave function. [29, 30]

1.3 Gauge Origin Dependence in the Localized Orbitals

If we only have static magnetic fields, then in the scale of molecules, we can usually regard the static magnetic fields as uniform, $\mathbf{B}(\mathbf{r}) = \mathbf{B}$, i.e., constant in the whole space. The vector potential can be defined as

$$\mathbf{A} = \frac{1}{2}\mathbf{B} \times (\mathbf{r} - \mathbf{O}) \tag{1.14}$$

where $\mathbf{O}$ is the chosen gauge origin.

A change of gauge origin can be seen as gauge transformation. If we change the gauge origin from $\mathbf{O}$ to $\mathbf{O}' = \mathbf{O} + \mathbf{\Delta O}$, then the new vector potential of the uniform magnetic field is

$$\begin{aligned}
\mathbf{A}' =& \frac{1}{2}\mathbf{B} \times (\mathbf{r} - \mathbf{O}') \\
=& \frac{1}{2}\mathbf{B} \times (\mathbf{r} - \mathbf{O} + \Delta\mathbf{O}) \\
=& \frac{1}{2}\mathbf{B} \times (\mathbf{r} - \mathbf{O}) + \nabla\left[\frac{1}{2}(\mathbf{B} \times \nabla\mathbf{O}) \cdot \mathbf{r}\right]
\end{aligned} \tag{1.15}$$

which match with the form of gauge transformation Eq. (1.3) with

$$f = \frac{1}{2}(\mathbf{B} \times \nabla\mathbf{O}) \cdot \mathbf{r} \tag{1.16}$$

.

In Hilbert space, the transformation of wave function Eq. (1.13) can easily be done. However, in quantum chemistry calculations, usually we use the linear combination of lo-

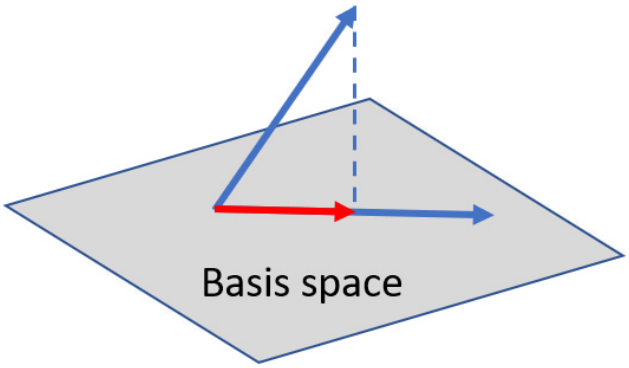

Figure 1.1. The wave function before gauge transformation is in the basis space. The gauge transformation rotate the wave function out of the space (the arrow out of the basis plane) if the basis space is not complete. The best approximation is the projection of transformed wave function in the basis space (red arrow).

calized atomic orbitals such as Gaussian orbital and Slater type orbitals to form the molecular orbital. Such localized atomic orbitals are not complete, limiting the transformation Eq. (1.13) in a subspace of the Hilbert space. As illustrated in Fig. 1.1, before gauge transformation, the projection of the wave function Ψ in the basis space $\{\chi\}$ is $\langle\chi\,|\,\Psi\rangle$. The gauge transformation rotate the state to $\exp(-iF)\Psi$ and the optimal solution obtained in the original basis space $\langle\chi\,|\exp(-iF)\Psi\rangle$. If the basis space is not complete, the expectation value of the energy before and after the transformation ($\langle\Psi\,|\,\chi\rangle\,\langle\chi\,|H|\,\chi\rangle\,\langle\chi\,|\,\Psi\rangle$ versus $\langle\exp(-iF)\Psi\,|\,\chi\rangle\,\langle\chi\,|\exp(-iF)H\exp(iF)|\,\chi\rangle\,\langle\chi\,|-\exp(iF)\Psi\rangle$) may not be identical, since the basis space $\{\chi\}$ may not be complete. However, if the basis space can also be transformed into $\{\exp(-iF)\chi\}$, the projection of the state becomes

$$\langle\exp(-iF)\chi\,|\exp(-iF)\Psi\rangle = \langle\chi\,|\,\Psi\rangle \tag{1.17}$$

, and the expectation value becomes

$$\langle \exp(-iF)\Psi \mid \exp(-iF)\chi\rangle \times \tag{1.18}$$

$$\langle \exp(-iF)\chi \mid \exp(-iF)H\exp(iF)\mid \exp(-iF)\chi\rangle \times \tag{1.19}$$

$$\langle \exp(-iF)\chi \mid \exp(-iF)\Psi\rangle \tag{1.20}$$

$$= \langle \Psi \mid \chi\rangle \langle \chi \mid H \mid \chi\rangle \langle \chi \mid \Psi\rangle \tag{1.21}$$

which is identical to the result before the gauge transformation even for an incomplete basis space. Usually in the quantum chemical simulation, we use localized basis function without transformation. Thus, the calculation result of molecular systems in the presence of magnetic fields with Gaussian basis function always shows gauge origin dependence. If we use a more complete Gaussian basis, the projection of the wave function and Hamiltonian in the basis space will approximate the complete space better. Thus, a bigger Gaussian basis set have less gauge origin dependence. However, in order to mitigate the gauge origin problem, the increase in the computational cost of using a more complete basis can be prohibitively high in the real cases.

1.4 Gauge Including Atomic Orbital: Defining Local Gauge Origin on Each Atom

In order to mitigate the gauge origin dependence for a localized atomic orbital without using a bigger basis set, the gauge including atomic orbital (GIAO) was proposed. In the presence of uniform magnetic field $\mathbf{B}$, it is defined as

$$\tilde{\chi}_\mu(\mathbf{r}, \mathbf{k}_A) = \chi_\mu(\mathbf{r} - \mathbf{R}_A) e^{i\mathbf{k}_A \cdot (\mathbf{r} - \mathbf{R}_A)} \tag{1.22}$$

where the vector is defined as

$$\mathbf{k}_A = \frac{\mathbf{R}_A \times \mathbf{B}}{2} \tag{1.23}$$

. $\{\chi_\mu(\mathbf{r}-\mathbf{R}_A)\}$ are localized atomic orbital (AO) basis functions centered at nuclear coordinate $\mathbf{R}_A$. The GIAO can be regarded as a localized atomic orbital attached with a phase factor. The phase factor defines the local gauge origin at each nuclear center in the presence of magnetic field with a plane wave. This can be shown as follows

$$\mathbf{k}_A \cdot (\mathbf{r}-\mathbf{R}_A) = \frac{\mathbf{R}_A \times \mathbf{B}}{2} \cdot (\mathbf{r}-\mathbf{R}_A) = -\frac{1}{2}(\mathbf{B} \times \mathbf{R_A}) \cdot \mathbf{r} \tag{1.24}$$

which satisfy the form of gauge origin trasformation factor $-f$ in Eq. (1.16) with $\Delta\mathbf{O} = \mathbf{R}_A - \mathbf{O}$, where the original gauge origin $\mathbf{O}$ is defined at $(0,0,0)$, $\mathbf{R}_A = \mathbf{R}_A - \mathbf{O}$, $\mathbf{r} = \mathbf{r} - \mathbf{O}$ and the fact that $\mathbf{R}_A \times \mathbf{B} \cdot \mathbf{R}_A = 0$. We have

$$\tilde{\chi}_\mu(\mathbf{r}, \mathbf{k}_A) = e^{-i\frac{1}{2}[\mathbf{B}\times(\mathbf{R_A}-\mathbf{O})]\cdot\mathbf{r}} \chi_\mu(\mathbf{r}-\mathbf{R}_A) \tag{1.25}$$

The Hamiltonian in the basis representation

$$\langle \tilde{\chi}_A | H | \tilde{\chi}_A \rangle = \left\langle \chi_A \left| e^{-i\frac{1}{2}[\mathbf{B}\times(\mathbf{R_A}-\mathbf{O})]} \, H \, e^{i\frac{1}{2}[\mathbf{B}\times(\mathbf{R_A}-\mathbf{O})]} \right| \chi_A \right\rangle \tag{1.26}$$

transform the gauge origin of the Hamiltonian from $\mathbf{O}$ to nuclear coordinate $\mathbf{R}_A$. Thus, the GIAO defines a local gauge origin on each atom in the basis representation. No matter what gauge origin is chosen in the vector potential, the calculation result does not change.

It should be pointed out that GIAO provides a uniform way of choosing gauge origin in the localized basis function. Whether or not it is the optimal way of defining a gauge origin is still under debate.

1.5 Interaction between the plane wave and matter

We can show that with only magnetic fields and radiation fields, the Hamiltonian in the Coulomb gauge is not dependent on the scalar field. The electrostatic interaction can be written as charge interaction.

Assume there is no source in the space of interest, in the Coulomb gauge, the scalar

potential $\phi = 0$. Only vector potential is needed to express the electromagnetic wave. The equation of motion for vector potential in vacuum is

$$\nabla^2 \mathbf{A} - \frac{1}{c^2}\frac{\partial^2}{\partial t^2}\mathbf{A} = 0 \tag{1.27}$$

the electric and magnetic field is given by

$$\mathbf{E} = -\frac{\partial \mathbf{A}}{\partial t} \tag{1.28}$$

$$\mathbf{B} = \nabla \times \mathbf{A} \tag{1.29}$$

For linearly polarized plane wave propagating in direction $\hat{\boldsymbol{\kappa}}$, with polarization unit vector $\hat{\boldsymbol{\varepsilon}}_i$, the complex vector potential

$$\tilde{\mathbf{A}} = A_0 \hat{\varepsilon}_i \exp[i(\omega t - \boldsymbol{\kappa} \cdot \mathbf{r})] \tag{1.30}$$

The real vector potential

$$\mathbf{A} = \tilde{\mathbf{A}} + \tilde{\mathbf{A}}^* = \frac{1}{2}\{A_0 \hat{\varepsilon}_i \exp[i(\omega t - \boldsymbol{\kappa} \cdot \mathbf{r})] + (A_0 \hat{\varepsilon}_i)^* \exp[-i(\omega t - \boldsymbol{\kappa} \cdot \mathbf{r})]\} \tag{1.31}$$

$\mathbf{r}$ is the coordinate of interest. the complex form of electric field

$$\tilde{\mathbf{E}} = E_0 \hat{\boldsymbol{\varepsilon}}_i \exp[i(\omega t - \boldsymbol{\kappa} \cdot \mathbf{r})] \tag{1.32}$$

and the real electric field is $\mathbf{E} = \frac{1}{2}(\tilde{\mathbf{E}} + \tilde{\mathbf{E}}^*)$

Eq. (1.28) gives the relation

$$E_0 = -i\omega A_0 \tag{1.33}$$

From Eq. (1.29), we can find the magnetic field of the plane wave

$$\tilde{\mathbf{B}} = -i(\boldsymbol{\kappa} \times \hat{\boldsymbol{\varepsilon}}_i) A_0 \exp[i(\omega t - \boldsymbol{\kappa} \cdot \mathbf{r})] \tag{1.34}$$

For circularly polarized light, assume the wave is propagating in direction z. The polarization unit vector is

$$\hat{\boldsymbol{\varepsilon}}_i = \hat{\boldsymbol{\varepsilon}}_\pm = \frac{1}{2}\big(\hat{\boldsymbol{\varepsilon}}_x \pm i\hat{\boldsymbol{\varepsilon}}_y\big) \tag{1.35}$$

where

$$\hat{\boldsymbol{\varepsilon}}_R = \hat{\boldsymbol{\varepsilon}}_+, \quad \hat{\boldsymbol{\varepsilon}}_L = \hat{\boldsymbol{\varepsilon}}_- \tag{1.36}$$

The non relativistic field-matter interaction term in the Hamiltonian Eqs. (1.7) and (1.9)

$$H_I = \sum_i^N \mathbf{A}\cdot\mathbf{p}_i \tag{1.37}$$

The light-matter interaction will be discussed in the response function section. Here we use the conclusion from Ref. 119 that the transition probability from the ground state to one excited state is proportional to the square of the norm of transition matrix element

$$P_{i\to f} \propto \left|\left\langle f\left|\sum_i^N \tilde{\mathbf{A}}^*\cdot\mathbf{p}_i\right|i\right\rangle\right|^2 N_i \tag{1.38}$$

where N_i is the population of initial state. Since this excitation absorb photon with positive frequency, the matter interact with the complex conjugate of $\tilde{\mathbf{A}}$. The absorption is proportional to the photon energy, concentration of the molecules, and transition probability and divided by the intensity of the light $A \propto N_i P_{i\to f}\hbar\omega/(E_0)^2$, thus

$$A \propto \omega\big|\langle f\,|\exp(i\boldsymbol{\kappa}\cdot\mathbf{r})\hat{\boldsymbol{\varepsilon}}_i^*\cdot\mathbf{p}|\,i\rangle\,\big|^2 N_i \tag{1.39}$$

where the time dependent part of the wave is taken out out the bracket and integrated to give a delta function of frequency.

For circularly polarized light propagating in z direction, $\mathbf{A}_\pm = \frac{\mathbf{A}_x \pm i\mathbf{A}_y}{\sqrt{2}}$, it is easy to show

that

$$\left|\left\langle f\left|\mathbf{A}_{\pm}^{*}\cdot\mathbf{p}\right|i\right\rangle\right|^{2}=\left|\left\langle f\left|A_{0}^{*}\exp(i\boldsymbol{\kappa}\cdot\mathbf{r})\hat{\boldsymbol{\varepsilon}}_{\mp}\cdot\mathbf{p}\right|i\right\rangle\right|^{2}=\left|\left\langle f\left|A_{0}^{*}\exp(i\boldsymbol{\kappa}\cdot\mathbf{r})p_{\mp}\right|i\right\rangle\right|^{2} \tag{1.40}$$

where

$$p_{\mp}=\frac{p_{x}\mp ip_{y}}{\sqrt{2}} \tag{1.41}$$

and the circular dichroism is defined as the difference of absorption of left and right polarized light, $A_{-}-A_{+}$. The circular dichroism can be calculated as

$$\Delta A\propto A_{-}-A_{+}=\omega N_{i}\left(\left|\left\langle f\left|\exp(i\boldsymbol{\kappa}\cdot\mathbf{r})p_{+}\right|i\right\rangle\right|^{2}-\left|\left\langle f\left|\exp(i\boldsymbol{\kappa}\cdot\mathbf{r})p_{-}\right|i\right\rangle\right|^{2}\right) \tag{1.42}$$

$$=\omega N_{i}\left(\left|\left\langle i\left|\exp(-i\boldsymbol{\kappa}\cdot\mathbf{r})p_{-}\right|f\right\rangle\right|^{2}-\left|\left\langle i\left|\exp(-i\boldsymbol{\kappa}\cdot\mathbf{r})p_{+}\right|f\right\rangle\right|^{2}\right) \tag{1.43}$$

where we use the relation

$$\left\langle f\left|\exp(i\boldsymbol{\kappa}\cdot\mathbf{r})p_{\pm}\right|i\right\rangle^{*}=\left\langle i\left|[\exp(i\boldsymbol{\kappa}\cdot\mathbf{r})p_{\pm}]^{*}\right|f\right\rangle=\left\langle i\left|\exp(-i\boldsymbol{\kappa}\cdot\mathbf{r})p_{\mp}\right|f\right\rangle \tag{1.44}$$

In the low frequency limit, $\boldsymbol{\kappa}\cdot\mathbf{r}$ is small, $\exp(i\boldsymbol{\kappa}\cdot\mathbf{r})\approx 1$. This is the electric dipole approximation. Using the commutator relation $[\mathbf{p}^{2},\mathbf{r}]=-2i\mathbf{p}$, we can write the matrix element as

$$\left\langle i\left|A_{0}p_{j}\right|f\right\rangle=A_{0}\left\langle i\left|i[H_{0},r_{j}]\right|f\right\rangle=i(E_{i}-E_{f})A_{0}\left\langle i\left|r_{j}\right|f\right\rangle=-i\omega A_{0}\left\langle i\left|r_{j}\right|f\right\rangle=E_{0}\left\langle i\left|r_{j}\right|f\right\rangle \tag{1.45}$$

where we used the relation Eq. (1.33). This is the length gauge. The transition probability

$$P_{i\to f}\propto\omega^{2}|A_{0}|^{2}\left|\left\langle f\left|\hat{\boldsymbol{\varepsilon}}_{i}^{*}\cdot\mathbf{r}\right|i\right\rangle\right|^{2}=|E_{0}|^{2}\left|\left\langle f\left|\hat{\boldsymbol{\varepsilon}}_{i}^{*}\cdot\mathbf{r}\right|i\right\rangle\right|^{2} \tag{1.46}$$

The absorption of linearly polarized light in the dipole approximation and length gauge can be written as

$$A\propto\omega\left|\left\langle f\left|\hat{\boldsymbol{\varepsilon}}_{i}^{*}\cdot\mathbf{r}\right|i\right\rangle\right|^{2}N_{i}=\omega\left|\left\langle i\left|\hat{\boldsymbol{\varepsilon}}_{i}\cdot\mathbf{r}\right|f\right\rangle\right|^{2}N_{i} \tag{1.47}$$

For circular dichroism, with dipole approximation,

$$\begin{aligned}\Delta A \propto & \quad \omega\big(\big|\langle i\,|\hat{\boldsymbol{\varepsilon}}_-\cdot\mathbf{r}|\,f\rangle\,\big|^2-\big|\langle i\,|\hat{\boldsymbol{\varepsilon}}_+\cdot\mathbf{r}|\,f\rangle\,\big|^2\big)N_i \\ = & \quad \omega\big(\big|\langle i\,|\mu_-|\,f\rangle\,\big|^2-\big|\langle i\,|\mu_+|\,f\rangle\,\big|^2\big)N_i \end{aligned} \tag{1.48}$$

where $\mu_\pm = (r_x \pm ir_y)/\sqrt{2}$. Without the presence of the magnetic fields, the dipole contribution to the circular dichroism is zero.

In relativistic case, the Heisenberg equation of motion gives

$$c\boldsymbol{\alpha} = -i[\mathbf{r}, H_0] \tag{1.49}$$

the light matter interaction can be written as

$$\langle f\,|H_I|\,i\rangle = \left\langle f\left|c\boldsymbol{\alpha}\cdot\tilde{\mathbf{A}}^*\right|i\right\rangle = -i\left\langle f\left|\mathbf{r}\cdot\tilde{\mathbf{A}}^*\right|i\right\rangle(E_i-E_f) = i\omega\left\langle f\left|\mathbf{r}\cdot\tilde{\mathbf{A}}^*\right|i\right\rangle \tag{1.50}$$

which is similar to the non-relativistic case.

Next, let us go beyond dipole approximation. If we do Taylor expansion of plane wave for the exponent and cut off at first order, Eq. (1.39) becomes

$$A \propto \omega\big|\langle i\,|(1-i\boldsymbol{\kappa}\cdot\mathbf{r})\hat{\boldsymbol{\varepsilon}}_i\cdot\mathbf{p}|\,f\rangle\,\big|^2 N_i \tag{1.51}$$

Focus on the second part $\langle i\,|(\boldsymbol{\kappa}\cdot\mathbf{r})(\hat{\boldsymbol{\varepsilon}}_i\cdot\mathbf{p})|\,f\rangle$.

$$\begin{aligned}(\boldsymbol{\kappa}\cdot\mathbf{r})(\hat{\boldsymbol{\varepsilon}}_i\cdot\mathbf{p}) = & \frac{1}{2}[(\boldsymbol{\kappa}\cdot\mathbf{r})(\hat{\boldsymbol{\varepsilon}}_i\cdot\mathbf{p})+(\boldsymbol{\kappa}\cdot\mathbf{p})(\hat{\boldsymbol{\varepsilon}}_i\cdot\mathbf{r})] \\ & +\frac{1}{2}[(\boldsymbol{\kappa}\cdot\mathbf{r})(\hat{\boldsymbol{\varepsilon}}_i\cdot\mathbf{p})-(\boldsymbol{\kappa}\cdot\mathbf{p})(\hat{\boldsymbol{\varepsilon}}_i\cdot\mathbf{r})]\end{aligned} \tag{1.52}$$

It can be shown that

$$(\boldsymbol{\kappa}\cdot\mathbf{r})(\hat{\boldsymbol{\varepsilon}}_i\cdot\mathbf{p})-(\boldsymbol{\kappa}\cdot\mathbf{p})(\hat{\boldsymbol{\varepsilon}}_i\cdot\mathbf{r}) = (\boldsymbol{\kappa}\times\hat{\boldsymbol{\varepsilon}}_i)\cdot(\mathbf{r}\times\mathbf{p}) \tag{1.53}$$

From Eq. (1.34) we can find that this term is the interaction between the magnetic field and the magnetic dipole (one half of the orbital angular momentum $\mathbf{l} = \mathbf{r} \times \mathbf{p}$).

From commutator $[\mathbf{p}^2, \mathbf{rr}] = -2i(\mathbf{pr} + \mathbf{rp})$, we have $\mathbf{pr} + \mathbf{rp} = i[H_0, \mathbf{rr}]$. The matrix element of the first term in Eq. (1.52)

$$\begin{aligned}\frac{1}{2}\boldsymbol{\kappa} \cdot \langle i \left| \mathbf{rp} + \mathbf{pr} \right| f \rangle \cdot \hat{\boldsymbol{\varepsilon}}_i =& \frac{i}{2}\boldsymbol{\kappa} \cdot \langle i \left| [H_0, \mathbf{rr}] \right| f \rangle \cdot \hat{\boldsymbol{\varepsilon}}_i = \frac{i(E_i - E_f)}{2}\boldsymbol{\kappa} \cdot \langle i \left| \mathbf{rr} \right| f \rangle \cdot \hat{\boldsymbol{\varepsilon}}_i \\ =& -\frac{i\omega\boldsymbol{\kappa}}{2} \cdot \langle i \left| \mathbf{rr} \right| f \rangle \cdot \hat{\boldsymbol{\varepsilon}}_i \end{aligned} \tag{1.54}$$

we notice that $\boldsymbol{\kappa} \cdot \hat{\boldsymbol{\varepsilon}}_i = 0$, thus $\boldsymbol{\kappa} \cdot \mathbf{I}_3 \cdot \hat{\boldsymbol{\varepsilon}}_i = 0$. And

$$-\frac{i\omega\boldsymbol{\kappa}}{2} \cdot \langle i \left| \mathbf{rr} \right| f \rangle \cdot \hat{\boldsymbol{\varepsilon}}_i = -\frac{i\omega\boldsymbol{\kappa}}{2} \cdot \left\langle i \left| \mathbf{rr} - \frac{\mathbf{r} \cdot \mathbf{r}\, \mathbf{I}_3}{3} \right| f \right\rangle \cdot \hat{\boldsymbol{\varepsilon}}_i = \frac{\boldsymbol{\kappa}}{2} \cdot \langle i \left| \mathbf{Q} \right| f \rangle \cdot \frac{\mathbf{E}_0}{A_0} \tag{1.55}$$

In summary,

$$\langle i \left| (1 - i\boldsymbol{\kappa} \cdot \mathbf{r})\hat{\boldsymbol{\varepsilon}}_i \cdot \mathbf{p} \right| f \rangle = -i\omega\hat{\boldsymbol{\varepsilon}}_i \cdot \langle i \left| \mathbf{r} \right| f \rangle - \frac{i}{2}(\boldsymbol{\kappa} \times \hat{\boldsymbol{\varepsilon}}_i) \cdot \langle i \left| \mathbf{l} \right| f \rangle - \frac{\omega\boldsymbol{\kappa}}{2} \cdot \langle i \left| Q \right| f \rangle \cdot \hat{\boldsymbol{\varepsilon}}_i \tag{1.56}$$

$$= \frac{1}{A_0}(\mathbf{E}_0 \cdot \langle i \left| \mathbf{r} \right| f \rangle + \frac{\mathbf{B}_0}{2} \cdot \langle i \left| \mathbf{l} \right| f \rangle - i\frac{\boldsymbol{\kappa}}{2} \cdot \langle i \left| Q \right| f \rangle \cdot \mathbf{E}_0) \tag{1.57}$$

For circularly polarized light, due to the right hand rule, $\boldsymbol{\kappa} \times \hat{\boldsymbol{\varepsilon}}_x = |\boldsymbol{\kappa}|\hat{\boldsymbol{\varepsilon}}_y$, $\boldsymbol{\kappa} \times \hat{\boldsymbol{\varepsilon}}_y = -|\boldsymbol{\kappa}|\hat{\boldsymbol{\varepsilon}}_x$, thus $\boldsymbol{\kappa} \times \hat{\boldsymbol{\varepsilon}}_+ = -i|\boldsymbol{\kappa}|\hat{\boldsymbol{\varepsilon}}_+$, $\boldsymbol{\kappa} \times \hat{\boldsymbol{\varepsilon}}_- = i|\boldsymbol{\kappa}|\hat{\boldsymbol{\varepsilon}}_-$. From Eq. (1.56), we have

$$\begin{aligned}\langle i \left| (1 - i\boldsymbol{\kappa} \cdot \mathbf{r})\hat{\boldsymbol{\varepsilon}}_\pm \cdot \mathbf{p} \right| f \rangle =& -i\omega\hat{\boldsymbol{\varepsilon}}_\pm \cdot \langle i \left| \mathbf{r} \right| f \rangle - \frac{i}{2}(\mp i)|\boldsymbol{\kappa}|\hat{\boldsymbol{\varepsilon}}_\pm \cdot \langle i \left| \mathbf{l} \right| f \rangle - \frac{\omega\boldsymbol{\kappa}}{2} \cdot \langle i \left| Q \right| f \rangle \cdot \hat{\boldsymbol{\varepsilon}}_\pm \\ =& -i\omega \langle i \left| r_\pm \right| f \rangle \mp \frac{1}{2}|\boldsymbol{\kappa}| \langle i \left| l_\pm \right| f \rangle - \frac{\omega\boldsymbol{\kappa}}{2} \cdot \langle i \left| Q_{\cdot\pm} \right| f \rangle \\ =& -i\omega \left[\langle i \left| r_\pm \right| f \rangle \mp \frac{i}{2} \cdot \langle i \left| l_\pm \right| f \rangle - \frac{i\omega\hat{\boldsymbol{\kappa}}}{2} \cdot \langle i \left| Q_{\cdot\pm} \right| f \rangle \right] \end{aligned} \tag{1.58}$$

where $|\boldsymbol{\kappa}| = \omega$. Since

$$iQ_\pm = i(Q_{xz} \pm iQ_{yz}) = iQ_{xz} \mp Q_{yz} = \mp(Q_{yz} \mp iQ_{xz}) = \mp Q_\mp \tag{1.59}$$

$$\langle i\,|(1-i\boldsymbol{\kappa}\cdot\mathbf{r})\hat{\boldsymbol{\varepsilon}}_{\pm}\cdot\mathbf{p}|\,f\rangle = -i\omega\left[\,\langle i\,|r_{\pm}|\,f\rangle \mp \frac{i}{2}\,\langle i\,|l_{\pm}|\,f\rangle \pm \frac{\omega\hat{\boldsymbol{\kappa}}}{2}\cdot\langle i\,|Q_{\cdot\mp}|\,f\rangle\,\right] \tag{1.60}$$

Thus

$$\begin{aligned} A_{\pm} \propto & \frac{1}{|\mathbf{E}_0|^2}|\,\langle i\,|(1-i\boldsymbol{\kappa}\cdot\mathbf{r})\hat{\boldsymbol{\varepsilon}}_{\pm}\cdot\mathbf{p}|\,f\rangle\,|^2 \\ = & |\,\langle i\,|r_{\pm}|\,f\rangle\,|^2 + \left|\frac{i}{2}\,\langle i\,|l_{\pm}|\,f\rangle\right|^2 + \left|\frac{\omega\hat{\boldsymbol{\kappa}}}{2}\cdot\langle i\,|Q_{\cdot\mp}|\,f\rangle\right|^2 \\ & \pm \mathrm{Im}(\langle f\,|r_{\mp}|\,i\rangle\,\langle i\,|l_{\pm}|\,f\rangle) \\ & \pm \mathrm{Re}(\langle f\,|r_{\mp}|\,i\rangle\,\langle i\,|Q_{\mp}|\,f\rangle) \\ & -\frac{\omega\hat{\boldsymbol{\kappa}}}{2}\mathrm{Im}(\langle f\,|l_{\mp}|\,i\rangle\,\langle i\,|Q_{\mp}|\,f\rangle) \end{aligned} \tag{1.61}$$

Then for

$$\Delta A \propto \frac{1}{|\mathbf{E}_0|^2}[|\,\langle i\,|(1-i\boldsymbol{\kappa}\cdot\mathbf{r})\hat{\boldsymbol{\varepsilon}}_{-}\cdot\mathbf{p}|\,f\rangle\,|^2 - |\,\langle i\,|(1-i\boldsymbol{\kappa}\cdot\mathbf{r})\hat{\boldsymbol{\varepsilon}}_{+}\cdot\mathbf{p}|\,f\rangle\,|^2] \tag{1.62}$$

without the presence of static magnetic field, the contribution to Eq. (1.62) from the second line of Eq. (1.61) is zero. The lowest contribution to Eq. (1.62) is the third line of Eq. (1.61),

$$\begin{aligned} \Delta A \propto & -\mathrm{Im}(\langle f\,|r_{+}|\,i\rangle\,\langle i\,|l_{-}|\,f\rangle) - \mathrm{Im}(\langle f\,|r_{-}|\,i\rangle\,\langle i\,|l_{+}|\,f\rangle) \\ = & -2[\mathrm{Im}(\langle f\,|r_x|\,i\rangle\,\langle i\,|l_x|\,f\rangle) + \mathrm{Im}(\langle f\,|r_y|\,i\rangle\,\langle i\,|l_y|\,f\rangle)] \end{aligned} \tag{1.63}$$

assuming the light propagation direction is z. After isotropic average, the electronic circular dichroism can be calculated by

$$\Delta A \propto \mathrm{Im}(\langle f\,|\mathbf{r}|\,i\rangle\cdot\langle i\,|\mathbf{l}|\,f\rangle) \tag{1.64}$$

1.6 Time Evolution of the Observable and the Response Function

In this section, we introduce the response function and relate it to the time evolution of the expectation value of the operator, i.e., observable. From the response function, we can obtain the absorption spectra and electronic circular dichroism signal of molecular systems. This section will provide the background knowledge for simulating MCD with real time dynamics in Chapter 5. The readers only interested in linear response TDDFT method can skip this section. In Secs. 1.6.1 and 1.6.2, we mainly follows and expand the derivation of time evolution of observable in Ref. 112 with more details.

1.6.1 Liouville Equation

Time dependent Schrödinger equation and its complex conjugate are

$$i\frac{\partial}{\partial t}\left|\psi\right\rangle = \left(H_0 + V_t\right)\left|\psi\right\rangle, \quad -i\frac{\partial}{\partial t}\left\langle\psi\right| = \left\langle\psi\right|\left(H_0 + V_t\right) \tag{1.65}$$

where V_t is a time dependent perturbation. It can also be represented in the Fourier transformed form

$$V_t(\mathbf{r}) = \int_{-\infty}^{\infty} d\omega V_\omega(\mathbf{r}) e^{-i\omega t} \tag{1.66}$$

Density matrix in Schrödinger picture and interaction picture are defined separately as

$$\rho = \left|\psi\right\rangle\left\langle\psi\right| \tag{1.67}$$

in interaction picture,

$$\rho_I(t) = e^{iH_0 t}\left|\psi\right\rangle\left\langle\psi\right| e^{-iH_0 t} \tag{1.68}$$

The equation of motion for density matrix in interaction picture is

$$i\frac{\partial}{\partial t}\rho_I = e^{iH_0 t} V_t \left|\psi\right\rangle\left\langle\psi\right| e^{-iH_0 t} - e^{iH_0 t}\left|\psi\right\rangle\left\langle\psi\right| V_t e^{-iH_0 t} \tag{1.69}$$

Define operator in interaction picture

$$V_t(t) = e^{iH_0 t} V_t e^{-iH_0 t} \tag{1.70}$$

note that subscript t denote the time in Schrödinger picture, t in parenthesis is the time in interaction picture. Then we have

$$e^{iH_0 t} V_t = V_t(t) e^{iH_0 t}, \quad V_t e^{-iH_0 t} = e^{-iH_0 t} V_t(t) \tag{1.71}$$

So

$$i\frac{\partial}{\partial t}\rho_I = [V_t(t), \rho_I(t)] \tag{1.72}$$

By integrating the time,

$$\rho_I(t) = \rho_0 - i\int_{-\infty}^{t} [V_{t'}(t'), \rho_I(t')] \tag{1.73}$$

or in Schrödinger picture

$$\begin{aligned} e^{iH_0 t}\rho(t)e^{-iH_0 t} =& \rho_0 - i\int_{-\infty}^{t} [e^{iH_0 t'} V_{t'} e^{-iH_0 t'} e^{iH_0 t'} \rho(t') e^{-iH_0 t'} \\ & - e^{iH_0 t'} \rho(t') e^{-iH_0 t'} e^{iH_0 t'} V_{t'} e^{-iH_0 t'}] dt' \end{aligned} \tag{1.74}$$

multiply $e^{-iH_0 t}$ on the left, $e^{iH_0 t}$ on the right:

$$\rho(t) = e^{-iE_0 t}\rho_0 e^{iE_0 t} - i\int_{-\infty}^{t} dt' [V_{t'}(t'-t), e^{iH_0(t-t')}\rho(t')e^{-iH_0(t-t')}] \tag{1.75}$$

In principle, we can plug the Eq. (1.75) in the right hand side of Eq. (1.75), and obtain an infinite expansion. In order to explain how real time dynamics works, we cut off the expansion at first order.

In linear response approximation, we use ρ_0 as the density operator on the right hand side

$$\rho(t) = \rho_0 - i\int_{-\infty}^{t} dt'[V_{t'}(t'-t), \rho_0]dt' \tag{1.76}$$

1.6.2 Time evolution of the observable

For operator $\hat{O}$, the expectation value at time t is

$$O(t) = \left\langle \psi \left| \hat{O} \right| \psi \right\rangle = Tr(\rho O) = \langle 0 \left| O \right| 0 \rangle - i\int_{-\infty}^{t} Tr([V_{t'}(t'-t)\rho_0 O - \rho_0 V_{t'}(t'-t)O])dt' \tag{1.77}$$

Notice that

$$Tr(V_{t'}(t'-t)\rho_0 O) = Tr(OV_{t'}(t'-t)\rho_0) = \langle 0 \left| OV_{t'}(t'-t) \right| 0 \rangle \tag{1.78}$$

and

$$Tr(\rho_0 V_{t'}(t'-t)O) = \langle 0 \left| V_{t'}(t'-t)O \right| 0 \rangle \tag{1.79}$$

So

$$\begin{aligned} O(t) =& O(0) - i\int_{-\infty}^{t} dt' \langle 0 \left| [O, V_{t'}(t'-t)] \right| 0 \rangle \\ =& O(0) - i\int_{-\infty}^{\infty} dt' \Theta(-(t'-t)) \langle 0 \left| [O, V_{t'}(t'-t)] \right| 0 \rangle \end{aligned} \tag{1.80}$$

where the step function is

$$\Theta(-(t'-t)) = \begin{cases} 1 & -(t'-t) > 0, \text{which is } t' < t \\ 0 & -(t'-t) < 0, \text{which is } t' > t \end{cases} \tag{1.81}$$

The step function is used such that the integral upper limit is changed from t to ∞, and it will be more convenient for the following derivations.

Define retarded polarization propagator in time domain,

$$\langle\langle \hat{O}; V_{t'}(t'-t) \rangle\rangle^r = -i\Theta(-(t'-t)) \langle 0 | [O, V_{t'}(t'-t)] | 0 \rangle \tag{1.82}$$

The time evolvement of the expectation value of operator $\hat{O}$ is

$$O(t) = O(0) + \int_{-\infty}^{\infty} \langle\langle \hat{O}; V_{t'}(t'-t) \rangle\rangle^r dt' \tag{1.83}$$

decompose $V_{t'}$ into frequency domain according to Eq. (1.66), we have

$$O(t) = O(0) + \int_{-\infty}^{\infty} d\omega \int_{-\infty}^{\infty} dt' \langle\langle \hat{O}; V_{\omega}(t'-t) \rangle\rangle^r e^{-i\omega t} \tag{1.84}$$

where $V_{\omega}(t'-t)$ is frequency component operator V_{ω} in interaction picture

$$V_{\omega}(t'-t) = e^{iH_0(t'-t)} V_{\omega} e^{-iH_0(t'-t)} \tag{1.85}$$

The purpose of doing this transformation is to take advantage that operator V_{ω} is independent of time, and it will be easier to analyze the polarization propagator $\langle\langle \hat{O}; V_{\omega}(t'-t) \rangle\rangle^r$.

1.6.3 Lehmann representation

$$\begin{aligned}
\langle\langle \hat{O}; V_{\omega}(t'-t) \rangle\rangle^r =& -i\Theta(-(t'-t)) \sum_n [\langle 0 | O | n \rangle \langle n | V_{\omega}(t'-t) | 0 \rangle - \langle 0 | V_{\omega}(t'-t) | n \rangle \langle n | O | 0 \rangle] \\
=& -i\Theta(-(t'-t)) \sum_n [\langle 0 | O | n \rangle \langle n | V_{\omega} | 0 \rangle e^{iE_n(t'-t)} e^{-iE_0(t'-t)} \\
& - \langle 0 | V_{\omega} | n \rangle \langle n | O | 0 \rangle e^{i(E_n - E_0)(t'-t)}]
\end{aligned} \tag{1.86}$$

Now we want to transform the function in time domain into frequency domain. Consider integral

$$-\int_{-\infty}^{\infty} d\omega \frac{1}{2\pi i} \sum_n \left[\frac{\langle 0 \left| O \right| n \rangle \langle n \left| V_{\omega'} \right| 0 \rangle}{\omega - (E_n - E_0) + i\eta} \right] e^{-i\omega(t-t')} \tag{1.87}$$

The pole is at $\omega = (E_n - E_0) - i\eta$, which is in the lower half plane. When $t - t' > 0$, the path go through the lower half plane, and the contour is clockwise Fig. 1.2.

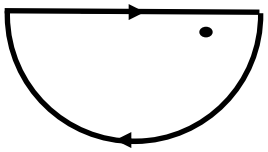

Figure 1.2. This is lower half plane contour with clockwise path. The dot is $(E_n - E_0) - i\eta$.

So the integral becomes

$$\begin{aligned}
&\lim_{\eta \to 0} -\int_{-\infty}^{\infty} d\omega \frac{1}{2\pi i} \sum_n \left[\frac{\langle 0 \left| O \right| n \rangle \langle n \left| V_{\omega'} \right| 0 \rangle}{\omega - (E_n - E_0) + i\eta} \right] e^{-i\omega(t-t')} \\
&= -\left(-\frac{2\pi i}{2\pi i} \sum_n \langle 0 \left| O \right| n \rangle \langle n \left| V_{\omega'} \right| 0 \rangle e^{-i(E_n - E_0)(t-t')} \right) \\
&= \sum_n \langle 0 \left| O \right| n \rangle \langle n \left| V_{\omega'} \right| 0 \rangle e^{-i(E_n - E_0)(t-t')}
\end{aligned} \tag{1.88}$$

when $t - t' < 0$, the path go through the upper half plane. Since the upper half plane has no poles, the integral becomes zero.

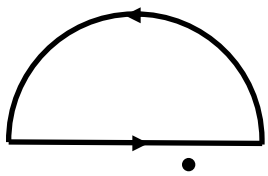

Figure 1.3. This is upper half plane contour with counterclockwise path. The dot is $(E_n - E_0) - i\eta$.

So in summary,

$$\begin{aligned}
&\lim_{\eta\to 0} -\int_{-\infty}^{\infty} d\omega \frac{1}{2\pi i} \sum_n \left[\frac{\langle 0\,|O|\,n\rangle\,\langle n\,|V_{\omega'}|\,0\rangle}{\omega - (E_n - E_0) + i\eta} \right] e^{-i\omega(t-t')} \\
&= \begin{cases} \sum_n \langle 0\,|O|\,n\rangle\,\langle n\,|V_{\omega'}|\,0\rangle\, e^{-i(E_n-E_0)(t-t')} & t-t' > 0 \\ 0 & t-t' < 0 \end{cases}
\end{aligned} \tag{1.89}$$

For the same reason,

$$\begin{aligned}
&\lim_{\eta\to 0} -\int_{-\infty}^{\infty} d\omega \frac{1}{2\pi i} \sum_n \left[\frac{\langle 0\,|V_{\omega'}|\,n\rangle\,\langle n\,|O|\,0\rangle}{\omega + (E_n - E_0) + i\eta} \right] e^{-i\omega(t-t')} \\
&= \begin{cases} \sum_n \langle 0\,|V_{\omega'}|\,n\rangle\,\langle n\,|O|\,0\rangle\, e^{+i(E_n-E_0)(t-t')} & t-t' > 0 \\ 0 & t-t' < 0 \end{cases}
\end{aligned} \tag{1.90}$$

So this integral with η is equivalent to a step function.

$$\begin{aligned}
&-i\left(-\int_{-\infty}^{\infty} d\omega \frac{1}{2\pi i} \sum_n \left[\frac{\langle 0\,|O|\,n\rangle\,\langle n\,|V_{\omega'}|\,0\rangle}{\omega - (E_n - E_0) + i\eta} - \frac{\langle 0\,|V_{\omega'}|\,n\rangle\,\langle n\,|O|\,0\rangle}{\omega + (E_n - E_0) + i\eta} \right] e^{-i\omega(t-t')} \right) \\
&= \langle\!\langle O; V_{\omega'}(t'-t) \rangle\!\rangle
\end{aligned} \tag{1.91}$$

the ω' in the subscript denote the fourier component of the perturbation V. ω is the frequency of response function.

Define

$$\langle\!\langle O; V_{\omega'} \rangle\!\rangle^r_\omega = \lim_{\eta\to 0^+} \sum_n \left[\frac{\langle 0\,|O|\,n\rangle\,\langle n\,|V_{\omega'}|\,0\rangle}{\omega - (E_n - E_0) + i\eta} - \frac{\langle 0\,|V_{\omega'}|\,n\rangle\,\langle n\,|O|\,0\rangle}{\omega + (E_n - E_0) + i\eta} \right] \tag{1.92}$$

Then the inverse Fourier transform is From Eq. (1.91), we have the relationship between response function in time and frequency domain

$$\langle\!\langle O; V_{\omega'}(t'-t) \rangle\!\rangle^r = \int_{-\infty}^{\infty} \frac{d\omega}{2\pi} \langle\!\langle O; V_{\omega'} \rangle\!\rangle^r_\omega e^{-i\omega(t-t')} = \int_{-\infty}^{\infty} \frac{d\omega}{2\pi} \langle\!\langle O; V_{\omega'} \rangle\!\rangle^r_\omega e^{i\omega(t'-t)} \tag{1.93}$$

in order to obtain the inverse Fourier transform, we look at

$$\begin{aligned}\int_{-\infty}^{\infty}\langle\langle O;V_{\omega''}(t')\rangle\rangle^{r}e^{-i\omega t'}dt' =& \int_{-\infty}^{\infty}dt'e^{-i\omega t'}\int_{-\infty}^{\infty}\frac{d\omega'}{2\pi}\langle\langle O;V_{\omega''}\rangle\rangle_{\omega'}^{r}e^{i\omega' t'}\\ =&\int_{-\infty}^{\infty}dt'\int_{-\infty}^{\infty}\frac{d\omega'}{2\pi}\langle\langle O;V_{\omega''}\rangle\rangle_{\omega'}^{r}e^{i(\omega'-\omega)t'}\\ =&\int_{-\infty}^{\infty}d\omega'\langle\langle O;V_{\omega''}\rangle\rangle_{\omega'}^{r}\delta(\omega'-\omega)\\ =&\langle\langle O;V_{\omega''}\rangle\rangle_{\omega}^{r}\end{aligned} \tag{1.94}$$

Then we will study the linear response function in frequency domain.

$$\begin{aligned}&\lim_{\eta\to 0^+}\frac{\langle 0\left|O\right|n\rangle\langle n\left|V_{\omega'}\right|0\rangle}{\omega-(E_n-E_0)+i\eta}\\ =&\lim_{\eta\to 0^+}\frac{\langle 0\left|O\right|n\rangle\langle n\left|V_{\omega'}\right|0\rangle[\omega-(E_n-E_0)-i\eta]}{[\omega-(E_n-E_0)]^2-(i\eta)^2}\\ =&\lim_{\eta\to 0^+}\frac{\langle 0\left|O\right|n\rangle\langle n\left|V_{\omega'}\right|0\rangle[\omega-(E_n-E_0)-i\eta]}{[\omega-(E_n-E_0)]^2+(\eta)^2}\\ =&\frac{\langle 0\left|O\right|n\rangle\langle n\left|V_{\omega'}\right|0\rangle}{\omega-(E_n-E_0)}-i\pi\langle 0\left|O\right|n\rangle\langle n\left|V_{\omega'}\right|0\rangle\delta(\omega-(E_n-E_0))\end{aligned} \tag{1.95}$$

where the last line use the property of delta function

$$\delta(x)=\frac{1}{\pi}\lim_{\varepsilon\to 0}\frac{\varepsilon}{x^2+\varepsilon^2} \tag{1.96}$$

1.6.4 Fourier transformation of the time dependent observable

The response function can be obtained from the time evolution of the expectation value of the observable after a delta kick. It will be discussed in Chapter 5. With a delta kick of the form

$$V_t=V\delta(t)\kappa \tag{1.97}$$

where κ is the strength of the perturbation, by applying a time-frequency transformation, we can obtain the response function

$$\int_{-\infty}^{\infty}(O(t)-O(0))e^{i\omega t}dt=\frac{\kappa}{2\pi}\int dt\,e^{i\omega t}\int d\omega' e^{-i\omega' t}\langle\!\langle\hat{O};V\rangle\!\rangle^{r}_{\omega'}=\kappa\langle\!\langle\hat{O};V\rangle\!\rangle^{r}_{\omega'} \tag{1.98}$$

1.6.5 Relating absorption spectra to response function

We use delta pulse of electric field as a perturbation, and electric dipole as an observable.

$$\langle\!\langle\mu_\alpha;\mu_\alpha\rangle\!\rangle^{r}_{\omega}=\lim_{\eta\to 0^+}\sum_n\left[\frac{\langle 0\,|\mu_\alpha|\,n\rangle\,\langle n\,|\mu_\alpha|\,0\rangle}{\omega-(E_n-E_0)+i\eta}-\frac{\langle 0\,|\mu_\alpha|\,n\rangle\,\langle n\,|\mu_\alpha|\,0\rangle}{\omega+(E_n-E_0)+i\eta}\right] \tag{1.99}$$

So

$$\begin{aligned}\mathrm{Im}(\langle\!\langle\mu_\alpha;\mu_\alpha\rangle\!\rangle^{r}_{\omega})=-\pi\sum_n[&\mathrm{Re}(\langle 0\,|\mu_\alpha|\,n\rangle\,\langle n\,|\mu_\alpha|\,0\rangle)\delta(\omega-(E_n-E_0))\\&-\mathrm{Re}(\langle 0\,|\mu_\alpha|\,n\rangle\,\langle n\,|\mu_\alpha|\,0\rangle)\delta(\omega+(E_n-E_0))]\end{aligned} \tag{1.100}$$

$$\sigma(\omega)=-\frac{1}{\pi}\sum_\alpha\mathrm{Im}(\langle\!\langle\mu_\alpha;\mu_\alpha\rangle\!\rangle^{r}_{\omega}) \tag{1.101}$$

1.6.6 Relating ECD to response function

In this case, we use delta pulse of electric as a perturbation, and magnetic dipole as observable. $\langle\!\langle m_\alpha;\mu_\beta\rangle\!\rangle^{r}_{\omega}$. The rotatory strength of ECD can be written as

$$R(\omega)=\sum_n\mathrm{Im}(\langle 0\,|\mu_\alpha|\,n\rangle\,\langle n\,|m_\alpha|\,0\rangle)\delta(\omega-(E_n-E_0)) \tag{1.102}$$

The response function

$$\langle\!\langle m_\alpha;\mu_\alpha\rangle\!\rangle^{r}_{\omega}=\lim_{\eta\to 0^+}\sum_n\left[\frac{\langle 0\,|m_\alpha|\,n\rangle\,\langle n\,|\mu_\alpha|\,0\rangle}{\omega-(E_n-E_0)+i\eta}-\frac{\langle 0\,|\mu_\alpha|\,n\rangle\,\langle n\,|m_\alpha|\,0\rangle}{\omega+(E_n-E_0)+i\eta}\right] \tag{1.103}$$

We defined $C_n = \langle 0 | m_\alpha | n \rangle \langle n | \mu_\alpha | 0 \rangle$ .The real part of the response function is

$$\begin{aligned}
\mathrm{Re}(\langle\langle m_\alpha; \mu_\alpha \rangle\rangle_\omega^r) = \lim_{\eta \to 0^+} \sum_n \Bigg[& \frac{\mathrm{Re}(C_n)[\omega - (E_n - E_0)] + \mathrm{Im}(C_n)\eta}{[\omega - (E_n - E_0)]^2 + (\eta)^2} \\
& - \frac{\mathrm{Re}(C_n^*)[\omega + (E_n - E_0)] + \mathrm{Im}(C_n^*)\eta}{[\omega + (E_n - E_0)]^2 + (\eta)^2} \Bigg] \\
= \lim_{\eta \to 0^+} \sum_n & \left[\frac{\mathrm{Im}(C_n)\eta}{[\omega - (E_n - E_0)]^2 + (\eta)^2} - \frac{\mathrm{Im}(C_n^*)\eta}{[\omega + (E_n - E_0)]^2 + (\eta)^2} \right] \\
= \pi \sum_n & [\mathrm{Im}(C_n)\delta(\omega - (E_n - E_0)) - \mathrm{Im}(C_n^*)\delta(\omega + (E_n - E_0)] \qquad (1.104)
\end{aligned}$$

the second line drop the real part of C_n because for real orbitals, $\langle 0 | m_\alpha | n \rangle$ is real and $\langle n | m_\alpha | 0 \rangle$ is pure imaginary, so $Re(C_n) = 0$. So

$$R(\omega) = -\frac{1}{\pi} \sum_\alpha \mathrm{Re}(\langle\langle m_\alpha; \mu_\alpha \rangle\rangle_\omega^r) \qquad (1.105)$$

The ECD signal can be simulated from the magnetic dipole-electric dipole resoponse function.

Chapter 2

GENERALIZED HARTREE-FOCK WITH A NON-PERTURBATIVE TREATMENT OF STRONG MAGNETIC FIELDS: APPLICATION TO MOLECULAR SPIN PHASE TRANSITIONS

In this chapter, we present a framework of an *ab initio* variational approach to effectively explore electronic spin phase transitions in molecular systems inside a homogenous magnetic field. In order to capture this phenomenon, the Complex generalized Hartree-Fock ($\mathbb{C}$-GHF) method is used in the spinor formalism with London orbitals. Recursive algorithms for computing the one- and two-electron integrals of London orbitals are also provided. A Pauli matrix representation of the $\mathbb{C}$-GHF method is introduced to separate spin contributions from the scalar part of the Fock matrix. Next, spin phase transitions in two different molecular systems are investigated in the presence of a strong magnetic field. Non-collinear spin configurations are observed during the spin phase transitions in H_2 and a di-Chromium complex, $[(H_3N)_4Cr(OH)_2Cr(NH_3)_4]^{4+}$, with an increase in magnetic field strength. The competing driving forces of exchange coupling and the spin Zeeman effect have been shown to govern the spin phase transition and its transition rate. Additionally, the energetic contributions of the spin Zeeman, orbital Zeeman, and diamagnetic terms to the potential energy surface are also analyzed. The work in this chapter is adapted with permission from S. Sun, D. Williams-Young, T. F. Stetina, and X. Li. Generalized hartree-fock with non-perturbative treatment of strong magnetic field: Application to molecular spin phasetransition. *J. Chem. Theory Comput.*, 15:348–356, 2019.

2.1 Introduction

Electron spin is a fundamental physical property that is important to a wide array of science and technological applications such as energy storage, quantum computing, and chemical catalysis. An atomic or molecular system has a spin-dependent many-electron response that can be perturbed by an external electromagnetic field. Although effective model Hamiltonians with perturbative treatments of external fields [47, 106, 108, 125] have their merits, they are limited in their description of spin-dependent processes in the strong perturbation limit. While molecular response to external electric fields has been a subject of extensive theoretical work, computational frameworks for modeling finite magnetic field effects have been lagging behind mainly due to three challenges; the gauge-origin problem, spin non-collinearity, and necessity of complex arithmetic.

For many-atom systems, electronic structure calculations in the presence of electromagnetic fields become dependent on the choice of the gauge-origin, mainly due to the basis set incompleteness of Gaussian type orbitals. [22, 29, 30, 38, 59, 84, 90, 127] Among various approaches to correct for the gauge-origin problem, electronic structure methods using London type orbitals [23, 101] provide the most satisfactory solution. [4, 10, 56–58, 80, 167] London orbitals are constructed from conventional atomic orbitals dressed by a complex phase factor that depends on the external vector potential, and are considered physically appropriate for modeling chemical systems in an external magnetic field. [59]

In the non-perturbative limit, such as in the presence of a strong magnetic field, variational treatment of the electronic structure using London orbitals is required. [1, 71, 83] For this purpose, Helgaker and coworkers have made algorithmic advances for evaluating one- and two-electron integrals using London orbitals, and applied a variational approach to study molecules in strong magnetic fields within the spin collinear framework at the level of Hartree-Fock [155, 156], coupled cluster [146], configuration interaction, [87] density functional theory, and current density functional theory. [35, 36, 157] While the electronic characteristics of spin states in a magnetic field can be obtained using a variational spin-

collinear method, the spin phase transition process, *e.g.*, from singlet to triplet, driven by a static magnetic field requires a spin-noncollinear treatment.

It is well known that certain symmetry breaking, such as an external static magnetic field breaking time reversal symmetry and geometric frustration breaking continuous translation symmetry, will cause noncollinear spin configurations to arise. [2, 34, 40, 45, 129] Thus, a proper description of spin processes must come from a solution of the first-principles spin-dependent Hamiltonian that allows a variational treatment of non-collinear spin. The generalized Hartree-Fock (GHF) method removes the spin collinear constraint from conventional restricted and unrestricted Hartree-Fock (RHF and UHF) methods so that spins are allowed to rotate freely in a non-collinear framework. A detailed history of the early GHF method can be found in Reference 102 and we refer readers to a recent review [40] on non-collinear spin. The GHF approach has been shown to be a convenient and inexpensive computational platform to simulate spin dynamics of a single spin center in a static magnetic field [20] and in a dissociated reaction. [21]

In this work, we introduce a variational spin non-collinear approach using the complex GHF ($\mathbb{C}$-GHF) method with London orbitals in the presence of a strong magnetic field. The method implemented herein is able to model both spin-collinear and noncollinear phenomena as well as the processes underlying the magnetic field induced spin phase transition. Note that during the preparation of this manuscript, a variational GHF approach has been applied to studies of orbital and spin effects in molecules subject to non-uniform magnetic fields. [131]

2.2 Methodology

2.2.1 Spinor Formalism of Generalized Hartree-Fock with London Orbitals

In order to treat non-collinear spins in a non-perturbative magnetic field, one needs to retain the full vector form of the magnetization $\mathbf{m}(\mathbf{r})$ and allow each spin quantization axis to rotate. This is equivalent to writing the spin orbitals as a superposition of the spin-up and spin-down manifolds. For Hartree-Fock, this leads to the generalized Hartree-Fock (GHF)

method, [20, 34, 40, 41, 102, 129, 148, 169] which is similar in structure to the wave function used in two-component relativistic models. [27, 28, 64, 86, 98, 100, 116–118, 164]

The spinor orbital is defined as

$$\psi_j(\mathbf{r}) = \begin{pmatrix} \phi_j^{\alpha}(\mathbf{r}) \\ \phi_j^{\beta}(\mathbf{r}) \end{pmatrix} \tag{2.1}$$

The spatial functions $\{\phi_j^{\alpha}(\mathbf{r}, \mathbf{k}_A)\}$, $\{\phi_j^{\beta}(\mathbf{r}, \mathbf{k}_A)\}$ are expanded in terms of a common set of complex London orbitals $\{\tilde{\chi}_\mu(\mathbf{r}, \mathbf{k}_A)\}$,

$$\phi_j^{\alpha}(\mathbf{r}, \mathbf{k}_A) = \sum_{\mu} C_{\mu j}^{\alpha} \tilde{\chi}_\mu(\mathbf{r}, \mathbf{k}_A) \tag{2.2}$$

$$\phi_j^{\beta}(\mathbf{r}, \mathbf{k}_A) = \sum_{\mu} C_{\mu j}^{\beta} \tilde{\chi}_\mu(\mathbf{r}, \mathbf{k}_A) \tag{2.3}$$

$$\tilde{\chi}_\mu(\mathbf{r}, \mathbf{k}_A) = \chi_\mu(\mathbf{r} - \mathbf{R}_A) e^{i\mathbf{k}_A \cdot (\mathbf{r} - \mathbf{R}_A)} \tag{2.4}$$

where $\{\chi_\mu(\mathbf{r} - \mathbf{R}_A)\}$ are real atomic orbital (AO) basis functions centered at $\mathbf{R}_A$. The exponential form of the London orbital phase factor defines the local gauge origin at each nuclear center in the presence of magnetic field with a plane wave vector described by $\mathbf{k}_A = \frac{\mathbf{R}_A \times \mathbf{B}}{2}$, where $\mathbf{B}$ is the external magnetic field.

In the spinor orbital basis defined in Eq. (2.1), the Fock matrix ($\mathbf{F}$) and the density matrix ($\mathbf{P}$ with $P_{\mu\nu}^{\sigma\sigma'} = \sum_j^{\text{occ}} C_{\mu j}^{\sigma} C_{\nu j}^{\sigma' *}$) have a spin-blocked form, [20] shown in Eq. (2.5)

$$\mathbf{X} = \begin{pmatrix} \mathbf{X}^{\alpha\alpha} & \mathbf{X}^{\alpha\beta} \\ \mathbf{X}^{\beta\alpha} & \mathbf{X}^{\beta\beta} \end{pmatrix}, \quad \mathbf{X} \in \{\mathbf{F}, \mathbf{P}\} \tag{2.5}$$

In the current implementation, we cast the rank-2 spin-blocked $\mathbf{F}$ and $\mathbf{P}$ matrices in the

Pauli matrix basis, [118]

$$\mathbf{F} = \sum_{n=0}^{3} \mathbf{F}_n \otimes \boldsymbol{\sigma}_n \tag{2.6}$$

$$\mathbf{P} = \sum_{n=0}^{3} \mathbf{P}_n \otimes \boldsymbol{\sigma}_n \tag{2.7}$$

$$\boldsymbol{\sigma}_0 = \begin{pmatrix} 1 & 0 \\ 0 & 1 \end{pmatrix}, \boldsymbol{\sigma}_1 = \begin{pmatrix} 0 & 1 \\ 1 & 0 \end{pmatrix}, \boldsymbol{\sigma}_2 = \begin{pmatrix} 0 & -i \\ i & 0 \end{pmatrix}, \boldsymbol{\sigma}_3 = \begin{pmatrix} 1 & 0 \\ 0 & -1 \end{pmatrix}$$

where the scalar ($\mathbf{F}_0$) and spin part ($\mathbf{F}_1, \mathbf{F}_2, \mathbf{F}_3$) of Fock matrix are defined as [118]

$$\mathbf{F}_0 = \mathbf{h}_0 + \mathbf{J}[\mathbf{P}_0] + \mathbf{K}[\mathbf{P}_0], \tag{2.8}$$

$$\mathbf{F}_n = \mathbf{h}_n + \mathbf{K}[\mathbf{P}_n], \quad n = 1, 2, 3. \tag{2.9}$$

The Coulomb ($\mathbf{J}$) and exchange ($\mathbf{K}$) matrices are,

$$J_{\mu\nu}[\mathbf{P}_0] = \sum_{\lambda\kappa} (\mu\nu|\kappa\lambda) P_{0,\lambda\kappa} \tag{2.10}$$

$$K_{\mu\nu}[\mathbf{P}_n] = \sum_{\lambda\kappa} (\mu\lambda|\kappa\nu) P_{n,\lambda\kappa}, \quad n = 0, 1, 2, 3 \tag{2.11}$$

where

$$(\mu\nu|\kappa\lambda) = \int \mathrm{d}^3\mathbf{r}_1 \int \mathrm{d}^3\mathbf{r}_2 \frac{\tilde{\chi}^*_\mu(\mathbf{r}_1, \mathbf{k}_A)\tilde{\chi}_\nu(\mathbf{r}_1, \mathbf{k}_B)\tilde{\chi}^*_\kappa(\mathbf{r}_2, \mathbf{k}_C)\tilde{\chi}_\lambda(\mathbf{r}_2, \mathbf{k}_D)}{|\mathbf{r}_1 - \mathbf{r}_2|} \tag{2.12}$$

are the electron repulsion integrals (ERIs). Note that since ERIs using London orbitals are complex valued, they only have a four-fold symmetry instead of eight, as in the case of real-valued ERIs,

$$(\mu\nu|\kappa\lambda) = (\kappa\lambda|\mu\nu) = (\nu\mu|\lambda\kappa)^* = (\lambda\kappa|\nu\mu)^* \tag{2.13}$$

2.2.2 The Non-Relativistic Hamiltonian in the Presence of a Static and Uniform Magnetic Field

In the non-relativistic framework, the interaction of an electron spin with external electromagnetic field is described by the Schrödinger-Pauli Hamiltonian:

$$\hat{h}^{\text{Pauli}} = \frac{1}{2}\left[\boldsymbol{\sigma}\cdot(\mathbf{p}+\mathbf{A})\right]^2 - \hat{U} \tag{2.14}$$

where $\mathbf{A}$ and $\hat{U}$ are the vector potential and scalar potential of the electromagnetic field, respectively. $\mathbf{p} = -i\boldsymbol{\nabla}$ is the momentum operator. Given the relationship between the vector potential and the magnetic field, $\mathbf{A} = \frac{1}{2}\mathbf{B}\times\mathbf{r}$, the one-electron Pauli Hamiltonian can be written as

$$h^{\text{Pauli}} = \hat{h}_0(\mathbf{r}) + \frac{1}{2}(\boldsymbol{\sigma} - i\mathbf{r}\times\boldsymbol{\nabla})\cdot\mathbf{B} + \frac{1}{8}(\mathbf{B}\times\mathbf{r})^2 \tag{2.15}$$

where $\hat{h}_0(\mathbf{r})$ is the field-free one-electron Hamiltonian. The second term includes spin and orbital Zeeman contributions. The third term is the diamagnetic contribution and is quadratic in the strength of magnetic field, which can be expanded as

$$\begin{aligned}(\mathbf{B}\times\mathbf{r})^2 =& (B_y^2+B_z^2)x^2 + (B_x^2+B_z^2)y^2 + (B_x^2+B_y^2)z^2 \\ &- 2B_xB_yxy - 2B_yB_zyz - 2B_xB_zxz\end{aligned} \tag{2.16}$$

The orbital Zeeman and the diamagnetic term do not directly contribute to the spin dynamics. [20] Although these two terms are relatively small, they are important contributions in diamagnetism. [49, 50, 120, 121] In the presence of a strong magnetic field, these two terms account for significant contributions to the interaction between the chemical system and the external field. [155]

Using the formalism of generalized Hartree-Fock in the Pauli matrix basis (Eq. (2.6)), spin contributions in Eq. (2.14) can be separated from the scalar part. The resulting scalar

Fock matrix is

$$\begin{aligned}\mathbf{F}_0 =&\mathbf{h}_0 + \mathbf{J}[\mathbf{P}_0] + \mathbf{K}[\mathbf{P}_0] - \frac{i}{2}\mathbf{L}\cdot\mathbf{B} + \frac{1}{8}\big\{(B_y^2+B_z^2)\mathbf{q}_{xx} + (B_x^2+B_z^2)\mathbf{q}_{yy} + (B_x^2+B_y^2)\mathbf{q}_{zz} \\ &- 2B_xB_y\mathbf{q}_{xy} - 2B_yB_z\mathbf{q}_{yz} - 2B_xB_z\mathbf{q}_{xz}\big\} \end{aligned} \tag{2.17}$$

where $\mathbf{L}_{\mu\nu} = \langle\tilde{\chi}_\mu|\mathbf{r}\times\boldsymbol{\nabla}|\tilde{\chi}_\nu\rangle$ is the orbital-angular momentum integral , and $(\mathbf{q}_{nm})_{\mu\nu} = \langle\tilde{\chi}_\mu|\hat{r}_n\hat{r}_m|\tilde{\chi}_\nu\rangle$ is the electric quadrupole integral. After spin separation using the Pauli matrices, spin components of the Fock matrix are

$$\mathbf{F}_n = \frac{1}{2}B_n\mathbf{S} + \mathbf{K}[\mathbf{P}_n], \quad n = 1,2,3. \tag{2.18}$$

where $\mathbf{S}$ is the overlap matrix.

2.2.3 Electron Integrals using London Type Orbitals

The electronic structure method introduced in this work requires the computation of one- and two-electron integrals of London orbitals. Integrals are evaluated in complex arithmetic, and corresponding recursion relationships are presented in the Appendix. In the current work, one- and two-electron integrals of London orbitals and the complex generalized Hartree-Fock method are implemented in the Chronus Quantum software package. [94]

2.3 Results and Discussion

The formalism of generalized Hartree-Fock in the spinor basis allows for calculations of non-collinear spin states within the *ab initio* framework. With the atomic London orbitals and associated one- and two-electron integrals, wave functions of chemical systems with multi-spin-centers in the presence of a static magnetic field can be variationally optimized. In this current work, we study the spin noncollinearity and magnetic phase transition of molecular systems driven by static magnetic fields. All $\mathbb{C}$-GHF calculations are done using the Chronus Quantum software package.

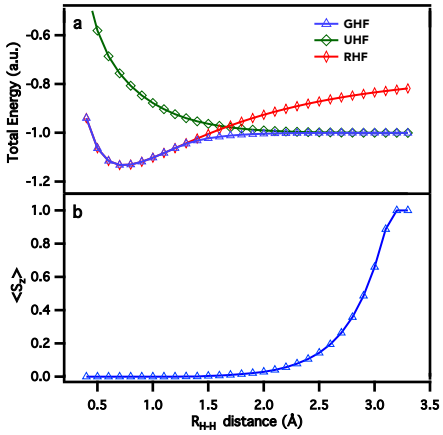

Figure 2.1. (**a**): The potential energy surface of an H_2 molecule in a homogenous magnetic field, $|B_z| = 0.001$ a.u. along the $-z$ direction. (**b**): The expectation value of S_z of the $\mathbb{C}$-GHF solution.

The first test case is a H_2 molecule in a uniform magnetic field. $\mathbb{C}$-GHF solutions in the presence of a static magnetic field were obtained with several different basis sets, including 6-31G, 6-31G(d,p), aug-cc-pVDZ, and aug-cc-pVTZ. Although differences in the absolute energy computed with different basis sets are noticeable, the expectation values of S_z at a given magnetic field only differ by less than 3%. In the following discussion, we will only present the results computed at the $\mathbb{C}$-GHF/aug-cc-pVTZ level of theory. [24] In this test system, the static magnetic field (1 a.u. $\approx 2.35\times10^5$ T, based on SI units for magnetic field) is aligned perpendicular to the molecular axis. Figure 2.1 plots the potential energy curve of an H_2 molecule in a uniform magnetic field ($|B_z| = 0.001$ a.u. along the $-z$ direction) computed using the complex generalized Hartree-Fock ($\mathbb{C}$-GHF), complex unrestricted Hartree-Fock ($\mathbb{C}$-UHF), and complex restricted Hartree-Fock ($\mathbb{C}$-RHF) with London orbitals. $\mathbb{C}$-UHF and $\mathbb{C}$-RHF calculations are restricted to spin triplet ($S_z = 1$) and singlet ($S_z = 0$) states, respectively. The $\mathbb{C}$-GHF solution is not spin restricted. As a result, at all bond distances, the $\mathbb{C}$-GHF solution is always the lowest in energy.

From the equilibrium bond length toward the asymptotic dissociation limit, the change in $\langle S_z \rangle$ of the $\mathbb{C}$-GHF solution suggests that the system undergoes a spin phase transition from

$\langle S_z \rangle = 0$ to 1. This spin phase transition is a result of the competing driving forces of the exchange coupling and paramagnetism. This can be understood from the perturbative and phenomenological spin Hamiltonian including both the spin exchange coupling and Zeeman effect,

$$H = -\frac{1}{2} J_{12} \mathbf{S}_1 \cdot \mathbf{S}_2 - g\mu_B \mathbf{B} \cdot (\mathbf{S}_1 + \mathbf{S}_2) \tag{2.19}$$

$$= -\frac{1}{2} J_{12} |\mathbf{S}_1||\mathbf{S}_2| \cos(\theta) - g\mu_B B_z (S_{1z} + S_{2z}) \tag{2.20}$$

where J_{12} is the exchange coupling strength, g is the spin g-factor, and μ_B is the Bohr magneton. For a non-collinear spin alignment in the presence of a static magnetic field in the z direction depicted in Fig. 2.2, the spin Hamiltonian can be written as in Eq. (2.20), with the angle between the two spin vectors defined as θ. In the collinear spin electronic structure framework, such as RHF and UHF, θ can only be 0° or 180°. Without spin-orbit coupling, the exchange coupling is isotropic.

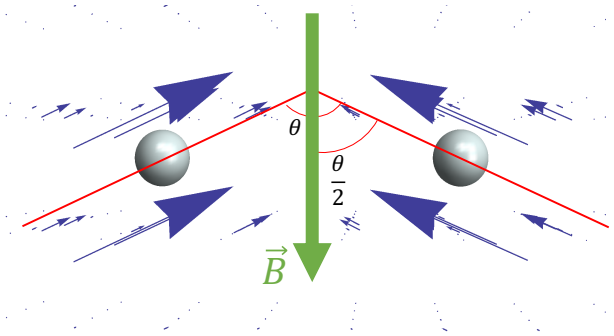

Figure 2.2. Illustration of non-collinearity of two spin vectors.

At the equilibrium bond distance, the exchange coupling is much stronger than the Zeeman term, giving rise to the antiparallel orientation of the two electrons, *i.e.*, a closed-shell configuration and $\theta = 180°$. As the bond length increases, the exchange coupling decreases exponentially, whereas the strength of the Zeeman effect remains constant. At certain bond lengths when the exchange coupling becomes weaker than the Zeeman term, the electronic

system undergoes a spin phase transition. This spin phase transition is a non-collinear process where θ can take on any value between 0° and 180°, and the non-collinear spin state has the lowest energy. In this regime, only the non-collinear ℂ-GHF can describe the electronic characteristics of the spin system.

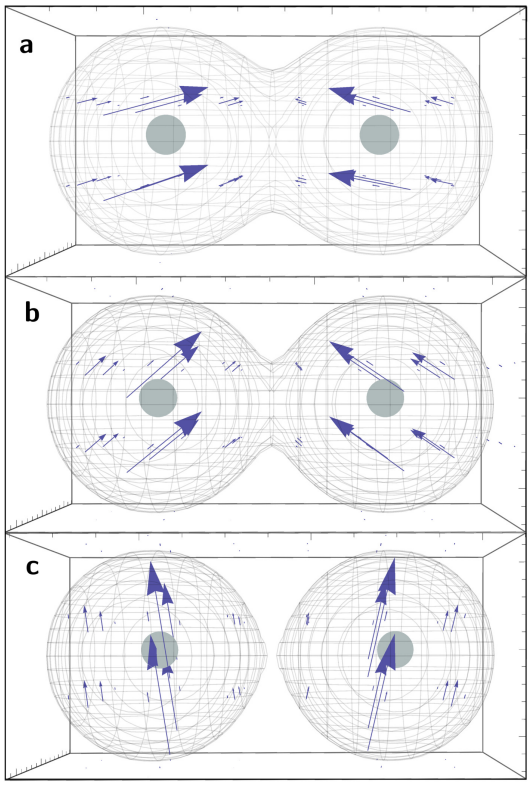

Figure 2.3. Spin magnetization vector at different H-H bond lengths. (**a**): R_{HH} = 2.6 Å, $\langle S_z \rangle$ =0.19428, (**b**): R_{HH} = 2.9 Å, $\langle S_z \rangle$ =0.48588, and (**c**): R_{HH} = 3.1 Å, $\langle S_z \rangle$ =0.88685. For all cases, the magnetic field strength is 0.001 a.u. along the $-z$ direction. The area enclosed by the mesh has a charge density > 0.002. The size of the 3D box is 550pm(W) × 300pm(H) × 300pm(D).

Figure 2.3 shows the progression of spin vectors during the spin phase transition when the bond length is stretched from 2.6 to 3.1 Å, while keeping the magnetic field strength constant, $|B_z| = 0.001$ a.u., along the $-z$ direction. When a non-zero $\langle S_z \rangle$ moment is obtained in the system, the overall spin vector is aligned opposite to the magnetic field arising from the spin

Zeeman effect. As the spins undergo a phase transition, the angle between local spin vectors decreases from 180° to 0°. At $R_{HH} \sim 2.9$ Å (Fig. 2.3b) the two local spin vectors are nearly orthogonal, exhibiting a strong non-collinearity in the presence of a magnetic field. The UHF and RHF solutions are restricted by collinear spin configuration, and therefore, can not capture the progression of spin phase transition via the spin noncollinear configuration.

The framework of $\mathbb{C}$-GHF with London orbitals also allows for a variational exploration of critical magnetic field strengths that can induce a spin phase transition in molecular systems. Figure 2.4 plots the spin magnetization vector at different field strengths while keeping the bond length fixed at 2.6 Å. As the magnetic field gets stronger, the expectation value of S_z becomes greater, and a non-collinear spin phase transition is observed. In contrast to the phenomenon in Fig. 2.3 where bond stretching weakens the exchange coupling, the spin phase transition in Fig. 2.4 arises from the increasing strength of the spin Zeeman effect, due to the increase in magnetic field strength. At $|B_z| = 0.005$ a.u., the spin phase transition is already complete, and the triplet spin-collinear configuration is the lowest energy state.

Figure 2.5 plots the expectation value of S_z as a function of H-H bond length and magnetic field strength. Figure 2.5 suggests that the rate of the spin phase transition sensitively depends on the strength of exchange coupling and spin Zeeman terms. At near the equilibrium bond distance with the strongest magnetic field ($|B_z| = 0.3$ a.u.) considered here, the spin configuration switches almost immediately. In the weak field or weak exchange coupling regime, spins can be seen to undergo a much slower phase transition compared to those in the strong field or strong exchange coupling regime.

Although the orbital Zeeman and diamagnetic terms in Eq. (15) do not directly modify the spin interaction with the external magnetic field, they are important contributions to the stability of molecular system in magnetic field and can indirectly influence spin dynamics through perturbing the spatial extent and energetics of molecular orbitals. [87] Figure 2.6 shows the magnitudes of spin Zeeman, orbital Zeeman, and diamagnetic contributions to the total potential energy. In the strong exchange couple regime ($R_{HH} \sim 0.4 - 0.6$ Å), the diamagnetic term has the largest contribution, followed by the orbital Zeeman term. These

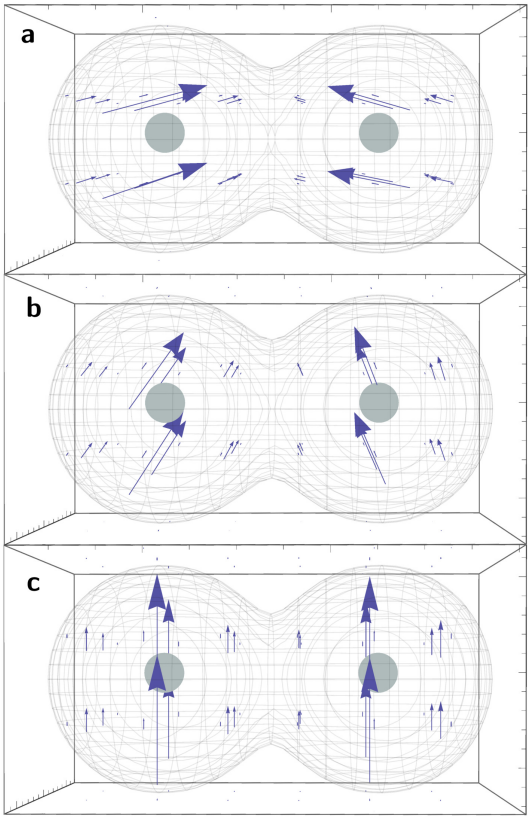

Figure 2.4. Spin magnetization vectors for H_2 at different field strengths. (**a**): $|B_z| = 0.001$ a.u., $\langle S_z \rangle$ =0.19428, (**b**): $|B_z| = 0.003$ a.u., $\langle S_z \rangle$ =0.59040, and (**c**): $|B_z| = 0.005$ a.u., $\langle S_z \rangle = 1.0000$. The H-H bond length is $R_{HH} = 2.6$ Å. The area enclosed by the mesh has a charge density > 0.002. The size of the 3D box is 550pm(W) $\times$ 300pm(H) $\times$ 300pm(D).

two terms are different in sign with the diamagnetic term destabilizing the system energy with respect to the field-free molecular system. In this regime, the system takes on a closed-shell configuration. As a result, the spin Zeeman contribution is zero. As the system undergoes a spin phase transition, the non-zero overall spin vector gives rise to an increasing spin Zeeman contribution that significantly stabilizes the molecular system. Analysis of Fig. 2.6 suggests that in a closed-shell configuration, orbital Zeeman and diamagnetic contributions are responsible for the interaction between the electronic system and the external magnetic field. In an open-shell system, the spin Zeeman is the dominant driving force underlying the

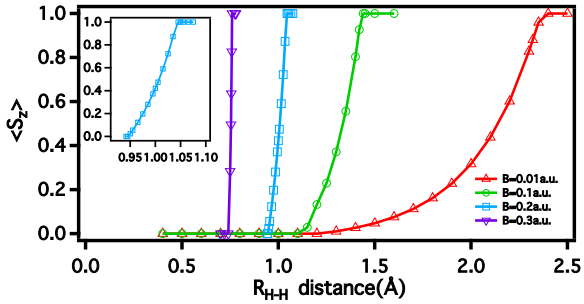

Figure 2.5. $\langle S_z \rangle$ as a function of H-H bond length and magnetic field strength.

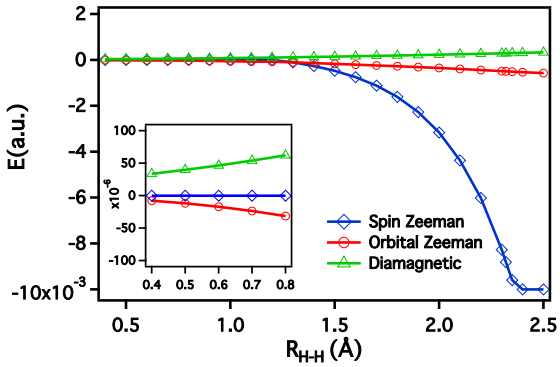

Figure 2.6. Energetic contributions of spin Zeeman, orbital Zeeman, and diamagnetic terms. $|B_z| = 0.01$ a.u.

system-magnetic-field interaction in the weak field regime. As the field strength increases, the diamagnetic term becomes non-negligible as it increases quadratically with respect to the field.

In order to probe the spin phase transition in a more complex magnetic molecular system, we study the spin characteristics of a di-chromium molecular complex, $[(H_3N)_4Cr(OH)_2Cr(NH_3)_4]^{4+}$, in a uniform magnetic field. Figure 2.7 illustrates the molecular structure and computational setup where the magnetic field is applied in $+z$ direction, perpendicular to the Cr-O-Cr-O plane. The molecular geometry was optimized [91] with the GAUSSIAN16 software package [32] at the B3LYP/6-31G level of theory. [9, 88, 144, 163] The electronic structures in

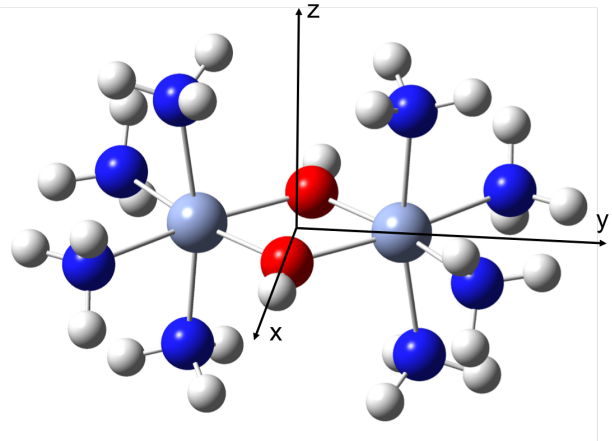

Figure 2.7. The molecular structure of a di-chromium molecular complex, $[(H_3N)_4Cr(OH)_2Cr(NH_3)_4]^{4+}$ that has D_{2h} symmetry. Each Cr atom is in a distorted octahedral coordination environment. The magnetic field is applied in the $+z$ direction, perpendicular to the Cr-O-Cr-O plane.

a magnetic field were calculated using ℂ-GHF with 6-31G London atomic orbitals in the Chronus Quantum software package.

In the di-Cr(III) molecular complex, the octahedral ligand field splits Cr d orbitals into e and t_2 sets where three unpaired electrons occupy the t_2 manifold (Fig. 2.8b). In contrast to the previous molecular H_2 system where the ground state at equilibrium bond length is in a non-magnetic closed-shell configuration, the ground state of the di-Cr(III) molecular complex exhibits a magnetic ℂ-GHF solution. Cr(III) cations in an octahedral coordination environment bridged by oxygen atoms are known to have antiferromagnetic super-exchange coupling. [18, 19, 46] The J constant in Eq. (2.20) for super-exchange coupling is negative in sign, favoring the antiferromagnetic spin alignment in the ground state ($\langle S_z \rangle = 0$, see Fig. 2.8b). The lack of electron correlation in Hartree-Fock calculation gives rise to an overestimation of the J constant magnitude because the correlation effect has an opposite contribution to the magnetism. [46] Nevertheless, qualitative characteristics and trends of spin phase transitions can still be captured by ℂ-GHF calculations with London atomic orbitals.

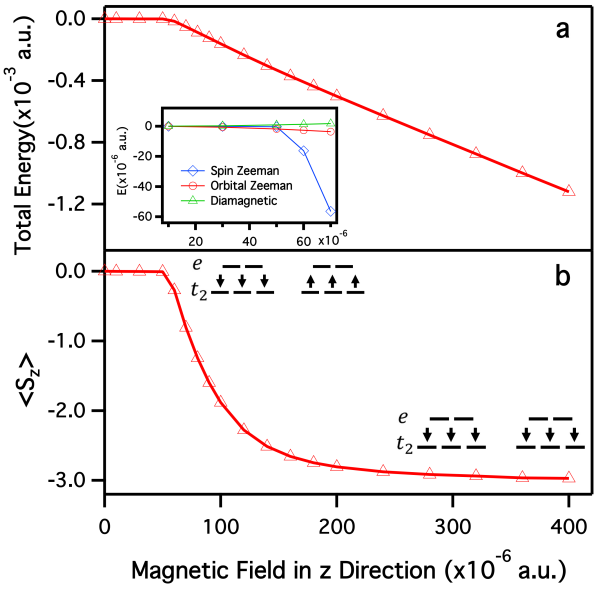

Figure 2.8. (**a**) Total energy of di-Cr(III) complex in a finite magnetic field. (**b**) The expectation value of S_z of the $\mathbb{C}$-GHF solution.

In the absence of an external magnetic field, the ground state wave function of the di-Cr(III) molecular complex obtained from the $\mathbb{C}$-GHF calculation is antiferromagnetic. Figure 2.8 plots the relative total energy compared to that in the absence of a magnetic field and the expectation value of S_z as a function of applied magnetic field strength. When the magnetic field is relatively weak, the system is in the antiferromagnetic state. In this region, the super-exchange coupling is constant and the small energy change is solely due to the orbital Zeeman and diamagnetic terms. As the magnetic field reaches a critical point ($\sim 60 \times 10^{-6}$ a.u.) where a small change in spin alignment can give rise to a spin Zeeman term strong enough to overcome the antiferromagnetic super-exchange coupling, the system starts to undergo a spin phase transition. As the magnetic field strength increases, the energy of the molecule decreases due to the increasing spin Zeeman contribution. The change of expectation value of S_z indicates that the spin state gradually switches from the antiferromagnetic $\langle S_z \rangle = 0$ to ferromagnetic $\langle S_z \rangle = -3$ configuration (Fig. 2.8b). This

case study suggests that ℂ-GHF calculations with London atomic orbitals can be used to investigate magnetic phase transitions in transition metal complexes.

2.4 Conclusion

Presented in this article is a framework of *ab initio* variational approach using complex generalized Hartree-Fock (ℂ-GHF) with London orbitals to effectively explore the spin phase space in the presence of a homogenous magnetic field. We introduced the implementation of the ℂ-GHF approach within the spinor formalism. In order to account for gauge origin-independence in the self-consistent field, the ℂ-GHF is represented in the London orbital basis with a magnetic field complex phase factor. Recursive algorithms for computing one- and two-electron integrals of London orbitals are provided in the Appendix. Additionally, a Pauli matrix representation of the ℂ-GHF is introduced in this work that allows for the separation of spin contributions from the scalar part of the Fock matrix.

ℂ-GHF with London orbitals in the presence of a homogenous magnetic field has been applied to study the spin phase transition in a molecular H_2 system. Non-collinear spin configurations have been observed during the phase transition from a singlet to triplet state. The competing driving forces of exchange coupling and the spin Zeeman effect have been shown to govern the spin phase transition and its transition rate. In addition, energetic analysis suggests that in the presence of a static magnetic field, orbital Zeeman and diamagnetic terms are important contributions in a closed-shell configuration, while the spin Zeeman term is the dominant interaction driving force in an open-shell state.

The variational ℂ-GHF method with London orbitals can also be used to compute magnetic phase transitions in molecular complexes driven by an external magnetic field. Results show that there exists a critical point where the spin Zeeman is large enough to compete with the super-exchange coupling so that the spin phase transition takes place and drives the magnetic phase transition.

The method presented in this work is based on the single Slater determinant wave function ansatz which lacks important electron correlation effects. Future developments will use the

variational $\mathbb{C}$-GHF reference for correlated electronic structure methods which will provide more accurate descriptions of spin and magnetic phase transitions.

Chapter 3

AN AB INITIO LINEAR RESPONSE METHOD FOR COMPUTING MAGNETIC CIRCULAR DICHROISM SPECTRA WITH NON-PERTURBATIVE TREATMENT OF MAGNETIC FIELD

Magnetic circular dichroism (MCD) experiments provide a sensitive tool for exploring geometric, magnetic, and electronic properties of chemical complexes and condensed matter systems. They are also challenging to simulate because of the need to simultaneously treat the perturbations of a finite magnetic field as well as an optical field. In this work, we introduce an *ab initio* approach that treats external magnetic field non-perturbatively with London orbitals for simulating the MCD spectra of closed-shell systems. Effects of a magnetic field are included variationally in the spin-free non-relativistic Hamiltonian, followed by a linear response formalism to directly calculate the difference in absorption between the left and right circularly polarized light. In addition to the presentation of underlying mathematical formalism and implementation, the method developed in this paper has been applied to simulations of MCD spectra of the sodium anion, 2,2,6,6-tetramethylcyclohexanone, and 3-methyl-2-hexanone. Results are discussed and compared to experiments. The work in this chapter is adapted with permission from S. Sun, D. Williams-Young, and X. Li. An Ab Initio Linear Response Method for Computing Magnetic Circular Dichroism Spectra with Non-Perturbative Treatment of Magnetic Field. *J. Chem. Theory Comput.*, 15:3162-3169, 2019.

3.1 Introduction

Magnetic circular dichroism (MCD) is an important class of magneto-optical spectroscopy in which the probing field is a circularly polarized optical light in the presence of a static

magnetic field. [6] The application of a magnetic field couples the (spin and/or orbital) angular momentum of the system to the field. This affects both the positions and intensities of peaks in the electronic spectrum: the former due to an energy shift of each electronic state, and the latter due to perturbations to the wavefunction. This often leads to a breaking of degeneracies and allows for the in-depth spectroscopic study of the fine structure of material systems. Excitingly, because optically active ("bright") and inactive ("dark") states can be coupled together, spectroscopic methods performed in a magnetic field can probe quantum states that are otherwise inaccessible at zero field. Because MCD experiments provide a sensitive tool for exploring geometric, magnetic, and electronic properties of chemical complexes and condensed matter systems, they are widely used in chemistry, biology, and materials research.

Interpreting and understanding MCD spectra has been traditionally based on the first-order perturbative model, [11, 73, 103, 119, 143]

$$\frac{\Delta A'}{\mathscr{E}} = \Gamma \mu_B B \sum_J \left[\mathscr{A}_J \left(-\frac{\partial f(\hbar\omega - \hbar\omega_{0J})}{\partial \hbar\omega} \right) + \left(\mathscr{B}_J + \frac{\mathscr{C}_J}{kT} \right) f(\hbar\omega - \hbar\omega_{0J}) \right] \tag{3.1}$$

$\mathscr{A}_J$ term, which has a derivative band-shape, arises when the degenerate excited states are split due to Zeeman effect. Perturbation of the transition dipole gives rise to $\mathscr{B}_J$ term, which is the most common effect in MCD. The $\mathscr{C}_J$ term is modulated by the Boltzmann distribution of the ground state when degenerate ground states are split by Zeeman effects. The $\mathscr{B}_J$ term is relatively weak compared to the $\mathscr{A}_J$ and $\mathscr{C}_J$ terms, as such it will only be obvious when there are no $\mathscr{A}_J$ and $\mathscr{C}_J$ term contributions, *e.g.*, in a low symmetry closed shell molecule.

Over the past two decades, there have been many successful developments to compute MCD spectra in the perturbative regime, including single residue of the quadratic response function; [17] the complex polarization propagator method; [82, 141, 142] a sum-over-states expression using truncated configuration interaction, with perturbative treatment of the magnetic field and spin-orbit coupling; [61, 62] magnetically perturbed time-dependent den-

sity functional theory (TDDFT); [133,134,137] and multi-configurational self-consistent-field with quasi-degenerate perturbation theory to include Zeeman effects with spin-couplings. [37, 39, 55] In addition, solvent effects on MCD spectra are also considered. [72, 140] Using London orbitals to remove the gauge-dependence of finite atom-centered basis set has been applied in the perturbative calculations of MCD at the level of coupled-cluster, [16, 74] Hartree-Fock, and DFT. [75, 81]

To the best of our knowledge, there are only two approaches to compute the MCD terms with *variational* treatment of magnetic field. Linderberg and coworkers used the random-phase-approximation (RPA) in the presence of a static magnetic field with semi-empirical evaluation of London orbital integrals to simulate the MCD $\mathscr{B}$ term [128]. Bertsch and coworkers included the orbital Zeeman effect in the local-density-approximation (LDA) using RT–TDDFT integrated over a spatial grid to simulate $\mathscr{A}$- and $\mathscr{B}$-term contributions. [89]

For many-atom systems, electronic structure calculations in the presence of electromagnetic fields become unphysically dependent on the choice of the arbitrary gauge-origin. This is due to the use of atomic-centered orbitals, basis set incompleteness, and truncated expansion of the field-matter interaction, *i.e*, physical observables become dependent on the origin of the electromagnetic field. [22, 29, 30, 38, 59, 84, 90, 127] Among various approaches to correct for the gauge-origin problem, electronic structure methods using London type orbitals [23, 101] provide the most satisfactory solution. [4, 10, 56, 57, 80, 167]

In the perturbative treatment of magnetic field effects, explicit electron integrals of London orbitals are not necessary. However, in the non-perturbative variational approach, complex-valued London orbital integrals must be explicitly evaluated in order to remove the gauge-origin dependence. General recursion relationships for one- and two-electron integrals using London orbitals were pioneered by Helgaker and were recently implemented in the complex generalized Hartree-Fock framework. [65, 124, 131, 153, 156]

In this work, we introduce an *ab initio* approach that treats external magnetic field non-perturbatively with London orbitals for simulating MCD spectra of closed-shell systems. This method can describe $\mathscr{A}$ and $\mathscr{B}$ term contributions to the MCD spectrum in a uniform

way. Effects of a magnetic field are included variationally in the spin-free non-relativistic Hamiltonian, followed by a linear response theory to obtain the MCD spectrum using a formalism that directly computes the difference of absorption between left- and right-circularly polarized light.

3.2 Methodology

3.2.1 MCD Hamiltonian of a Closed-Shell System

In order to simulate MCD spectra, the fundamental Hamiltonian needs to address perturbations from both a static magnetic field and an oscillating optical field. In the non-relativistic framework, the interaction of an electron with external fields in an MCD experiment can be described by the following one-electron Hamiltonian. In this work, we focus on MCD spectra of closed-shell molecular systems, therefore, the spin-Zeeman contributions do not enter the Hamiltonian.

$$h = \frac{1}{2}(\mathbf{p} + \mathbf{A})^2 - U + V \tag{3.2}$$

$$= -\frac{1}{2}\boldsymbol{\nabla}^2 + \frac{1}{2}(-i\mathbf{r} \times \nabla) \cdot \mathbf{B}_M + \frac{1}{8}(\mathbf{B}_M \times \mathbf{r})^2 + \sum_A \frac{Z_A}{|\mathbf{r} - R_A|}$$

$$- U_W + \mathbf{A}_W \cdot \mathbf{p} + \frac{1}{2}\mathbf{A}_W^2 + \mathbf{A}_W \cdot \mathbf{A}_M \tag{3.3}$$

where $\mathbf{A}$ and U are the total vector potential and scalar potential of the external fields, respectively. $\mathbf{p} = -i\boldsymbol{\nabla}$ is the momentum operator and V is the nuclear attraction potential. The total vector potential $\mathbf{A}$ includes an applied static magnetic field and a probing optical field (or a plane wave), $\mathbf{A} = \mathbf{A}_M + \mathbf{A}_W$. Since $U_M = 0$ for a static magnetic field, only the scalar potential of the probing plane wave remains in Eq. (3.3). We used the relationship between the vector potential and the static magnetic field ($\mathbf{B}_M$), $\mathbf{A}_M = \frac{1}{2}\mathbf{B}_M \times \mathbf{r}$.

Using the electric-dipole approximation in the length gauge for the interaction between the system and the probing plane wave and the relationship $\mathbf{E}_W(\mathbf{r}, t) = -\boldsymbol{\nabla} U_W(\mathbf{r}, t) -$

$\frac{\partial}{\partial t}\mathbf{A}_W(\mathbf{r},t)$, the final working Hamiltonian for simulating MCD experiment is:

$$h = -\frac{1}{2}\boldsymbol{\nabla}^2 + \frac{1}{2}(-i\mathbf{r}\times\nabla)\cdot\mathbf{B}_M + \frac{1}{8}(\mathbf{B}_M\times\mathbf{r})^2 + \sum_A \frac{Z_A}{|\mathbf{r}-R_A|} - \mathbf{r}\cdot\mathbf{E}_W \tag{3.4}$$

Note that in Eq. (3.4), higher order perturbations arising from interactions between the electronic system and the probing optical field, such as the electric-quadrupole and magnetic-dipole terms, are ignored.

In the following discussion, we remove the subscript notations "M" and "W" for simplicity, however, readers should keep in mind that $\mathbf{B}$ and $\mathbf{E}$ fields originate from two different external perturbations.

The second term in Eq. (3.4) includes orbital Zeeman contributions, and the third term is the diamagnetic contribution. This is quadratic in the strength of the magnetic field, which is expanded in Eq. (2.16)

The total one-electron Hamiltonian Eq. (3.4) can be separated as $h(t) = h_0 + V(t)$, where the time-dependent perturbation, $V(t) = -\mathbf{r}\cdot\mathbf{E}(t)$, is the electric-dipole interaction, and h_0 is the time-independent reference Hamiltonian,

$$h_0 = -\frac{1}{2}\boldsymbol{\nabla}^2 + \frac{1}{2}(-i\mathbf{r}\times\nabla)\cdot\mathbf{B}_M + \frac{1}{8}(\mathbf{B}_M\times\mathbf{r})^2 + \sum_A \frac{Z_A}{|\mathbf{r}-R_A|} \tag{3.5}$$

The separation of time-dependent and time-independent contributions to the total Hamiltonian allows different procedures to treat the separate external perturbations in an MCD calculation. Instead of using perturbative treatments for both the static magnetic and oscillating optical fields, we introduce a semi-variational approach in which the wave function is variationally optimized in the presence of a static magnetic field (Sec. 3.2.2) and the response to the oscillating circularly polarized optical field is taken at the weak-field limit (Sec. 3.2.3).

3.2.2 Ground State with Variational Treatment of Magnetic Field using London Orbitals

In the numerical implementation developed in this work, the Hamiltonian is cast in an atomic basis. In restricted Hartree-Fock, the molecular orbitals $\{\phi_j(\mathbf{r})\}$ are expanded in terms of a set of complex London orbitals $\{\tilde{\chi}_\mu(\mathbf{r}, \mathbf{k}_A)\}$,

$$\phi_j(\mathbf{r}) = \sum_\mu C_{\mu j} \tilde{\chi}_\mu(\mathbf{r}, \mathbf{k}_A) \tag{3.6}$$

$$\tilde{\chi}_\mu(\mathbf{r}, \mathbf{k}_A) = \chi_\mu(\mathbf{r} - \mathbf{R}_A) e^{i\mathbf{k}_A \cdot (\mathbf{r} - \mathbf{R}_A)} \tag{3.7}$$

where $\{\chi_\mu(\mathbf{r} - \mathbf{R}_A)\}$ are real Gaussian type atomic orbital (AO) basis functions centered at $\mathbf{R}_A$. The exponential form of the London orbital phase factor defines the local gauge origin at each nuclear center in the presence of magnetic field with a plane wave vector described by $\mathbf{k}_A = \frac{\mathbf{R}_A \times \mathbf{B}}{2}$, where $\mathbf{B}$ is the external magnetic field.

The one-electron integral for any one-electron operator $\hat{O}_1$ with London orbitals can be defined as

$$O_{1,\mu\nu} = (\mu|O_1|\nu) = \int \mathrm{d}^3\mathbf{r} \tilde{\chi}^*_\mu(\mathbf{r}, \mathbf{k}_A)\, \hat{O}_1\, \tilde{\chi}_\nu(\mathbf{r}, \mathbf{k}_B) = \int \mathrm{d}^3\mathbf{r} \tilde{\chi}_\mu(\mathbf{r}, -\mathbf{k}_A)\, \hat{O}_1\, \tilde{\chi}_\nu(\mathbf{r}, \mathbf{k}_B) \tag{3.8}$$

and the electron repulsion integrals (ERIs) are,

$$(\mu\nu|\kappa\lambda) = \int \mathrm{d}^3\mathbf{r}_1 \int \mathrm{d}^3\mathbf{r}_2 \frac{\tilde{\chi}^*_\mu(\mathbf{r}_1, \mathbf{k}_A) \tilde{\chi}_\nu(\mathbf{r}_1, \mathbf{k}_B) \tilde{\chi}^*_\kappa(\mathbf{r}_2, \mathbf{k}_C) \tilde{\chi}_\lambda(\mathbf{r}_2, \mathbf{k}_D)}{|\mathbf{r}_1 - \mathbf{r}_2|} \tag{3.9}$$

In a perturbative treatment of the static magnetic field, explicit electron integrals using London orbitals with a finite field are not needed. [16, 74, 75, 81] However, for the variational approach, complex-valued London orbital integrals must be evaluated. For details on integral evaluation using London orbitals, we refer readers to Refs. 65, 153, 156. Integrals are evaluated in complex arithmetic, implemented in the Chronus Quantum software package. [94]

Using the formalism of restricted Hartree-Fock for closed-shell systems, the time-independent

Fock matrix is defined in Eq. (2.17), which can be written as,

$$\begin{aligned}\mathbf{F}_0 = \quad & \mathbf{T} + \mathbf{V} + \mathbf{J}[\mathbf{P}_0] - \frac{1}{2}\mathbf{K}[\mathbf{P}_0] - \frac{i}{2}\mathbf{L}\cdot\mathbf{B} \\ & + \frac{1}{8}\big\{(B_y^2 + B_z^2)\mathbf{q}_{xx} + (B_x^2 + B_z^2)\mathbf{q}_{yy} + (B_x^2 + B_y^2)\mathbf{q}_{zz} \\ & - 2B_xB_y\mathbf{q}_{xy} - 2B_yB_z\mathbf{q}_{yz} - 2B_xB_z\mathbf{q}_{xz}\big\} \end{aligned} \tag{3.10}$$

where $\mathbf{L}_{\mu\nu} = (\tilde{\chi}_\mu|\mathbf{r}\times\boldsymbol{\nabla}|\tilde{\chi}_\nu)$ is the orbital-angular momentum integral , and $(\mathbf{q}_{nm})_{\mu\nu} = (\tilde{\chi}_\mu|\hat{r}_n\hat{r}_m|\tilde{\chi}_\nu)$ is the electric quadrupole integral. The density matrix is defined as

$$P_{0,\mu\nu} = 2\sum_{i}^{N/2} C_{\mu i}C_{\nu i}^* \tag{3.11}$$

where N is the number of electrons.

The Coulomb ($\mathbf{J}$) and exchange ($\mathbf{K}$) matrix elements are,

$$J_{\mu\nu}[\mathbf{P}_0] = \sum_{\lambda\kappa}(\mu\nu|\kappa\lambda)P_{0,\lambda\kappa} \tag{3.12}$$

$$K_{\mu\nu}[\mathbf{P}_0] = \sum_{\lambda\kappa}(\mu\lambda|\kappa\nu)P_{0,\lambda\kappa} \tag{3.13}$$

Because the fundamental electron integrals are complex-valued, in this work, we use complex restricted Hartree-Fock ($\mathbb{C}$-RHF) as our reference. Note that since ERIs using London orbitals are complex-valued, they only have a four-fold symmetry instead of eight, as in the case of real-valued ERIs,

$$(\mu\nu|\kappa\lambda) = (\kappa\lambda|\mu\nu) = (\nu\mu|\lambda\kappa)^* = (\lambda\kappa|\nu\mu)^* \tag{3.14}$$

3.2.3 Perturbation of Left/Right Circularly Polarized Light

In this work, we only consider the electric-dipole contribution to the MCD spectrum (Eq. (3.4)). Higher order multipole moment contributions, such as electric-quadrupole and magnetic-

dipole arising from the system-light interaction, are ignored.

In an MCD experiment, the direction of magnetic field is usually made parallel to the propagation direction of incident light. Defining the direction of the incident light as γ, where γ can be $\{x, y, z\}$, the circularly polarized dipoles are

$$\mu_\gamma^- = \frac{1}{\sqrt{2}}(\mu_\alpha - i\mu_\beta) \tag{3.15}$$

$$\mu_\gamma^+ = \frac{1}{\sqrt{2}}(\mu_\alpha + i\mu_\beta) \tag{3.16}$$

where $\{\alpha, \beta, \gamma\} \equiv \{x, y, z\}$, $\{y, z, x\}$ or $\{z, x, y\}$, following the right hand rule. The difference of absorbance between left- and right-polarized light per photon energy can be written as

$$\frac{\Delta A'}{\mathscr{E}} = \frac{\epsilon'_- - \epsilon'_+}{\mathscr{E}} d\ l = \Gamma \sum_J \sum_\gamma \frac{1}{3}(|\left\langle 0 \left| \mu_\gamma^- \right| J \right\rangle'|^2 - |\left\langle 0 \left| \mu_\gamma^+ \right| J \right\rangle'|^2) f(\hbar\omega - \hbar\omega'_{0J}) \tag{3.17}$$

where primed notations refer to quantities calculated in the presence of a static magnetic field, $\mathscr{E} = \hbar\omega$ is the energy per photon, d is concentration of solution in mol/L, l is the length of the path through the sample in centimeters, [119] γ is the direction of propagation of incident photon, $f(\hbar\omega - \hbar\omega'_{0J})$ is the band shape function, and $\hbar\omega'_{0J}$ is the excitation energy from ground state to the excited state J in the presence of a static magnetic field. Note that Eq. (3.17) takes on an isotropic average of all directions of incident light and applied magnetic field where the summation of γ runs over x, y, z. The derivation of the rotational average can be found in Reference 119.

Γ is the a collection of physical constants defined as [119]

$$\Gamma = \frac{N_0 \pi^2 \alpha^2 d\ l\ \log_{10} e}{250\ \hbar\ c\ n} \tag{3.18}$$

where α is the permittivity and n is the index of refraction.

The difference between oscillator strengths of left- and right-circularly polarized light for

excited state J can be written as [119]:

$$\sum_{\gamma}(|\left\langle 0\left|\mu_{\gamma}^{-}\right|J\right\rangle'|^2-|\left\langle 0\left|\mu_{\gamma}^{+}\right|J\right\rangle'|^2)=i\sum_{\alpha\beta\gamma}\epsilon_{\alpha\beta\gamma}\left\langle 0\left|\mu_{\alpha}\right|J\right\rangle^{\gamma}\left\langle J\left|\mu_{\beta}\right|0\right\rangle^{\gamma} \tag{3.19}$$

where $\epsilon_{\alpha\beta\gamma}$ is Levi-Civita symbol ($\epsilon_{xyz}=\epsilon_{yzx}=\epsilon_{zxy}=1$, $\epsilon_{yxz}=\epsilon_{xzy}=\epsilon_{zyx}=-1$, otherwise 0). We use superscript γ to explicitly denote the direction of the applied magnetic field.

Substituting Eq. (3.19) in Eq. (3.17), we reach the working formalism for computing MCD spectra,

$$\frac{\Delta A'}{\mathscr{E}}=\Gamma\sum_{J}\frac{1}{3}\left(i\sum_{\alpha\beta\gamma}\epsilon_{\alpha\beta\gamma}\left\langle 0\left|\mu_{\alpha}\right|J\right\rangle^{\gamma}\left\langle J\left|\mu_{\beta}\right|0\right\rangle^{\gamma}\right)f(\hbar\omega-\hbar\omega_{0J}^{\gamma}) \tag{3.20}$$

Compared to the conventional definition of the $\mathscr{B}$ term in perturbation theory, one can define the MCD strength of excited state $|J\rangle$ as

$$R_J=\frac{i}{3}\frac{\sum_{\alpha\beta\gamma}\epsilon_{\alpha\beta\gamma}\left\langle 0\left|\mu_{\alpha}\right|J\right\rangle^{\gamma}\left\langle J\left|\mu_{\beta}\right|0\right\rangle^{\gamma}}{\mu_B|\mathbf{B}|} \tag{3.21}$$

where μ_B is Bohr magneton. If the magnetic field does not split excited states of different M_L that belong to a same orbital angular momentum quantum number, the first order approximation of R_J becomes $\mathscr{B}_J$ in the perturbative treatment. The MCD strength (Eq. (3.21)) is written in atomic units, whereas the conventional experimentally reported unit is $D^2\cdot\mathrm{cm}$, where D is Debye. [119] The conversion for R_J from atomic units to the conventional unit of $D^2\cdot\mathrm{cm}$ is 1 a.u. $=2.944\times10^{-5}D^2\cdot\mathrm{cm}$.

The perturbative approach (Eq. (3.1)) is formulated in terms of the state-specific field-free parameters $\mathscr{A}_J,\mathscr{B}_J,\mathscr{C}_J$. In contrast, Eq. (3.20) directly computes MCD observables using a variational treatment of the external finite magnetic field. Compared to the perturbative approach, the expression in Eq. (3.20) contains $\mathscr{A}_J$ and $\mathscr{B}_J$ terms, and their higher order contributions.

Without an applied magnetic field, the absorbance difference between left- and right-

circularly polarized light is zero for electric circular dichroism (ECD) inactive molecules (or natural optical inactive molecules). In the presence of a static magnetic field, the imaginary part of transition dipole ($\langle 0 \left| \mu_\alpha \right| J \rangle^\gamma$ and $\langle 0 \left| \mu_\alpha \right| J \rangle^\gamma$) has nonzero contribution to the MCD strength, [6] which can be understood directly from Eq. (3.20). Since the excitation energy ω^γ is computed in the presence of a magnetic field, the breaking of excited state degeneracies, *i.e.* the $\mathscr{A}_J$ term, as a result of orbital Zeeman and diamagnetic effects are also included in Eq. (3.20). For closed-shell molecules, there is no spin degeneracy in the unperturbed ground state. In addition, the optical gap of a molecular system is usually larger than $k_B T$, where k_B is the Boltzmann constant. As a result, almost all molecules are in the ground state in experimental temperature, and thus the equivalent $\mathscr{C}$ term contribution can be ignored.

The computational approach introduced here (Eq. (3.20)) has a unique advantage that it only requires the computation of a single response to external optical perturbation due to the variational treatment of a finite magnetic field in the reference state. In contrast, perturbative approaches, such as the sum-over-states expression, require computations of all excited states. [82, 132] Complex polarization propagator methods [141, 142] need to numerically resolve quadratic response functions at different frequencies, but can be advantageous in the high density-of-state region. Alternatively, $\mathscr{A}_J$ and $\mathscr{B}_J$ terms can be computed via the evaluation of the derivatives of transition density and excitation energy with respect to magnetic perturbation. [133, 134]

3.2.4 Linear Response $\mathbb{C}$*-TDHF*

In order to compute MCD spectra using Eq. (3.20), electronic optical excitations need to be computed in the presence of a finite magnetic field. In this work, this is achieved using the linear response complex time-dependent Hartree-Fock ($\mathbb{C}$-TDHF) approach. The reference of $\mathbb{C}$-TDHF is the solution of $\mathbb{C}$-HF with the finite magnetic field included variationally.

The working equation of TDHF is given as

$$\begin{pmatrix} \mathbf{A}^{\gamma} & \mathbf{B}^{\gamma} \\ \mathbf{B}^{\gamma *} & \mathbf{A}^{\gamma *} \end{pmatrix} \begin{pmatrix} \mathbf{X}^{\gamma} \\ \mathbf{Y}^{\gamma} \end{pmatrix} = \omega^{\gamma} \begin{pmatrix} \mathbf{I} & \mathbf{0} \\ \mathbf{0} & -\mathbf{I} \end{pmatrix} \begin{pmatrix} \mathbf{X}^{\gamma} \\ \mathbf{Y}^{\gamma} \end{pmatrix} \tag{3.22}$$

$$B_{ai,bj} = (ai||bj) \tag{3.23}$$

$$A_{ai,bj} = (ai||jb) + \delta_{ab}\delta_{ij}(\epsilon_a - \epsilon_i) \tag{3.24}$$

where γ is the direction of the applied finite magnetic field in the ground state reference. Note, since the GIAO integrals and $\mathbb{C}$-HF are used, matrix elements in Eq. (3.22) are complex valued.

Given the direction γ of the applied uniform magnetic field, the corresponding transition dipole can be assembled from the transition density.

$$\langle 0 \left| \mu_\alpha \right| J \rangle^{\gamma} = \sum_i \sum_a \left(\langle i \left| \mu_\alpha \right| a \rangle^{\gamma} X^{\gamma}_{J,ai} + \langle a \left| \mu_\alpha \right| i \rangle^{\gamma} Y^{\gamma}_{J,ai} \right), \qquad \mu_\alpha \in \{\mu_x, \mu_y, \mu_z\} \tag{3.25}$$

where i and a sum over occupied and virtual molecular orbitals (MOs), respectively, and $\langle a \left| \mu_\alpha \right| i \rangle^{\gamma}$ and $\langle i \left| \mu_\alpha \right| a \rangle^{\gamma}$ are the dipole integrals in MO basis.

3.3 Computational Detail

To obtain the transition dipoles required in Eq. (3.20), three separate linear response $\mathbb{C}$-TDHF calculations were carried out with a magnetic field applied in the x, y, and z directions. Gauge including atomic orbitals (GIAO) were used to eliminate the gauge origin dependence in the variational treatment of the finite magnetic field described in Sec. 3.2.2. The geometries of molecules were optimized with the B3LYP functional [9,88,107] with a 6-31G(d) basis set [31,52] without a magnetic field using the GAUSSIAN16 computational chemistry software package. [33] $\mathbb{C}$-TDHF calculations in magnetic field using the GIAO 6-31G(d) basis set were performed in the CHRONUS QUANTUM open source package. [94] Computed spectra are

broadened with a normalized Gaussian function.

$$f_J(\omega) = \frac{1}{\sqrt{\pi}\sigma_J} \exp\left[-\left(\frac{\omega - \omega'_J}{\sigma_J} \right)^2 \right] \tag{3.26}$$

where ω and ω'_J are in atomic units. A major advantage of MCD over absorption spectra of linear polarized light is that MCD can resolve Zeeman effects with a higher resolution. This can be seen via a simple mathematical exercise using Gaussian broadening function, as shown in the Appendix.

3.4 Benchmark and Discussion

3.4.1 Sodium Anion

The existence of sodium anion was experimentally confirmed from an MCD measurement, with an absorption peak at ∼600 nm resulting from the $s \rightarrow p$ orbital transition. [139] An external magnetic field introduces orbital Zeeman interactions that break the three-fold degeneracy of the p orbitals, illustrated in Fig. 3.1. This gives rise to two peaks of opposite sign which leads to a derivative shape, shown in Fig. 3.2. The effects of magnetic field on the wave functions and properties of the ground and excited states are fully accounted for by treating the magnetic field variationally. As a result, $\mathscr{A}$ and $\mathscr{B}$ terms as well as their higher-order contributions are included in the simulated results. In comparison, it is required by perturbation theory to include infinite orders of magnetic field perturbations to fully describe the effects.

Computed excitation energies and associated MCD strengths are listed in Tab. 3.1. In this calculation, a magnetic field of 5.0×10^{-5} a.u. (∼11.75 T) was applied and the MCD spectrum was computed using the method introduced here. The relatively large magnitude of the magnetic field is chosen in the calculation to avoid numerical noise and instability. Note that we only present the MCD intensity in arbitrary unit because the concentration, d, and length of the path of light, l, are not defined in the experimental literature. The center of the computed MCD band is located at ∼720 nm. We do not expect a quantitative

ω'_{0J}/eV	$R/\times 10^5$ a.u.
1.72587	−11.1937
1.72655	0.0000
1.72723	11.1937

Table 3.1. Excitation energies and MCD strengths of Na^- $s \rightarrow p$ transitions in a 5×10^{-5} a.u. ($\sim$11.75 T) magnetic field.

agreement with the experiment as the experimental conditions are not modeled in this work. Nevertheless, the derivative band-shape of the Na^- MCD spectrum is obtained using the variational method introduced here.

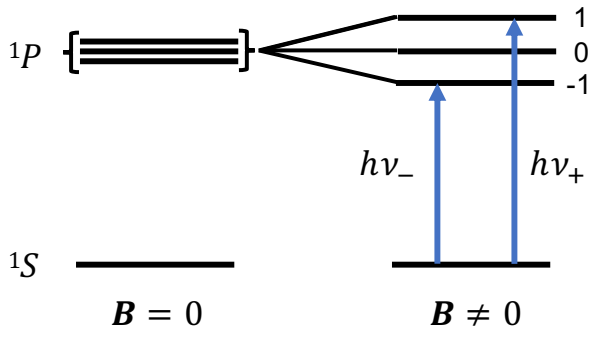

Figure 3.1. Illustration of splitting of the Na^- $s \rightarrow p$ transition. Without the external magnetic field, the excited states have a three-fold degeneracy. In the presence of a finite magnetic field, excited states of different M_L values split.

3.4.2 2,2,6,6-tetramethylcyclohexanone

In the absence of excited state splitting, the main effect of an external magnetic field comes from the perturbed transition dipole moment, giving rise to the perturbation-theory equivalent $\mathscr{B}_J$ term contribution.

MCD calculation of 2,2,6,6-tetramethylcyclohexanone in a 2.106×10^{-5} a.u. ($\sim$4.95 T) magnetic field is carried out. In order to be consistent with experimental measurements,

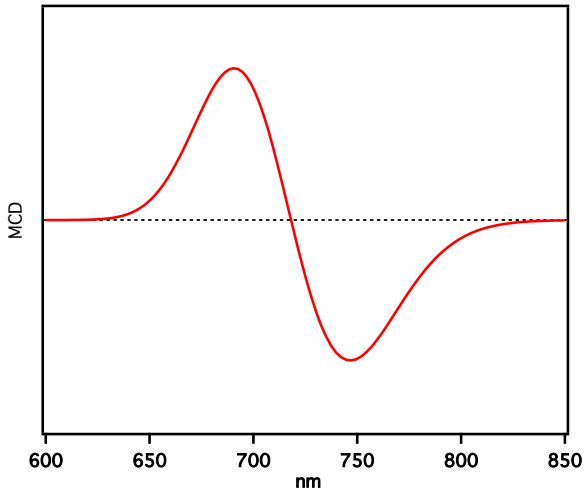

Figure 3.2. Simulated MCD spectra of Na^- $s \rightarrow p$ transitions in a 5×10^{-5} a.u. ($\sim$11.75 T) magnetic field. An arbitrary unit and Gaussian broadening with $\sigma = 0.035$ are used.

the computed MCD spectrum is presented as the magnetic-field normalized molar ellipticity, $[\theta]_M$. The calculation of $[\theta]_M$, in the conventional unit of Degree$(\text{mol/L})^{-1}\text{m}^{-1}\text{Gauss}^{-1}$, is $[\theta]_M = 0.0014802 \sum_J R_J \omega f(\hbar\omega - \hbar\omega_{0J}^{\gamma})$ where R_J, ω, and f are computed in atomic units. [134]

The computed MCD spectrum of 2,2,6,6-tetramethylcyclohexanone is shown in Fig. 3.3, and the associated excitation energy and MCD strength are reported in Tab. 3.2. The peak at $\sim$4.8 eV is characterized as the $n \rightarrow \pi^*$ transition. Although the computed result is of the correct + sign, the center of the peak is blue-shifted compared to the experimental value of 4.1 eV. [7] In addition, the magnitude of peak intensity is higher than that measured in experiment. This is likely due to the lack of solvent effects and electron correlation in the current work.

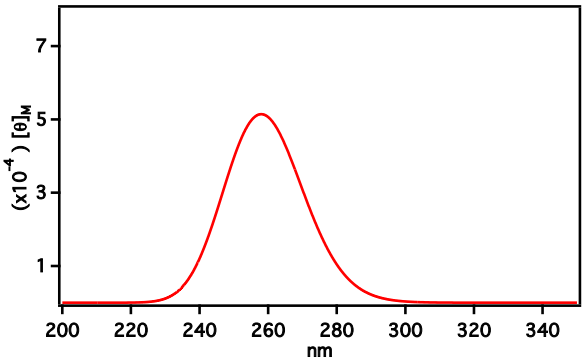

Figure 3.3. Simulated MCD spectrum of 2,2,6,6-tetramethylcyclohexanone in a 2.106×10^{-5} a.u. ($\sim$4.95 T) magnetic field. Gaussian broadening with $\sigma = 0.011$ is used.

ω'_{0J}/eV	R/a.u.
4.79665719	0.038400153724942

Table 3.2. Excitation energies and MCD strengths of 2,2,6,6-tetramethylcyclohexanone $n \rightarrow \pi^*$ transition in a 2.106×10^{-5} a.u. ($\sim$4.95 T) magnetic field.

3.4.3 3-methyl-2-hexanone

For natural optical active molecules, such as (R,S)-3-methyl-2-hexanone shown in Fig. 3.4.1 and Fig. 3.4.2, [7] electronic circular dichroism (ECD) spectra can be obtained in the absence of a magnetic field, however, ECD signals disappear if the ensemble consists of equal amounts of R- and S-enantiomers. In this case, MCD spectra are particularly useful as the effect of an external magnetic field can make the MCD signal visible.

Figure 3.5 shows the simulated MCD spectra of 3-methyl-2-hexanone in a 2.106×10^{-5} a.u. ($\sim$4.95 T) magnetic field and the associated numerical values are reported in Tab. 3.3. The strength of the magnetic field used is comparable to that used in the experiment. [7] The calculated MCD spectra of (R)- and (S)-3-methyl-2-hexanone are of the same '$-$' sign, in agreement with experiment. [7] As a result, even if the sample consists of equal amounts

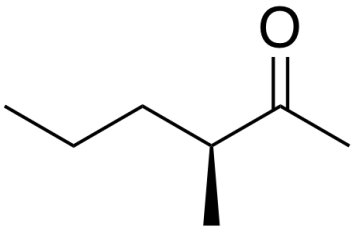

Figure 3.4.1. Molecular structure of (R)-3-methyl-2-hexanone

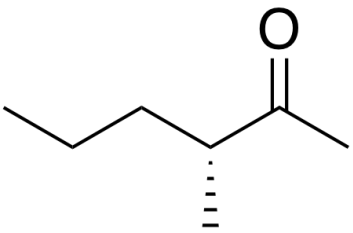

Figure 3.4.2. Molecular structure of (S)-3-methyl-2-hexanone

of R- and S-enantiomers, one still can measure the MCD signal. The excitation at ∼4.97 eV (∼250 nm) arises from the excitation from the lone pair electron of oxygen to the π^* anti-bonding orbital of the CO double bond. The peak position of the calculated spectrum is about 20 nm blue-shifted compared to the experimental value, [7] however, the height of the peak is similar to experiment.

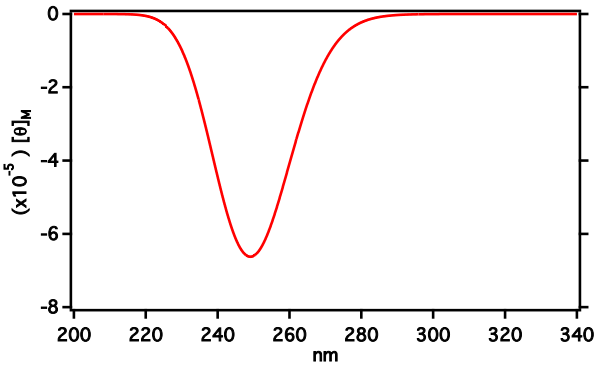

Figure 3.5. Simulated MCD spectra of 3-methyl-2-hexanone in a 2.106×10^{-5} a.u. (∼4.95 T) magnetic field. Gaussian broadening with $\sigma = 0.011$ is used.

ω'_{0J}/eV	R/a.u.
4.96819	−0.002011

Table 3.3. Excitation energies and MCD strengths of 3-methyl-2-hexanone in a 2.106×10^{-5} a.u. (∼4.95 T) magnetic field.

3.5 Conclusion

In this paper, we presented a mathematical formalism and implementation of an *ab initio* method with non-perturbative treatment of magnetic field for computing magnetic circular dichoism spectra of closed-shell systems. The approach developed in this work utilizes a spin-free non-relativistic Hamiltonian as the ground state reference that variationally includes the effects of a finite magnetic field, including orbital Zeeman and diamagnetic terms. MCD spectra are computed using the linear response formalism and direct calculation of left- and right-circular polarizations. In order to remove the gauge-origin dependence, London orbitals are used explicitly in the non-perturbative treatment of the finite magnetic field.

The method developed in this paper has been applied to simulations of MCD spectra of sodium anion, 2,2,6,6-tetramethylcyclohexanone, and 3-methyl-2-hexanone. Results are discussed and compared to experiments, and all computed benchmark spectra were able to return spectra with the correct sign. Particularly, the derivative band-shape of Na^- MCD spectrum was obtained using the variational method developed here, however, due the lack of electron correlation effect, the computed peak positions are not in good agreement with experiment. Nevertheless, the electronic transition characteristics in an MCD measurement can be correctly obtained at a low computational cost using the method developed in this work.

Chapter 4

RELATIVISTIC EFFECTS IN MAGNETIC CIRCULAR DICHROISM: RESTRICTED MAGNETIC BALANCE AND TEMPERATURE DEPENDENCE

Magnetic circular dichroism of transition metal complexes and open-shell systems are challenging to simulate and analyze, mainly due to the interplay of spin-orbit couplings and finite-magnetic-field induced Zeeman effects with the complex selection rules dictated by the circularly polarized light. In this work, we introduce an *ab initio* relativistic two-component formalism based on the restricted magnetic-balanced Hamiltonian for simulating MCD spectra. Both homogeneous finite magnetic field and relativistic effects are included variationally in the ground state reference. Finite-field London orbitals are used to enforce the constrained gauge-origin independence in the calculation using localized atomic orbitals. Through benchmark studies of $AuCl_4^-$, $Pt(CN)_4^{2-}$, and $Mo(CN)_8^{3-}$, we discuss how relativistic effects are manifested in MCD for both closed-shell and open-shell molecular complexes and how the interplay between spin-orbit coupling and magnetic field modulates the MCD selection rules. Finally, an investigation on temperature-dependent MCD is carried out and compared to experiment. The work in this chapter is adapted with permission from S. Sun and X. Li. Relativistic Effects in Magnetic Circular Dichroism: Restricted Magnetic Balance and Temperature Dependence. *J. Chem. Theory Comput.*, accepted.

4.1 Introduction

Computational modeling of spectroscopy is an indispensable tool for characterizing optical properties of molecular complexes. Although excited state calculations are routinely used to interpret linear absorption spectra and successful stories abound, computational methods

for studying magnetic circular dichroism (MCD) are not at the same level of practicality for analyzing experimental spectra and providing theoretical insights. Due to the complexity of the underlying MCD transition mechanism, the peak assignment can be difficult and ambiguous without the aid of an accurate theoretical method.

An MCD spectrum is the difference in absorption between left- and right-circularly polarized light, measured in the presence of a uniform magnetic field with a component in the direction of the propagation of the light. MCD is considered a relativistic spectroscopic method in which absorption signals are driven by the interplay of an external magnetic field, spin-orbit coupling, and probing circularly polarized light, which are described through the use of the Dirac Hamiltonian. Spin-orbit coupling is essential for both open-shell molecules as it gives rise to a unique temperature-dependence in the MCD spectra, and for closed-shell transition metal or heavy-element complexes as it allows for spin-forbidden transitions which appear in the spectra. Accurate prediction of MCD spectra requires appropriate treatment of magnetic field and spin-orbit coupling on equal footing. Simulations of MCD spectra can be generally categorized into perturbative and variational approaches.

In the perturbative regime, numerous approximations have been developed including single residue of the quadratic response function; [17] the complex polarization propagator method; [82, 141, 142] a sum-over-states expression using truncated configuration interaction, with perturbative treatment of the magnetic field and spin-orbit coupling; [61, 62] magnetically perturbed time-dependent density functional theory (TDDFT) with spin-orbit coupling treated perturbatively using the ZORA Hamiltonian; [133, 134, 137, 138] and multiconfigurational self-consistent-field with quasi-degenerate perturbation theory to include Zeeman effects with spin-couplings. [37, 39, 55]

Variational approaches are more challenging to develop due to the need to use a multicomponent, complex-valued wave funtion requiring novel integrals. In the Dirac Hamiltonian, magnetic field effects can be introduced through the minimal coupling $\boldsymbol{\pi} = \mathbf{p} + \mathbf{A}$, where $\mathbf{p}$ is the linear momentum and $\mathbf{A}$ is the vector potential for electrons. By variationally including spin-orbit coupling and magnetic field effects in the reference Dirac Hamiltonian, a time-

dependent perturbation theory can be used to simulate MCD spectra and, in principle, the resulting spectrum satisfies the MCD selection rules, which are discussed later. There are only a few developments in the variational domain which consider the effects of magnetic field within the random-phase-approximation (RPA), linear response TDHF, [128,152] or the real-time time-dependent density functional theory (RT-TDDFT) frameworks. [89, 151] In this previous work, only magnetic field effects were variationally included in the non-relativistic Hamiltonian. As a result, they can only be applied to simulations of MCD spectra on closed-shell systems with light elements. Open-shell molecular complexes can give rise to a temperature-dependent MCD feature which requires the inclusion of varationally-treated spin-orbit coupling.

When both spin-orbit coupling and magnetic field are considered in the Dirac equation, cast in a Gaussian basis, the magnetic balance condition between the large and small component bases is preferred over the kinetic balance condition. [3,85,115] The restricted magnetic balance was implemented with four-component methods for the simulation of nuclear magnetic resonance shielding constants. [78] It was later combined with gauge-including atomic orbitals (GIAO) to enforce the gauge-origin independence in both the four- [14, 77, 113, 124] and two-component [53, 96, 150, 170, 171] relativistic formalism.

In this work, we introduce a fully variational two-component relativistic approach for computing the temperature-dependent MCD spectrum with a special theoretical focus on the magnetic balance condition in the presence of a finite magnetic field. Through benchmark studies we will discuss how relativistic effects are manifested in MCD for both closed- and open-shell molecular complexes, and how the interplay between spin-orbit coupling and magnetic field modulates the MCD selection rules. Finally, an investigation on temperature-dependent MCD is carried out.

4.2 Theory of Exact-Two-Component in the Uniform External Magnetic Field

4.2.1 One-Electron Dirac Hamiltonian in Magnetic Field

The one-electron Dirac equation (in the atomic units) in the magnetic field is:

$$\begin{pmatrix} V & c\boldsymbol{\sigma}\cdot\boldsymbol{\pi} \\ c\boldsymbol{\sigma}\cdot\boldsymbol{\pi} & V-2c^2 \end{pmatrix} \begin{pmatrix} \psi^L \\ \psi^S \end{pmatrix} = E \begin{pmatrix} \psi^L \\ \psi^S \end{pmatrix} \tag{4.1}$$

where c is the speed of light, and ψ^L and ψ^S are the large and small components of the bi-spinor wave function. In Eq. (4.1), we used the mechanical momentum $\boldsymbol{\pi} = \mathbf{p} + \mathbf{A}$ that includes the linear momentum $\mathbf{p} = -i\boldsymbol{\nabla}$ and the vector potential $\mathbf{A}$ for electrons.

The relationship between the small component relative to the large component can be obtained from Eq. (4.1):

$$\psi^S = -\frac{c}{(V-E-2c^2)}(\boldsymbol{\sigma}\cdot\boldsymbol{\pi})\psi^L \tag{4.2}$$

As the vector potential in the mechanical momentum is related to the magnetic field through the expression, $\mathbf{A} = \frac{1}{2}\mathbf{B}\times\mathbf{r}$, Eq. (4.2) gives rise to the restricted magnetic balance condition between the large and small components of the wave function:

$$\lim_{c\to+\infty} 2mc\psi^S = \boldsymbol{\sigma}\cdot\boldsymbol{\pi}\psi^L \tag{4.3}$$

or the basis set relation:

$$\chi^S = \boldsymbol{\sigma}\cdot\boldsymbol{\pi}\chi^L \tag{4.4}$$

Equation (4.4) is the so-called restricted magnetic balance condition. [115]

In order to obtain a Hamiltonian expression that fulfills the magnetic balance condition, the four-component wave function is transformed into a large and pseudo-large component

basis:

$$\begin{pmatrix} \psi^L \\ \phi^L \end{pmatrix} = \mathcal{T} \begin{pmatrix} \psi^L \\ \psi^S \end{pmatrix} \tag{4.5}$$

using the following transformation matrix:

$$\mathcal{T} = \begin{pmatrix} \mathbf{I}_2 & \mathbf{0}_2 \\ \mathbf{0}_2 & \frac{\boldsymbol{\sigma}\cdot\boldsymbol{\pi}}{2c} \end{pmatrix}. \tag{4.6}$$

In the basis of large and pseudo large component, the one-electron modified Dirac equation is:

$$\begin{pmatrix} V\mathbf{I}_2 & \frac{1}{2}(\boldsymbol{\sigma}\cdot\boldsymbol{\pi})(\boldsymbol{\sigma}\cdot\boldsymbol{\pi}) \\ \frac{1}{2}(\boldsymbol{\sigma}\cdot\boldsymbol{\pi})(\boldsymbol{\sigma}\cdot\boldsymbol{\pi}) & \frac{1}{4c^2}(\boldsymbol{\sigma}\cdot\boldsymbol{\pi})V(\boldsymbol{\sigma}\cdot\boldsymbol{\pi}) - \frac{(\boldsymbol{\sigma}\cdot\boldsymbol{\pi})(\boldsymbol{\sigma}\cdot\boldsymbol{\pi})}{2} \end{pmatrix} \begin{pmatrix} \psi^L \\ \phi^L \end{pmatrix} = E \begin{pmatrix} \mathbf{I}_2 & \mathbf{0}_2 \\ \mathbf{0}_2 & -\frac{(\boldsymbol{\sigma}\cdot\boldsymbol{\pi})(\boldsymbol{\sigma}\cdot\boldsymbol{\pi})}{4c^2} \end{pmatrix} \begin{pmatrix} \psi^L \\ \phi^L \end{pmatrix} \tag{4.7}$$

In the non-relativistic limit, *i.e.*, the speed of light, c, goes to positive infinity, Eq. (4.7) is reduced to:

$$\frac{1}{2}(\boldsymbol{\sigma}\cdot\boldsymbol{\pi})(\boldsymbol{\sigma}\cdot\boldsymbol{\pi})\phi^L + V\psi^L = E\psi^L \tag{4.8}$$

which is the non-relativistic Pauli Hamiltonian in the presence of a magnetic field. [145, 151–153] The asymptotic, non-relativistic limit of Eq. (4.7) as $c \to \infty$ suggests that restricted magnetic balance can give rise to a smooth transition from a fully relativistic to non-relativistic treatment of electronic structure.

In a uniform magnetic field, the following expressions can be derived for Eq. (4.7):

$$\frac{1}{2}(\boldsymbol{\sigma}\cdot\boldsymbol{\pi})(\boldsymbol{\sigma}\cdot\boldsymbol{\pi}) = -\frac{1}{2}\boldsymbol{\nabla}^2 + \frac{1}{2}(\boldsymbol{\sigma} - i\mathbf{r}\times\boldsymbol{\nabla})\cdot\mathbf{B} + \frac{1}{8}(\mathbf{B}\times\mathbf{r})^2 \tag{4.9}$$

$$\begin{aligned}(\boldsymbol{\sigma}\cdot\boldsymbol{\pi})V(\boldsymbol{\sigma}\cdot\boldsymbol{\pi}) &= (\boldsymbol{\sigma}\cdot\mathbf{p})V(\boldsymbol{\sigma}\cdot\mathbf{p}) + (\mathbf{p}V\cdot\mathbf{A} + \mathbf{A}V\cdot\mathbf{p}) \\ &\quad + i\boldsymbol{\sigma}\cdot(\mathbf{p}V\times\mathbf{A} + \mathbf{A}V\times\mathbf{p}) + \mathbf{A}V\cdot\mathbf{A}\end{aligned} \tag{4.10}$$

The first term in Eq. (4.10), $(\boldsymbol{\sigma}\cdot\mathbf{p})V(\boldsymbol{\sigma}\cdot\mathbf{p})$ gives rise to $\mathbf{p}V\cdot\mathbf{p} + i\boldsymbol{\sigma}\cdot\mathbf{p}V\times\mathbf{p}$, which are

the spin-free and spin-coupling terms. Vector potential dependent terms in Eq. (4.10) can be written in terms of the magnetic field **B**:

$$\begin{aligned}\mathbf{p}V\cdot\mathbf{A}+\mathbf{A}V\cdot\mathbf{p} = \frac{i}{2}\big\{&B_x[(\nabla_y V r_z + r_z V\nabla_y)-(\nabla_z V r_y + r_y V\nabla_z)]\\ &B_y[(\nabla_z V r_x + r_x V\nabla_z)-(\nabla_x V r_z + r_z V\nabla_x)]\\ &B_z[(\nabla_x V r_y + r_y V\nabla_x)-(\nabla_y V r_x + r_x V\nabla_y)]\big\} \qquad (4.11)\end{aligned}$$

$$(\mathbf{p}V\times\mathbf{A}+\mathbf{A}V\times\mathbf{p})_\kappa = \sum_\mu \frac{1}{2}B_\mu(r_\kappa V p_\mu - p_\mu V r_\kappa)+\frac{1}{2}B_\kappa(p_\mu V r_\mu - r_\mu V p_\mu) \qquad (4.12)$$

$$\begin{aligned}\mathbf{A}V\cdot\mathbf{A} = &\, xVx(B_y^2+B_z^2)+yVy(B_x^2+B_z^2)+zVz(B_x^2+B_y^2)\\ &-xVy2B_xBy - yVz2B_yB_z - 2xVzB_xB_z \qquad (4.13)\end{aligned}$$

where $\kappa,\mu\in\{x,y,z\}$. It is clear that operator $\nabla_\beta V r_\alpha - r_\alpha V\nabla_\beta$ is Hermitian, thus Eq. (4.12) is anti-Hermitian, and the operator $r_\alpha V\nabla_\beta + \nabla_\beta V r_\alpha$ is anti-Hermitian, thus Eq. (4.11) is Hermitian.

4.2.2 Exact-Two-Component Transformation in Magnetic-Balance Condition

The four- to two-component transformation seeks to decouple the positive and negative energy solutions in the Dirac equation. The magnetic-balanced, modified Dirac Hamiltonian (Eq. (4.7)) allows the same basis to be used for the large and pseudo-large components in the bi-spinor representation. Each spinor is formed as a product of spatial basis with spin functions $f=\{\tilde{\chi}\}\otimes\{\alpha,\beta\}$ where $\tilde{\chi}$ is a gauge-including atomic orbital basis. In the spinor basis, the matrix representation of the restricted magnetically-balanced Dirac equation is:

$$\begin{pmatrix}\mathbf{V} & \mathbf{M}\\ \mathbf{M} & \frac{1}{4c^2}\mathbf{W}-\mathbf{M}\end{pmatrix}\begin{pmatrix}\mathbf{C}_L^+ & \mathbf{C}_L^-\\ \mathbf{C}_S^+ & \mathbf{C}_S^-\end{pmatrix} = \begin{pmatrix}\mathbf{S} & \mathbf{0}\\ \mathbf{0} & \frac{1}{2c^2}\mathbf{M}\end{pmatrix}\begin{pmatrix}\mathbf{C}_L^+ & \mathbf{C}_L^-\\ \mathbf{C}_S^+ & \mathbf{C}_S^-\end{pmatrix}\begin{pmatrix}\boldsymbol{\epsilon}^+ & \mathbf{0}\\ \mathbf{0} & \boldsymbol{\epsilon}^-\end{pmatrix} \qquad (4.14)$$

$$M_{\mu\nu} = \langle f_\mu|\frac{1}{2}(\boldsymbol{\sigma}\cdot\boldsymbol{\pi})(\boldsymbol{\sigma}\cdot\boldsymbol{\pi})|f_\nu\rangle \qquad (4.15)$$

$$W_{\mu\nu} = \langle f_\mu|(\boldsymbol{\sigma}\cdot\boldsymbol{\pi})V(\boldsymbol{\sigma}\cdot\boldsymbol{\pi})|f_\nu\rangle \qquad (4.16)$$

where $\mathbf{S}$ and $\mathbf{V}$ are the block-diagonal two-component overlap and potential energy matrix, and $\{\epsilon_p^+\}$, $\{\epsilon_p^-\}$ are the sets of positive/negative eigenvalues with corresponding molecular orbital coefficients $(\mathbf{C}_L^+ \quad \mathbf{C}_S^+)^T$ for the positive and $(\mathbf{C}_L^- \quad \mathbf{C}_S^-)^T$ for the negative energy solutions.

Following the procedure in Ref. 117, the non-unit metric of the magnetically-balanced four-component equation, Eq. (4.14), is eliminated through the transformation:

$$\mathbb{K}^\dagger \begin{pmatrix} \mathbf{S} & \mathbf{0} \\ \mathbf{0} & \frac{1}{2c^2}\mathbf{M} \end{pmatrix} \mathbb{K} = \begin{pmatrix} \mathbf{I} & \mathbf{0} \\ \mathbf{0} & \mathbf{I} \end{pmatrix} \tag{4.17}$$

$$\mathbb{K} = \begin{pmatrix} \mathbf{K} & \mathbf{0} \\ \mathbf{0} & 2c\mathbf{K}\sqrt{2\mathbf{t}}^{-1} \end{pmatrix} \tag{4.18}$$

where the two-component matrix $\mathbf{K}$ is obtained by solving the following eigenvalue equation:

$$\mathbf{MK} = \mathbf{SKt} \tag{4.19}$$

where $\mathbf{t}$ is the diagonal matrix of the eigenvalues. Note that in the presence of magnetic fields, the full two-component matrices of $\mathbf{M}$ and $\mathbf{K}$ must be used in the orthogonalization procedure, since the magnetic field breaks the time-reversal symmetry of the Hamiltonian.

It is easy to show that $\mathbf{K}$ diagonalizes both the magnetic balance $\mathbf{M}$ matrix and the overlap $\mathbf{S}$ matrix:

$$\mathbf{K}^\dagger \mathbf{M} \mathbf{K} = \mathbf{t}, \qquad \mathbf{K}^\dagger \mathbf{S} \mathbf{K} = \mathbf{I} \tag{4.20}$$

The four-component, magnetically-balanced Hamiltonian can then be transformed:

$$\mathbb{H}^\pi = \mathbb{K}^\dagger \mathbb{H} \mathbb{K} = \begin{pmatrix} \mathbf{K}^\dagger \mathbf{V} \mathbf{K} & c\sqrt{2\mathbf{t}} \\ c\sqrt{2\mathbf{t}} & \sqrt{2\mathbf{t}}^{-1} \mathbf{K}^\dagger (\boldsymbol{\sigma} \cdot \boldsymbol{\pi}) V (\boldsymbol{\sigma} \cdot \boldsymbol{\pi}) \mathbf{K} \sqrt{2\mathbf{t}}^{-1} - 2c^2 \end{pmatrix} \tag{4.21}$$

Upon diagonalizing the orthonormalized four-component Hamiltonian (Eq. (4.21)), the exact-two-component (X2C) [27,28,42,64,79,86,95,98–100,116,117,126,154] transformation

in the restricted magnetically-balanced condition can be carried out. The two-component electron-only X2C Hamiltonian can be constructed as:

$$\mathbf{H}_{\mathrm{X2C}} = (\mathbf{K}^{-1})^{\dagger}\mathbf{R}^{\dagger}\{\mathbf{K}^{\dagger}V\mathbf{K}+c\sqrt{2\mathbf{t}}\mathbf{X}+\mathbf{X}c\sqrt{2\mathbf{t}}+\mathbf{X}^{\dagger}[\sqrt{2\mathbf{t}}^{-1}\mathbf{K}^{\dagger}(\boldsymbol{\sigma}\cdot\boldsymbol{\pi})V(\boldsymbol{\sigma}\cdot\boldsymbol{\pi})\mathbf{K}\sqrt{2\mathbf{t}}^{-1}-2c^{2}]\mathbf{X}\}\mathbf{R}\mathbf{K}^{-1} \tag{4.22}$$

where the $\mathbf{X}$ matrix is built using the MOs in the orthogonal basis:

$$\mathbf{X} = \mathbf{C}'^{+}_{S}(\mathbf{C}'^{+}_{L})^{-1} \tag{4.23}$$

and the normalization matrix $\mathbf{R}$ is:

$$\mathbf{R} = (\mathbf{I} + \mathbf{X}^{\dagger}\mathbf{X})^{-\frac{1}{2}} \tag{4.24}$$

The restricted magnetically-balanced two-component Hamiltonian in Eq. (4.22) allows for including magnetic field perturbations variationally in the relativistic Dirac equation. It ensures that the solution is bound from below in the two-component formalism so that variational procedures can be applied to obtain the ground state wave function in the presence of a magnetic field. The restricted magnetic balance was used with X2C to calculate nuclear and electronic magnetic resonance parameters, including the hyperfine coupling, J-coupling, and g-tensor, within a response theory at the zero-field limit. [5, 149, 166]

4.2.3 Gauge-including Atomic Orbital

For many-atom systems, electronic structure calculations in the presence of electromagnetic fields become unphysically dependent on the choice of the arbitrary gauge-origin. [22, 29, 30, 38, 59, 84, 90, 127] Among various approaches to correct for the gauge-origin problem, electronic structure methods using London type orbitals [23, 101] provide the most satisfactory solution. [4, 10, 56, 57, 80, 167] Using London orbitals to enforce the constrained gauge origin independence for finite atom-centered basis set has been applied in the per-

turbative calculations of MCD at the level of coupled-cluster, [16, 74] Hartree-Fock, and DFT. [75, 81] Variational approaches require the use of finite-field gauge-including atomic orbital (GIAO) which has been implemented in Hartree-Fock and time-dependent Hartree-Fock [124,130,131,145,152,153,156], coupled-cluster [51,146], configurational interaction, [87] DFT and TDDFT methods [123, 151, 157]. Recently, finite-field GIAO has been used in variational calculations of MCD for closed-shell systems. [151, 152] In this work, finite-field GIAOs are implemented in a non-collinear formalism of the two-component relativistic DFT/TDDFT framework. [28, 76, 118]

4.3 Theory of Temperature-Dependent Magnetic Circular Dichroism

Interpreting and understanding MCD spectra has been traditionally based on the first-order perturbative model: [11, 73, 103, 119, 143]

$$\frac{\Delta A'}{\mathscr{E}} = \Gamma \mu_B B \sum_J \left[\mathscr{A}_J \left(- \frac{\partial f(\hbar\omega - \hbar\omega_{0J})}{\partial \hbar\omega} \right) + \left(\mathscr{B}_J + \frac{\mathscr{C}_J}{kT} \right) f(\hbar\omega - \hbar\omega_{0J}) \right] \tag{4.25}$$

where μ_B is Bohr magneton and Γ is a collection of physical constants [119]. $\mathscr{E} = \hbar\omega$ is the energy per photon. $f(\hbar\omega - \hbar\omega_{0J})$ is the band shape function, which is often chosen to be a Gaussian function. $\hbar\omega_{0J}$ is the excitation energy from ground state to the J^{th} excited state in the absence of a electromagnetic field. $\mathscr{A}_J$ term arises when the degenerate excited states are split due to Zeeman effects. Perturbation of the transition dipole gives rise to $\mathscr{B}_J$ term, which is the most common effect in MCD. The $\mathscr{C}_J$ term is modulated by the Boltzmann distribution of the ground state when degenerate ground states are split by Zeeman effects, and is the origin of the temperature dependent features in MCD spectra. Given that the degenerate ground state will split due to the spin Zeeman effect, in the case of an open-shell system, the population of the resulting split system will have a temperature dependence giving rise to different features in the MCD spectra.

The perturbative approach (Eq. (4.25)) for computing MCD spectra is formulated in terms of the state-specific field-free parameters $\mathscr{A}_J, \mathscr{B}_J, \mathscr{C}_J$, assuming perturbation expan-

sions for both the optical and magnetic fields, however, with the variational treatment of the magnetic fields, the $\mathscr{A}, \mathscr{B}, \mathscr{C}$ terms are not well defined because the non-perturbative magnetic field effect is already included in the molecular orbitals and energy eigenvalues.

In our previous work we derived mathematical expressions to compute MCD spectra in a variational framework and response function formalism for closed-shell systems. [151, 152] The computation of temperature-dependent MCD requires considering spin-Zeeman splitting in the ground state arising from the interaction with a static magnetic field. Assume there are N_0 and N_K numbers of spin-degenerate micro-states that belong to a same spatial ground and excited state wave function, $|0\rangle$ and $|K\rangle$, respectively, in the absence of a static magnetic field. The effects of magnetic-field-split ground and excited micro-states enter the expression of the MCD equation as an explicit summation over all micro-states with a Boltzmann factor:

$$\frac{\Delta A'}{\mathscr{E}} = \Gamma \sum_{a}^{N_0} \frac{N_a}{N_0} \sum_{K} \sum_{b}^{N_K} \frac{1}{3} \left(i \sum_{\alpha\beta\gamma} \epsilon_{\alpha\beta\gamma} \langle 0_a | \mu_\alpha | K_b \rangle^\gamma \langle K_b | \mu_\beta | 0_a \rangle^\gamma \right) f(\hbar\omega - \hbar\omega^\gamma_{0_a,K_b}) \quad (4.26)$$

where $|0_a\rangle$ and $|K_b\rangle$ are the a-th and b-th micro-state of the ground and excited state, respectively. μ is the electric dipole operator, $\{\alpha, \beta, \gamma\} \equiv \{x, y, z\}$, $\{y, z, x\}$ or $\{z, x, y\}$, following the right hand rule. $\epsilon_{\alpha\beta\gamma}$ is Levi-Civita symbol ($\epsilon_{xyz} = \epsilon_{yzx} = \epsilon_{zxy} = 1$, $\epsilon_{yxz} = \epsilon_{xzy} = \epsilon_{zyx} = -1$, otherwise 0). We use superscript γ to explicitly denote the direction of the applied magnetic field, which is also the direction of propagation of incident photon. Note that Eq. (4.26) takes on an isotropic average of all directions of incident light and applied magnetic fields since the summation of γ runs over x, y, z. The prefactor $\frac{N_a}{N_0}$ describes the Boltzmann distribution of the near-degenerate micro-state populations in the ground state:

$$N_a = \exp\left(-\frac{E_a}{kT} \right) \quad (4.27)$$

where k is Boltzmann constant, and T is the temperature. E_a is the energy of micro-state $|0_a\rangle$ relative to the lowest micro-state. For a single transition between micro-states, $|0_a\rangle \rightarrow |K_b\rangle$,

the MCD strength can be defined as

$$R = \frac{i}{3}\frac{\sum_{\alpha\beta\gamma}\epsilon_{\alpha\beta\gamma}\left\langle 0_a\left|\mu_\alpha\right|K_b\right\rangle^\gamma\left\langle K_b\left|\mu_\beta\right|0_a\right\rangle^\gamma}{\mu_B|\mathbf{B}|} \tag{4.28}$$

where μ_B is the Bohr magneton ($\mu_B = 1/2$ in atomic units).

For closed shell systems without ground state degeneracy, Eq. (4.26) can be reduced to: [151, 152]

$$\frac{\Delta A'}{\mathscr{E}} = \Gamma\sum_K\frac{1}{3}\left(i\sum_{\alpha\beta\gamma}\epsilon_{\alpha\beta\gamma}\left\langle 0\left|\mu_\alpha\right|K\right\rangle^\gamma\left\langle K\left|\mu_\beta\right|0\right\rangle^\gamma\right)f(\hbar\omega-\hbar\omega_{0J}^\gamma). \tag{4.29}$$

Equation (4.29) can also be used to compute the MCD spectrum of an open-shell system at the low temperature limit when only the lowest energy micro-state is populated.

4.4 Benchmark and Discussion

4.4.1 Computational Detail

Using Eq. (4.26) to compute temperature-dependent MCD, all micro-states in the ground state manifold and excitations out of these micro-states have to be calculated. In the linear response TDDFT formalism, this is a non-trivial task. Some attempts using TDDFT were made for certain special cases to simulate excitations of multiple unpaired electron systems [135, 136] by choosing a non-degenerate excited state as the reference of TDDFT. In the current work, we present a different approach to compute temperature-dependent MCD of a spin doublet ground state using Kramers unrestricted X2C-TDDFT, [28, 118] that relies on variationally including the magnetic field in the initial state preparation.

To obtain the transition dipoles required in Eq. (4.26), three separate linear response X2C-TDDFT calculations were carried out with a magnetic field $\mathbf{B}$ applied in the x, y, and z directions for each micro-state in the ground state manifold. Gauge including atomic orbitals (GIAO) were used to enforce a constrained gauge-origin independence in the variational treatment of the finite magnetic field. [151, 152] The geometries of the molecules were

optimized using the GAUSSIAN16 computational chemistry software package [33] with the non-relativistic B3LYP functional [9,88,107] in the absence of a magnetic field. X2C-TDDFT calculations in the presence of a magnetic field using the GIAO basis sets were performed in the CHRONUS QUANTUM open source package. [165] Computed spectra are broadened with a normalized Gaussian function:

$$f_J(\omega) = \frac{1}{\sqrt{\pi}\sigma_J} \exp\left[-\left(\frac{\omega - \omega_J}{\sigma_J} \right)^2 \right] \tag{4.30}$$

where ω and ω_J are in atomic units. The peak width σ_J is chosen to fit experimental spectra.

For an open-shell spin-doublet molecule, the lowest micro-state is when the spin is anti-parallel with respect to the magnetic field. The excitation energy and transition dipole from this state can be directly computed using X2C-TDDFT from the converged ground state wave function in the presence of a magnetic field. In order to obtain transitions from the higher-energy micro-state, the spin-parallel configuration with respect to the magnetic field must be used as the X2C-TDDFT reference state. An initial guess for the higher-energy micro-state can be obtained using a magnetic field in the negative x, y, z direction, $-\mathbf{B}$. Using such an initial guess, a second SCF procedure is applied using the magnetic field in positive x, y, z direction to converge the wave function to the high-energy micro-state solution. This technique can be successful if the applied magnetic field is small enough that it does not induce any spin flip or phase transition. [153]

The MCD selection rule requires that the total angular momentum change by one during the excitation, $\Delta M_J = \pm 1$ in double group symmetry. This can arise from changes in the orbital angular momentum in point group symmetry ($\Delta M_L = \pm 1$) or in the spin symmetry ($\Delta M_S = \pm 1$). In the following discussion, we will mainly use the point group, instead of double group symmetry for analysis because it is more intuitive for understanding the excited-state splitting and selection rules giving rise to the resulting MCD spectrum. The point group assignments are chosen to be the dominant molecular orbital contribution to the TDDFT transition.

4.4.2 Charge Transfer Excitations in $AuCl_4^-$ and $Pt(CN)_4^{2-}$

Historically, MCD spectra of $AuCl_4^-$ and $Pt(CN)_4^{2-}$ molecular complexes were used to study optical characteristics of square planar coordination. [66,68,104] The intense peaks in the UV-Vis region are charge transfer excitations. Arising from their unique molecular orbital alignments (see molecular orbital diagrams in Ref. 104), the CT bands in $AuCl_4^-$ and $Pt(CN)_4^{2-}$ have the ligand-to-metal (LMCT) and metal-to-ligand (MLCT) characters, respectively.

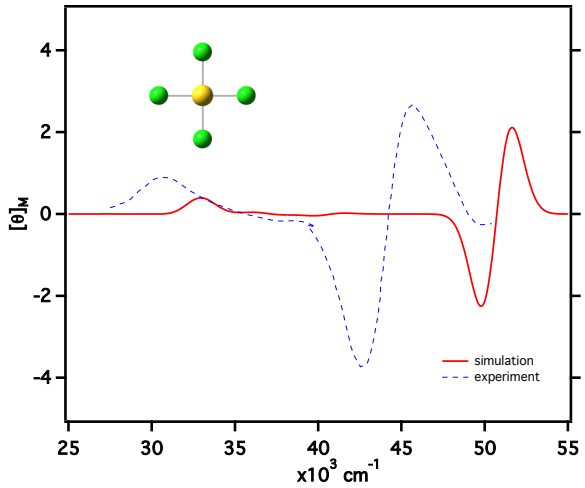

Figure 4.1. Simulated MCD spectra of $AuCl_4^-$ LMCT in a 2.9787×10^{-5} a.u. ($\sim$7 T) magnetic field. An arbitrary unit and Gaussian broadening with $\sigma = 0.006$ are used.

Figure 4.1 shows the computed MCD spectrum of $AuCl_4^-$ with excitation energies and MCD strengths of bright excited states listed in Tab. 4.1, compared to experiments. Calculations were carried out using X2C-B3LYP with the GIAO-Sapporo-DKH3-DZP-NO basis [111] for Au and the GIAO-Sapporo-DZP-2012-NO basis [110] for Cl. These electronic excitations are LMCT transitions from Au-d to Cl-p orbitals. The ground state of $AuCl_4^-$ has an $^1A_{1g}$ symmetry which does not split in a magnetic field. The first peak at $\sim 33 \times 10^3$ cm^{-1} ($\sim$4 eV) corresponds to excitations to the low-lying ^1E_u state. The derivative shaped peaks at $47 \sim 53 \times 10^3$ cm^{-1} are characterized as higher energy ^1E_u states. These peaks mainly

state	ω_{0J}/eV	ω_{0J}/cm^{-1}	R/a.u.
^1E_u	4.0239	32455	−6586.8
^1E_u	4.0241	32457	6604.7
^1E_u	5.0135	40436	−400.1
^1E_u	5.0142	40442	399.5
^1E_u	6.2836	50682	−58983.5
^1E_u	6.2838	50684	58975.9

Table 4.1. Excitation energies and MCD strengths of $AuCl_4^-$ LMCT transitions in a 2.9787×10^{-5} a.u. (∼7 T) magnetic field.

involve the ligand e_u orbitals with two-fold degeneracy. Since this is a singlet state, spin Zeeman effect is absent. The splitting is solely due to the magnetic field induced orbital Zeeman effect. Transitions to E_u states with angular momenta $M_L = \pm 1$ are allowed by right- and left-circularly polarized lights, giving rising to a derivative shaped peak.

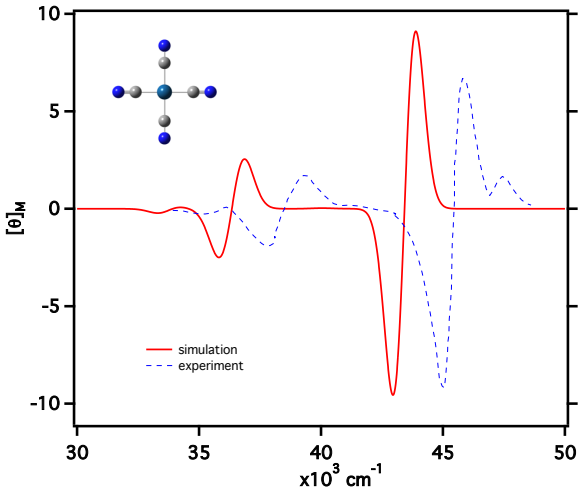

Figure 4.2. Simulated MCD spectrum of $Pt(CN)_4^{2-}$ in a 4.468×10^{-6} a.u. (∼1.05 T) magnetic field. Gaussian broadening with $\sigma = 0.003$ is used.

All bright transitions in $AuCl_4^-$ are characterized as singlet→singlet excitations. Spin-orbit coupling in this molecular system is weak, and, therefore, does not enable strong

singlet→triplet excitations. As such, the most important relativistic effect for this system is the scalar relativity. As the strength of spin-orbit coupling increases in a molecular system, additional MCD spectral features will appear, and the spectral assignments become more complex.

Figure 4.2 and Tab. 4.2 present the computed MCD spectrum of $Pt(CN)_4^{2-}$. Calculations were carried out using X2C-B3LYP with the GIAO-Sapporo-DKH3-DZP-ALL basis [111] for Pt and the GIAO-Sapporo-DZP-2012-ALL basis [110] for C and N. In contrast to the $AuCl_4^-$ molecule, the observed MCD peaks of $Pt(CN)_4^{2-}$ have MLCT characters, arising from the excitation of the Pt-d electron to the π^* orbitals of CN^- groups. The first peak at $33.7 \sim 36.6 \times 10^3$ cm^{-1} corresponds to singlet→triplet MLCT excitations. This peak can only be observed in a relativistic TDDFT approach because of the spin-orbit coupling. Because the $^3A_{2u}$ ($J = 1$) state does not give rise to an orbital Zeeman splitting, the observed peak is due to the spin Zeeman effect. Zero-field-splitting induced by the out-of-state spin-orbit coupling splits the $M_J = 0$ level from $M_J = \pm 1$ manifolds to the $^3A_{2u}$ state. Excitation to the $M_J = 0$ micro-state is forbidden because the change in angular momentum is zero from the $^1A_{1g}$ ground state. The spin Zeeman effect further splits $M_J = \pm 1$ into $M_J = -1$ and $M_J = 1$ micros-tates that give rise to the derivative-shaped peak.

The more intense peak at 36.6×10^3 cm^{-1} also arises from the singlet→triplet MLCT excitation, however, with a ^3E_u symmetry excited state. Analysis of allowed transitions is more complex because both spin and orbital angular momenta are split in the ^3E_u state by the magnetic field. Among the zero-field-split levels ($J = 0, 1, 2$) of the ^3E_u state, only the $J = 1$ level satisfies the MCD selection rule. As such, the observed derivative-shaped peak at 36.6×10^3 cm^{-1} consists of $M_J = -1$ and $M_J = 1$ micro-states of the ^3E_u ($J = 1$) level.

The intense peak at 43.4×10^3 cm^{-1} arises from singlet MLCT excitations. Because they are singlet states, the derivative lineshape is only due to the orbital Zeeman effect. Since they originate from the singlet excited states, the strengths of these peaks are greater than the triplet MLCT band. In the experimental spectrum, the small shoulder peak above the singlet states is the vibronic peak, arising from the coupling of ^1E_u electronic state and

state	ω_{0J}/eV	ω_{0J}/cm^{-1}	R/a.u.
$^3A_{2u}$	4.1761	33683	−1015.5
$^3A_{2u}$	4.1765	33686	1014.6
^3E_u	4.5319	36553	−5321.4
^3E_u	4.5323	36556	5376.3
^1E_u	5.3779	43376	−43085.0
^1E_u	5.3780	43378	42685.2

Table 4.2. Excitation energies and MCD strengths of $Pt(CN)_4^{2-}$ MLCT transitions in a 4.468×10^{-6} a.u. ($\sim$1.05 T) magnetic field.

vibrational modes of CN bonds.

Both computed MCD spectra of $AuCl_4^-$ and $Pt(CN)_4^{2-}$ are in excellent agreement with experiment in terms of the spectral shape. In the absence of ground state degeneracy, the computed spectral features are equivalent to the $\mathscr{A}$ and $\mathscr{B}$ terms from the point of view of perturbation theory. The temperature dependent $\mathscr{C}$ can only arise from an open-shell ground state configuration. The associated MCD features are rich and spectral assignments are much more complicated than those from a closed-shell ground state.

4.4.3 Temperature-Dependent MCD of Mo(CN)$_8^{3-}$

Octacyanometallate complex $Mo(CN)_8^{3-}$ has a D_{2d} symmetry in solution. [67] In the D_{2d} ligand field (Fig. 4.3), d orbitals split into $b_1(xy)$, $a_1(z^2)$, $e(xz, yz)$, and $b_2(x^2 - y^2)$, with increasing energy. In the ground state of $Mo(CN)_8^{3-}$, a single electron occupies the b_1 orbital of Mo(V), leading to a doublet ground state, $^2B_1$. For open-shell systems, both orbital and spin angular momenta play an equally important role in the MCD spectral assignment, leading to a feature rich and temperature-dependent MCD spectrum. For the following discussion, we define spin aligned in the $+z$ direction as 'α' and $-z$ as 'β'. We only discuss the computed result when the magnetic field is aligned in the $+z$ direction, which has the largest spectral amplitude in the rotational averaged MCD spectra.

Table 4.3 lists the bright excited states with point-group symmetry assignments, com-

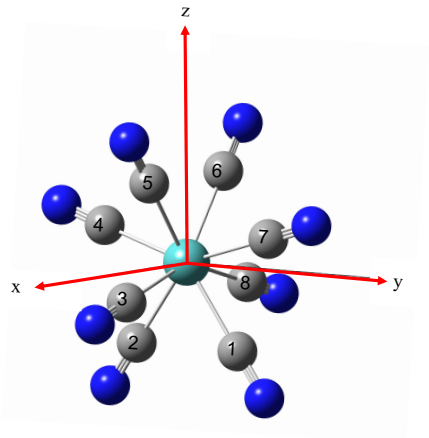

Figure 4.3. Molecular structure of D_{2d} $Mo(CN)_8^{3-}$. Ligands labelled as 3, 5, 6, 8 are in the xz plane, and 1, 2, 4, 7 are in the yz plane.

puted using B3LYP with a GIAO-Sapporo-DKH3-DZP-NO basis for Mo and a GIAO-Sapporo-DZP-2012-NO basis for C and N. The simulated spectrum is shown in Fig. 4.4. For the $Mo(CN)_8^{3-}$ molecular complex, the computed MCD peaks are mainly of the *d-d* and LMCT transition characters. In the simulated energy range, no MLCT excitation is observed.

The $^2B_1$ ground state of $Mo(CN)_8^{3-}$ does not split by the orbital Zeeman effect. The spin Zeeman effect splits the ground state to $^2B_1(\alpha)$ and $^2B_1(\beta)$ micro-states, separated by $|\mathbf{B}|$, with $^2B_1(\beta)$ level lower in energy. Due to the small splitting, both micro-states can be populated when $T > 0$ K, giving rise to the temperature dependent MCD spectrum (discussed later).

The first two peaks at 24.8×10^3 cm^{-1} and 25.0×10^3 cm^{-1} correspond to a linear combination of $e \rightarrow b_1$ and $b_2 \rightarrow b_1$ LMCT transitions with b_1 mainly consisting of Mo-d_{xy} orbitals. These orbital transitions lead to states with mixed $^2B_2$ and ^2E characters, making it difficult to analyze how MCD selection rules in term of the change of angular momentum are manifested in the optical excitations. They also highlight the need for *ab initio* method as presented herein to compute MCD spectral features that are too complex to predict based

State	ω_{0J}/eV	ω_{0J}/cm^{-1}	R/a.u.	Type
$^2B_2 + {}^2E$	3.0812	24852	1608.7	LMCT
$^2B_2 + {}^2E$	3.1006	25008	−1178.4	LMCT
^2E	3.2379	26116	1230.1	LMCT
^2E	3.2400	26132	−1290.2	LMCT
^2E	3.4220	27601	1263.2	LMCT
^2E	3.4224	27604	−1334.5	LMCT
$^2A_1$	3.4618	27922	60.6	*d*-*d*
^2E	4.0133	32369	843.5	*d*-*d*
$^2B_2$	4.5215	36468	1989.0	LMCT
$^2B_2$	4.5262	36506	−846.4	LMCT
^2E	4.5599	36778	−1277.7	LMCT
$^2B_2$	4.6005	37105	−64.5	*d*-*d*

Table 4.3. Excitation energies and the z-component of MCD strengths of $Mo(CN)_8^-$ bright transitions in a 3.404×10^{-5} a.u. ($\sim$8.0 T) magnetic field aligned in the $+z$ direction (see Fig. 4.3 for molecular structure and orientation).

on selection rules.

The third and fourth peaks at 26.1×10^3 cm^{-1} correspond to the $e \rightarrow b_1$ LMCT transition and ^2E excited state. In contrast to the B symmetry, the ^2E symmetry of the second excited state will split into $^2E_+$ and $^2E_-$ due to the orbital Zeeman effect. In addition, the spin Zeeman effect will further split $^2E_+$ and $^2E_-$ into $^2E_+(\alpha)$, $^2E_+(\beta)$, $^2E_-(\alpha)$, and $^2E_-(\beta)$ micro-states. A transition from the $^2B_1$ ground state to the ^2E excited state is associated with $\Delta L = 1$. Because the change in orbital angular momentum already satisfies the MCD selection rule, spin angular momentum must be conserved. As a result, only $^2B_1(\beta) \rightarrow {}^2E_+(\beta)$ and $^2B_1(\beta) \rightarrow {}^2E_-(\beta)$ transitions are allowed from the $^2B_1(\beta)$ ground state and these two transitions form a derivative lineshape as they absorb left- and right-circularly polarized photons, respectively. As the temperature increases, the population of the $^2B_1(\alpha)$ ground micro-state also increases. The allowed transitions from the $^2B_1(\alpha)$ ground micro-state are $^2B_1(\alpha) \rightarrow {}^2E_+(\alpha)$, and $^2B_1(\alpha) \rightarrow {}^2E_-(\alpha)$, whose MCD strengths have an opposite sign compared to those originated from the $^2B_1(\beta)$ micro-state. Similar

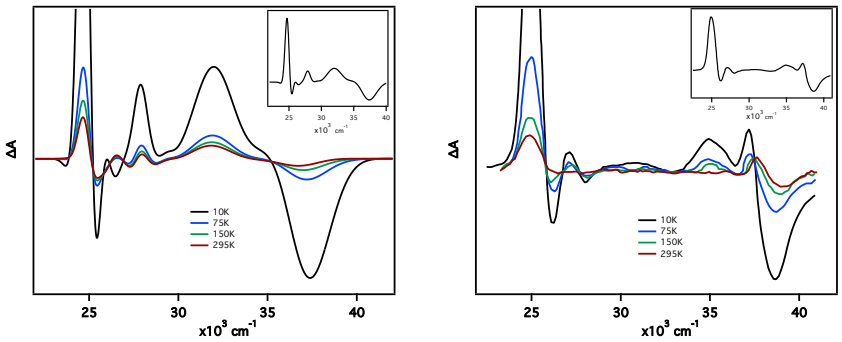

Figure 4.4. (**Left**) Simulated temperature-dependent MCD spectra of $Mo(CN)_8^{3-}$ in a 3.404×10^{-5} a.u. ($\sim$8.0 T) magnetic field. An arbitrary unit is used for the MCD strength. In order to produce a spectrum with a similar band shape compared to experiment, two different Gaussian broadening parameters are used at different energy ranges. For peaks with energies below 0.1341 a.u., Gaussian broadening with $\sigma = 0.0023$ was used; above 0.1341 a.u., $\sigma = 0.008$ was used. (**Right**) Experimental temperature dependent MCD spectra of $Mo(CN)_8^{3-}$, digitized from Ref. 67. Insets are the MCD spectra at 10K.

explanations also hold for the two peaks at 27.6×10^3 cm^{-1} in Tab. 4.3.

The peak at 27.9×10^3 cm^{-1} is a *d*-*d* transition from $b_1(d_{xy})$ to $a_1(d_{z^2})$, giving rise to a $^2A_1$ excited state. The magnetic field splits the $^2A_1$ state into $^2A_1(\alpha)$ and $^2A_1(\beta)$ microstates through the spin Zeeman effect. In the absence of orbital Zeeman splitting in the $^2B_1$ ground state and $^2A_1$ excited state, the MCD selection rule dictates that spin angular momentum must change sign during a transition. As a result, only $^2B_1(\beta) \rightarrow {}^2A_1(\alpha)$ and $^2B_1(\alpha) \rightarrow {}^2A_1(\beta)$ are allowed, with the former dominating at low temperature and the latter seeing more population as the temperature increases. Since these two transitions are of different signs of the MCD strength, their temperature dependent populations will lead to a temperature dependent MCD spectrum. Similarly, the excitation at 37.1×10^3 cm^{-1} is also a spin-flip *d*-*d* transition from $b_1(d_{xy})$ to $b_2(d_{x^2-y^2})$.

The peak around 32.1×10^3 cm^{-1} is the *d*-*d* transition from d_{xy} to d_{xz} and d_{yz} orbitals, resulting in a ^2E excited state. This transition is weakly allowed due to the spin-orbit coupling. Like in the ^2E LMCT state, where the spin angular momentum is conserved since

the transition changes the orbital angular momentum.

The analysis above suggests that all transitions from a B symmetry ground state to a A or B symmetry excited state requires a change in spin angular momentum to be MCD active; transitions to E symmetry excited state must conserve spin. All transitions from the higher energy $^2B_1(\alpha)$ micro-state are of an opposite sign of MCD strength compared to those from the $^2B_1(\beta)$ micro-state. As a result, the overall MCD spectrum depends on the relative population of the ground micro-states.

The temperature dependent MCD spectrum of $Mo(CN)_8^{3-}$ is computed using Eq. (4.26). Figure 4.4 shows that the temperature dependence of the main MCD features is correctly simulated with the method introduced here. At the low temperature ($T = 10$ K), the $^2B_1(\beta)$ ground micro-state has a much greater population (64%) than the $^2B_1(\alpha)$ micro-state. Thus, the averaged MCD is dominated by features arising from the $^2B_1(\beta)$ micro-state. As the temperature increases, the population of the $^2B_1(\alpha)$ micro-state increases, and the resulting MCD intensity cancels that from the $^2B_1(\beta)$ micro-state. As a result, the overall strength of the peaks decreases as the temperature increases.

4.5 Conclusion

In the current work, we present a relativistic, two-component TDDFT response theory for simulating temperature-dependent magnetic circular dichroism spectra of molecular complexes. The method is based on a two-component non-collinear formalism that variationally includes both relativistic corrections and magnetic field perturbation. In order to correctly model magnetic field effects within a relativistic Dirac equation, restricted magnetic-balance condition is used in conjunction with the four- to two-component transformation.

We investigated the relativistic effects in MCD spectra for both closed-shell and open-shell molecular systems. MCD selection rules were discussed in conjunction with orbital and spin symmetries. The simulated spectra are in very good agreement with the experiment measurements. In all test cases, relativistic effects play an important role, particularly, spin-orbit coupling introduces additional MCD spectral features arising from spin-forbidden

excitations in closed-shell and open-shell systems. The temperature-dependence of the MCD spectrum of an open-shell metal complex was satisfactorily demonstrated using the method introduced in this work.

However, for systems with more than one unpaired electron, the linear response TDDFT is not able to capture all the micro-states of a nearly degenerate ground state. One has to resort to variational, relativistic, multi-reference electronic structure theories. [63, 69]

Chapter 5

SIMULATING MAGNETIC CIRCULAR DICHROISM SPECTRA WITH REAL-TIME TIME-DEPENDENT DENSITY FUNCTIONAL THEORY IN GAUGE INCLUDING ATOMIC ORBITALS

Magnetic circular dichroism (MCD) spectra are able to provide insights to the geometric, electronic, and magnetic properties of chemical systems. However, they can be challenging to understand and simulate given the need to simultaneously treat both the finite magnetic and optical fields. Thus, efficient simulations are desired to understand the spectra and resolve the molecular electronic states. Real-time dynamics are used widely in the simulation of electronic spectroscopies such as absorption as well as electronic circular dichroism, but simulating MCD with real-time dynamics is technically and theoretically challenging. In this work, we introduce a real-time dynamics based *ab initio* method with a non-perturbative treatment of a static magnetic field with London orbitals for simulating the MCD spectra of closed-shell systems. Effects of a magnetic field are included variationally in the spin-free non-relativistic Hamiltonian. Real-time time dependent density functional theory dynamics are then performed, from which we compute the response function in the presence of the external magnetic field, giving the MCD spectrum. The method developed in this paper is applied to simulate the MCD spectra for pyrimidine, pyrazine, and 1,4-naphthoquinone. Results are discussed and compared to experiment. The work in this chapter is adapted with permission from S. Sun, R. Beck, D. Williams-Young, and X. Li. Simulating Magnetic Circular Dichroism Spectra with Real-Time Time-Dependent Density Functional Theory in Gauge Including Atomic Orbitals. *J. Chem. Theory Comput.*, 15:6824-6831, 2019.

5.1 Introduction

In magnetic circular dichroism (MCD) experiments, the breaking of degeneracies due to the application of a magnetic field, which couples the (spin and/or orbital) angular momentum to the field, giving rise to additional spectroscopic features that are otherwise inaccessible at zero field. [6] There have been many successful developments to compute MCD spectra with response theory including single residue of the quadratic response function, [17] the complex polarization propagator method, [82, 141, 142] and magnetically perturbed time-dependent density functional theory (TDDFT). [133, 134, 137] Configuration interaction (CI) base techniques include truncated CI with a sum-over-states expression and a perturbative treatment of the magnetic field and spin-orbit coupling, [61, 62] as well as a multi-configurational self-consistent-field (MC-SCF) with quasi-degenerate perturbation theory to include Zeeman effects with spin-couplings. [37, 39, 55] The technique of using London orbitals at zero magnetic field has been applied in the *perturbative* calculation of MCD at the level of EOM-CC, TDHF, and TDDFT, mitigating the gauge-origin dependence of finite atom-centered basis sets. [16, 74, 75, 81] Recently, a new class of *ab initio* computational MCD methods using a variational treatment of the magnetic field has been developed within the linear response complex time-dependent Hartree-Fock (ℂ-TDHF) framework. [152]

Compared to response theory based methods, real-time time-dependent theory has many unique advantages. Real-time approaches can resolve a broad spectra in a single short time simulation. This is particularly useful for systems with high density of states. For DFT based methods, real-time dynamics also avoid the implementation of functional second derivatives. We refer readers to Ref. 43 for a recent review on real-time electronic structure theory. For absorption spectra and electronic circular dichroism, [44, 168] real-time approaches only need to treat the perturbing electric field. The calculation of MCD spectra, however, requires the inclusion of both static magnetic and perturbing electric fields. Real-time electronic dynamics using a real-space local density approximation (LDA) have been applied to simulate effective $\mathscr{A}$ and $\mathscr{B}$ terms of MCD spectra. [89]

Within the density functional theory framework, advanced functional formalisms have been developed to describe molecules in the presence of a magnetic field. The inclusion of a magnetic field effect has been represented either by the functional dependence of current density in current-density-functional theory (CDFT) [12, 157–161] or the functional dependence of the magnetic field in magnetic-field density functional theory (BDFT), [122, 123] where both of these methods can be mathematically shown as equivalent. [48] When compared to full-configuration interaction, it has been observed that the exchange-correlation functional does not depend strongly on the magnetic field. [122]

In this paper, we introduce a real-time TDDFT approach using the generalized gradient approximation (GGA) of the magnetic-field density functional theory in an atomic orbital basis. In the time-dependent variational approach, the treatment of the magnetic perturbation is included non-perturbatively. Effects of a static, uniform magnetic field are included variationally with London orbitals, [4, 10, 23, 56, 57, 80, 101, 152, 153, 167] which provide the most satisfactory solution to correct for the gauge-origin problem when an incomplete Gaussian-type basis is used. [22, 29, 30, 38, 59, 84, 90, 127]

5.2 Methodology

5.2.1 Computing MCD Spectrum with Real-Time Electronic Structure Methods

MCD spectrum measures the response of a molecular system perturbed by a static magnetic field and probed by left and right circularly polarized light. This type of measurement can be described by a time-dependent Hamiltonian which consists of a time-independent and a time-dependent component, $H = H_0 + V_t$.

The magnetic field perturbations can be described by the time-independent Hamiltonian, $H_0 = h_0 + W$, where W is the two-electron interaction, and h_0 is the one-electron Hamiltonian defined in Eq. (3.4). [152, 153] It can be written as

$$h_0 = -\frac{1}{2}\boldsymbol{\nabla}^2 + \frac{1}{2}(-i\mathbf{r} \times \nabla) \cdot \mathbf{B} + \frac{1}{8}(\mathbf{B} \times \mathbf{r})^2 + \sum_A \frac{Z_A}{|\mathbf{r} - \mathbf{R}_A|} \tag{5.1}$$

The second term in Eq. (5.1) includes orbital Zeeman contributions, and the third term describes diamagnetism of a molecular system.

Using the electric-dipole approximation in the length gauge, $V_t = -\mathbf{r} \cdot \mathbf{E}_W$, for the interaction between the system and the probing optical field, the MCD spectra (in molar ellipticity with the conventional unit of Degree$(\mathrm{mol/L})^{-1}\mathrm{m}^{-1}\mathrm{Gauss}^{-1}$) can be computed using the following expression [134]

$$[\theta]_M = \Gamma \sum_J R_J \omega f(\omega - \omega_{0J}^{\gamma}) \tag{5.2}$$

where the rotatory strength R_J is defined as:

$$R_J = -\frac{1}{3} \frac{\sum_{\alpha\beta\gamma} \varepsilon_{\alpha\beta\gamma} \mathrm{Im}(\langle 0 \left|\mu_\alpha\right| J\rangle^{\gamma} \langle J \left|\mu_\beta\right| 0\rangle^{\gamma})}{\mu_B |\mathbf{B}|} \tag{5.3}$$

$\langle 0 \left|\mu_\alpha\right| J\rangle$ is the transition dipole and ω_{0J}^{γ} is the excitation energy from ground state to the excited state J in the presence of a static magnetic field. $f(\omega - \omega_{0J}^{\gamma})$ is the band shape function, which for fixed molecular structures we assume infinite excited state lifetime, thus $f(\omega - \omega_{0J}^{\gamma})$ can be written as a delta function, $\delta(\omega - \omega_{0J}^{\gamma})$. $\epsilon_{\alpha\beta\gamma}$ is Levi-Civita symbol ($\epsilon_{xyz} = \epsilon_{yzx} = \epsilon_{zxy} = 1$, $\epsilon_{yxz} = \epsilon_{xzy} = \epsilon_{zyx} = -1$, otherwise 0). Γ is a collection of physical constants. [119] R_J, ω, and f are in atomic units. We use superscript γ to explicitly denote the direction of the applied magnetic field. For detailed derivation of this expression, we refer readers to Reference 152.

Relating MCD Spectrum to Response Function Formalism

Thus, in order to compute MCD spectra using Eq. (5.2), one needs to extract the imaginary component of the quantity $\langle 0 \left|\mu_\alpha\right| J\rangle^{\gamma} \langle J \left|\mu_\beta\right| 0\rangle^{\gamma}$ from RT-TDDFT electronic dynamics. However, this is not a quantity that can be easily obtained from direct analyses of time-dependent observables, *e.g.*, Fourier transformation of electric dipoles. In this work, we propose a response function based technique that can be used to resolve MCD spectra from

real-time electronic structure simulations. In the following, we will present derivations that transform Eq. (5.2) into a response function formalism of the time-dependent signals.

We start by using the following expression,

$$\sum_J \mathrm{Im}(A_{0J}^{\alpha\beta,\gamma})\delta(\omega-\omega_{0J}^{\gamma}) \approx \sum_J [\mathrm{Im}(A_{0J}^{\alpha\beta,\gamma})\delta(\omega-\omega_{0J}^{\gamma}) - \mathrm{Im}(A_{0J}^{\beta\alpha,\gamma})\delta(\omega+\omega_{0J}^{\gamma})] \tag{5.4}$$

where

$$A_{0J}^{\alpha\beta,\gamma} = \langle 0\,|\mu_\alpha|\,J\rangle^\gamma \langle J\,|\mu_\beta|\,0\rangle^\gamma = (A_{0J}^{\beta\alpha,\gamma})^* \tag{5.5}$$

The δ function in Eq. (5.4) can be defined as the following limit, [26]

$$\delta(\omega-\omega_{0J}^{\gamma}) = \frac{1}{\pi}\lim_{\eta\to 0^+}\frac{\eta}{(\omega-\omega_{0J}^{\gamma})^2+\eta^2} \tag{5.6}$$

Using this relationship, Eq. (5.4) can be written as,

$$\begin{aligned}
&\sum_J \mathrm{Im}(A_{0J}^{\alpha\beta,\gamma})\delta(\omega-\omega_{0J}^{\gamma}) \\
&\approx \frac{1}{\pi}\sum_J \lim_{\eta\to 0^+}\left[\frac{\mathrm{Im}(A_{0J}^{\alpha\beta,\gamma})\eta}{(\omega-\omega_{0J}^{\gamma})^2+\eta^2} - \frac{\mathrm{Im}(A_{0J}^{\beta\alpha,\gamma})\eta}{(\omega+\omega_{0J}^{\gamma})^2+\eta^2}\right] \\
&= \frac{1}{\pi}\sum_J \lim_{\eta\to 0^+}\left[\frac{\mathrm{Im}(A_{0J}^{\alpha\beta,\gamma})\eta}{(\omega-\omega_{0J}^{\gamma}+i\eta)(\omega-\omega_{0J}^{\gamma}-i\eta)} - \frac{\mathrm{Im}(A_{0J}^{\beta\alpha,\gamma})\eta}{(\omega+\omega_{0J}^{\gamma}+i\eta)(\omega+\omega_{0J}^{\gamma}-i\eta)}\right]
\end{aligned} \tag{5.7}$$

Recognizing that $\mathrm{Re}[A_{0J}^{\alpha\beta,\gamma} - (A_{0J}^{\alpha\beta,\gamma})^*] = 0$ and $\mathrm{Im}[A_{0J}^{\alpha\beta,\gamma} - (A_{0J}^{\alpha\beta,\gamma})^*] = 2\mathrm{Im}(A_{0J}^{\alpha\beta,\gamma})$, we can

rewrite Eq. (5.7) and factor out $\omega - \omega_{0J}^{\gamma} - i\eta$ and $\omega + \omega_{0J}^{\gamma} - i\eta$ in the denominators,

$$\begin{aligned}
&\frac{1}{2\pi}\sum_J \lim_{\eta\to 0^+}\begin{pmatrix} \frac{\mathrm{Re}[A_{0J}^{\alpha\beta,\gamma}-(A_{0J}^{\alpha\beta,\gamma})^*](\omega-\omega_{0J}^{\gamma})+\mathrm{Im}[A_{0J}^{\alpha\beta,\gamma}-(A_{0J}^{\alpha\beta,\gamma})^*]\eta}{(\omega-\omega_{0J}^{\gamma}+i\eta)(\omega-\omega_{0J}^{\gamma}-i\eta)} \\ -\frac{\mathrm{Re}[A_{0J}^{\beta\alpha,\gamma}-(A_{0J}^{\beta\alpha,\gamma})^*](\omega+\omega_{0J}^{\gamma})+\mathrm{Im}[A_{0J}^{\beta\alpha,\gamma}-(A_{0J}^{\beta\alpha,\gamma})^*]\eta}{(\omega+\omega_{0J}^{\gamma}+i\eta)(\omega+\omega_{0J}^{\gamma}-i\eta)} \end{pmatrix} \\
&= \frac{1}{2\pi}\sum_J \lim_{\eta\to 0^+}\mathrm{Re}\left[\frac{[A_{0J}^{\alpha\beta,\gamma}-(A_{0J}^{\alpha\beta,\gamma})^*](\omega-\omega_{0J}^{\gamma}-i\eta)}{(\omega-\omega_{0J}^{\gamma}+i\eta)(\omega-\omega_{0J}^{\gamma}-i\eta)} - \frac{[A_{0J}^{\beta\alpha,\gamma}-(A_{0J}^{\beta\alpha,\gamma})^*](\omega+\omega_{0J}^{\gamma}-i\eta)}{(\omega+\omega_{0J}^{\gamma}+i\eta)(\omega+\omega_{0J}^{\gamma}-i\eta)}\right] \\
&= \frac{1}{2\pi}\sum_J \lim_{\eta\to 0^+}\mathrm{Re}\left[\frac{A_{0J}^{\alpha\beta,\gamma}-(A_{0J}^{\alpha\beta,\gamma})^*}{\omega-\omega_{0J}^{\gamma}+i\eta} - \frac{A_{0J}^{\beta\alpha,\gamma}-(A_{0J}^{\beta\alpha,\gamma})^*}{\omega+\omega_{0J}^{\gamma}+i\eta}\right] \qquad (5.8)
\end{aligned}$$

Using the definition of the response function $\langle\!\langle \mu_\alpha; \mu_\beta \rangle\!\rangle_\omega^\gamma$, [112, 114]

$$\langle\!\langle \mu_\alpha; \mu_\beta \rangle\!\rangle_\omega^\gamma = \lim_{\eta\to 0^+} \frac{\langle 0 |\mu_\alpha| J\rangle^\gamma \langle J |\mu_\beta| 0\rangle^\gamma}{\omega - \omega_{0J} + i\eta} - \frac{\langle 0 |\mu_\beta| J\rangle^\gamma \langle J |\mu_\alpha| 0\rangle^\gamma}{\omega + \omega_{0J} + i\eta} \qquad (5.9)$$

it is easy to see that Eq. (5.4) in the form of Eq. (5.8) can be simplified to

$$\sum_J \mathrm{Im}(A_{0J}^{\alpha\beta,\gamma})\delta(\omega - \omega_{0J}^{\gamma}) \approx \frac{1}{2\pi}\sum_J \mathrm{Re}(\langle\!\langle \mu_\alpha; \mu_\beta \rangle\!\rangle_\omega^r - \langle\!\langle \mu_\beta; \mu_\alpha \rangle\!\rangle_\omega^r) \qquad (5.10)$$

The final working equation for calculating MCD spectra becomes,

$$\begin{aligned}
[\theta]_M &= -\frac{\Gamma}{3\mu_B|\mathbf{B}|}\sum_{\alpha\beta\gamma}\omega\varepsilon_{\alpha\beta\gamma}\mathrm{Im}(\langle 0 |\mu_\alpha| n\rangle^\gamma \langle n |\mu_\beta| 0\rangle^\gamma)\delta(\omega - \omega_{0J}^{\gamma}) \\
&= -\frac{\Gamma}{6\pi\mu_B|\mathbf{B}|}\sum_{\alpha\beta\gamma}\omega\varepsilon_{\alpha\beta\gamma}\mathrm{Re}(\langle\!\langle \mu_\alpha; \mu_\beta \rangle\!\rangle_\omega^\gamma - \langle\!\langle \mu_\beta; \mu_\alpha \rangle\!\rangle_\omega^\gamma) \qquad (5.11)
\end{aligned}$$

Calculating MCD spectra using the first expression in Eq. (5.11) requires the computation of the transition dipole moments and excitation energies in the presence of an external magnetic field. These quantities can be obtained using the linear response formalism of the TDHF/TDDFT equation. [152] Alternatively, MCD spectra can be evaluated using the second expression in Eq. (5.11) which works with real-time time-dependent electronic structure methods.

Relating Time-Dependent Signals to Response Function Formalism

In this section, we will derive the relationship between the response function formalism in Eq. (5.11) and time-dependent signals obtained from real-time simulations. We will assume a variational treatment of the static magnetic field applied in the $\gamma \in x, y, z$ direction and that all time-dependent observables are collected in the presence of the magnetic field.

With an electrical δ-kick of intensity κ applied at $t = 0$ in direction $\beta \in x, y, z$, the perturbation Hamiltonian of the electric field can be expanded in the frequency domain as

$$\hat{V}_t = \delta(t)\hat{\mu}_\beta^\gamma \kappa_\beta = \frac{\hat{\mu}_\beta^\gamma \kappa_\beta}{2\pi} \int_{-\infty}^{\infty} e^{-i\omega t} d\omega \tag{5.12}$$

where all the frequencies have the same amplitude. Such an electric field perturbation will lead to the time-evolution of the dipole moment of a molecular system.

The time-evolution of the α-component of the dipole moment, μ_α, can be expressed as [112]

$$\mu_\alpha^\gamma(t) - \mu_\alpha^\gamma(0) = -\int_{-\infty}^{t} i\langle 0|[\hat{\mu}_\alpha, e^{i\hat{H}_0(t'-t)}\hat{V}_{t'}\, e^{-i\hat{H}_0(t'-t)}]|0\rangle^\gamma \; dt' \tag{5.13}$$

Substituting Eq. (5.12) into the Eq. (5.13) followed by a time-frequency transformation, we have

$$\begin{aligned} \mu_\alpha^\gamma(\omega) &= \int_{-\infty}^{\infty} (\mu_\alpha^\gamma(t) - \mu_\alpha^\gamma(0)) e^{i\omega t} dt \\ &= -\frac{\kappa_\beta}{2\pi} \int_{-\infty}^{\infty} e^{i\omega t} dt \int_{-\infty}^{\infty} e^{-i\omega' t} d\omega' \int_{-\infty}^{t} i\langle 0|[\hat{\mu}_\alpha, e^{i\hat{H}_0(t'-t)}\hat{\mu}_\beta\, e^{-i\hat{H}_0(t'-t)}]|0\rangle^\gamma \; dt' \end{aligned} \tag{5.14}$$

One can show that Eq. (5.14) can be equivalently written in a response function form, [112, 114]

$$\mu_\alpha^\gamma(\omega) = \kappa_\beta \langle\!\langle \mu_\alpha; \mu_\beta \rangle\!\rangle_\omega^\gamma \tag{5.15}$$

where the response function is defined in Eq. (5.9). For detailed derivation, we refer readers to Reference 112.

Using Eq. (5.15) in Eq. (5.11), we can write the final expression for computing the MCD molar ellipticity in Degree$(\mathrm{mol/L})^{-1}\mathrm{m}^{-1}\mathrm{Gauss}^{-1}$ using quantities in atomic units calculated from real-time electronic dynamics:

$$[\theta]_M = -0.0014802 \times \frac{1}{6\pi|\mathbf{B}|} \sum_{\alpha\beta\gamma} \omega\, \varepsilon_{\alpha\beta\gamma} \mathrm{Re}\left(\frac{\mu_\alpha^\gamma(\omega)}{\kappa^\beta} - \frac{\mu_\beta^\gamma(\omega)}{\kappa^\alpha} \right) \tag{5.16}$$

where $\mu_\alpha^\gamma(\omega)$, ω, $|\mathbf{B}|$, κ^β are in atomic units.

Note that the working equation Eq. (5.16) is similar to that in Reference 89 which was derived via the perturbation of wave function. The derivation presented here builds a connection between the real-time signal and the response function formalism. This approach is also generally applicable to other types of spectra. Observables computed using the linear response function with the non-perturbative treatment of magnetic field derived herein are similar to those calculated using the quadratic response function [17] or the gradient of linear response [133, 134, 137].

Since the non-perturbative treatment of magnetic field can account for the splitting of excited states and perturbation of transition dipole at the orbital level, the response theory based formalism presented here is able to treat the effects equivalent to $\mathscr{A}$ and $\mathscr{B}$ terms. However, the simulation of $\mathscr{C}$ term effect of open-shell system requires the inclusion of spin-orbit coupling, which cannot be simulated directly using the non-relativistic formalism.

5.2.2 Density-Functional Theory with Complex-Valued Orbitals

The molecular orbitals are expanded in a basis of complex-valued London orbitals [101].

$$\phi_j(\mathbf{r}) = \sum_\mu C_{\mu j} \tilde{\chi}_\mu(\mathbf{r}, \mathbf{k}_A) \tag{5.17}$$

$$\tilde{\chi}_\mu(\mathbf{r}, \mathbf{k}_A) = \chi_\mu(\mathbf{r} - \mathbf{R}_A) e^{i\mathbf{k}_A \cdot (\mathbf{r} - \mathbf{R}_A)} \tag{5.18}$$

where $\{\chi_\mu(\mathbf{r}-\mathbf{R}_A)\}$ are real atomic orbital (AO) basis functions centered at $\mathbf{R}_A$. The exponential form of the London orbital phase factor defines the local gauge origin at each nuclear center in the presence of magnetic field with a plane wave vector described by $\mathbf{k}_A = \frac{\mathbf{R}_A \times \mathbf{B}}{2}$, where $\mathbf{B}$ is the external magnetic field.

In the presence of an external magnetic field, the Kohn-Sham matrix in the London orbital basis for a closed-shell system is defined as [157]:

$$\begin{aligned}\mathbf{F}' = \quad & \mathbf{T} + \mathbf{V} + \mathbf{J}[\mathbf{P}'] + \mathbf{V}^{\mathrm{xc}}[\mathbf{P}'] - \frac{1}{2}c_{\mathrm{x}}\mathbf{K}[\mathbf{P}'] - \frac{i}{2}\mathbf{L}\cdot\mathbf{B} \\ & + \frac{1}{8}\big\{(B_y^2+B_z^2)\mathbf{q}_{xx} + (B_x^2+B_z^2)\mathbf{q}_{yy} + (B_x^2+B_y^2)\mathbf{q}_{zz} \\ & - 2B_xB_y\mathbf{q}_{xy} - 2B_yB_z\mathbf{q}_{yz} - 2B_xB_z\mathbf{q}_{xz}\big\} \end{aligned} \tag{5.19}$$

where $\mathbf{L}_{\mu\nu} = \langle\tilde{\chi}_\mu|\mathbf{r}\times\boldsymbol{\nabla}|\tilde{\chi}_\nu\rangle$ and $\langle\mathbf{q}_{nm}\rangle_{\mu\nu} = (\tilde{\chi}_\mu|\hat{r}_n\hat{r}_m|\tilde{\chi}_\nu\rangle$ are the orbital-angular momentum and electric quadrupole integrals, respectively. We also use a primed notation for the magnetic field perturbed Kohn-Sham ($\mathbf{F}'$) and density ($\mathbf{P}'$) matrices. Equation (5.19) corresponds to a pure density functional when $c_{\mathrm{x}} = 0$.

The magnetic-field density functional theory formalism [122, 123] is used in this implementation, where the functional does not explicitly depend on the magnetic field. Since the magnetic field perturbs the electron density and its derivatives, the density functional will implicitly depend on the magnetic field.

The Coulomb ($\mathbf{J}$) and exchange ($\mathbf{K}$) matrix elements are defined as:

$$J_{\mu\nu}[\mathbf{P}'] = \sum_{\lambda\kappa}(\tilde{\chi}_\mu\tilde{\chi}_\nu|\tilde{\chi}_\kappa\tilde{\chi}_\lambda)P'_{\lambda\kappa} \tag{5.20}$$

$$K_{\mu\nu}[\mathbf{P}'] = \sum_{\lambda\kappa}(\tilde{\chi}_\mu\tilde{\chi}_\lambda|\tilde{\chi}_\kappa\tilde{\chi}_\nu)P'_{\lambda\kappa} \tag{5.21}$$

The recursive relationships for evaluating one- and two-electron integrals using complex valued London orbitals have been presented in Ref. 118.

Using London atomic orbitals in Kohn-Sham DFT also implies that the evaluation of

matrix elements of $\mathbf{V}^{\text{xc}}$ requires a careful scrutiny because the density matrix and atomic orbitals are complex-valued. For GGA, the following quantities need to be evaluated on a numerical grid in order to compute the matrix element of $V^{\text{xc}}_{\mu\nu}$

$$\begin{aligned} V^{\text{xc}}_{\mu\nu} &= \frac{\partial E^{\text{xc}}}{\partial P_{\nu\mu}} \\ &= \sum_i w_i \left[\frac{\partial f^{\text{xc}}}{\partial \rho(\mathbf{r})} \tilde{\chi}^*_\mu(\mathbf{r}) \tilde{\chi}_\nu(\mathbf{r}) \right]_{\mathbf{r}=\mathbf{r}_i} + \sum_i w_i \left[\frac{\partial f^{\text{xc}}}{\partial \nabla\rho(\mathbf{r})} (\nabla\tilde{\chi}^*_\mu(\mathbf{r}) \tilde{\chi}_\nu(\mathbf{r}) + \tilde{\chi}^*_\mu(\mathbf{r}) \nabla\tilde{\chi}_\nu(\mathbf{r})) \right]_{\mathbf{r}=\mathbf{r}_i} \end{aligned} \tag{5.22}$$

where i runs over all the grid points. f^{xc} defines a density functional that depends on density variables. The expressions for evaluating $\frac{\partial f^{\text{xc}}}{\partial \rho}$ and $\frac{\partial f^{\text{xc}}}{\partial \nabla \rho}$ are usually obtained through a chain rule using auxiliary density variables (see Refs. 28, 118 for implementation details for both spin collinear and non-collinear cases.). $\{w_i\}$ are weights of the integration grid points based on the Becke multi-center numerical integration scheme. [8, 147]. Note that because London orbitals are complex valued, the $\mathbf{V}^{xc}$ becomes a complex-valued quantity, even though $\frac{\partial f^{\text{xc}}}{\partial \rho(\mathbf{r})}$, and $\frac{\partial f^{\text{xc}}}{\partial \nabla \rho(\mathbf{r})}$ are real-valued quantities in the KS formalism and real-time dynamics.

In the evaluation of density and basis set gradients, the derivative of primitive London atomic orbitals with respect to electronic coordinate $\mathbf{r}_j$ is needed. The following expression is derived and used in this work,

$$\begin{aligned} &\frac{\partial}{\partial r_j} \tilde{g}_\mu(\mathbf{r} - \mathbf{R}_A; \mathbf{k}_A; \mathbf{a}; \zeta_\alpha) \\ &= -2\zeta_\alpha \tilde{g}_\mu(\mathbf{r} - \mathbf{R}_A; \mathbf{k}_A; \mathbf{a} + \mathbf{1}_j; \zeta_\alpha) + a_j \tilde{g}_\mu(\mathbf{r} - \mathbf{R}_A; \mathbf{k}_A; \mathbf{a} - \mathbf{1}_j; \zeta_\alpha) + i(k_A)_j \tilde{g}_\mu(\mathbf{r} - \mathbf{R}_A; \mathbf{k}_A; \mathbf{a}; \zeta_\alpha) \end{aligned} \tag{5.23}$$

where g is the primitive London atomic orbitals centered at $\mathbf{R}_A$ with orbital angular momentum $\mathbf{a}$ and Gaussian exponent ζ.

5.2.3 Equation-of-Motion of Real-Time TDDFT

The evolvement of the system is by a time-integration of the Liouville-von Neumann equation:

$$i\frac{\partial \mathbf{P}}{\partial t} = [\mathbf{F}, \mathbf{P}] \tag{5.24}$$

with the modified midpoint and unitary transformation (MMUT) approach. [15,43,92,93,97] See 43 for a recent review on RT-TDDFT.

5.3 Computational Detail

All molecular geometries were optimized [91] in the absence of a magnetic field using the GAUSSIAN16 computational chemistry software package [33] using the B3LYP [9, 88, 107] functional and the 6-31G(d) basis. [31, 52]

RT-TDDFT calculations in a magnetic filed with a GIAO basis were carried out with the CHRONUS QUANTUM open source package [165]using the B3LYP [9, 88, 107] functional and the London-6-31G(d) basis. [31, 52]. The magnetic field strength is 2.238×10^{-5} a.u. ($\sim$5.26 T), comparable to that used in experiments. [13, 70] At $t < 0$, the ground state SCF was converged with a magnetic field applied in direction γ. The external magnetic field is applied throughout the RT-TDDFT dynamics. At $t = 0$, an electrical δ-kick is applied in the direction β. After the pulse, the system evolves according to Eq. (5.24). At each timestep, the expectation value of electric dipole $\boldsymbol{\mu}(t)$ is evaluated. In order to obtain a spectral broadening, a damping factor, Γ, in the Fourier transformation is used:

$$\mu_\alpha^\gamma(\omega) = \int_{-\infty}^{\infty} (\mu_\alpha^\gamma(t) - \mu_\alpha^\gamma(0)) \exp\big(-\frac{t}{\Gamma}\big) e^{i\omega t} dt \tag{5.25}$$

The value of Γ is determined in order to reproduce the experimental linewidth. Six separate dynamics for each test molecule are carried out with the external magnetic fields applied in the x, y, and z directions and a pulsed electric field in two directions orthogonal to the magnetic field. The simulation stepsize is 0.05 a.u. ($\sim$ 0.0012 fs). The simulation time is

100 fs for pyrimidine, pyrazine and 1,4-naphthoquinone and 500 fs for sodium anion. The electric field strength is 10^{-5} a.u.

5.4 Benchmark and Discussion

5.4.1 Sodium Anion

Figure 5.1 compares the MCD spectra of sodium anion in a 5.0×10^{-5} a.u. ($\sim$11.75 T) magnetic field, computed with the real-time TDHF and the linear response TDHF formalisms, respectively. [152] The MCD spectra computed using these two different methods are indistinguishable. An external magnetic field introduces orbital Zeeman interactions that break the three-fold degeneracy of the p orbitals, giving rise to two peaks of opposite sign which leads to a derivative shape, shown in Fig. 5.1. This benchmark shows that the real-time and the linear response approaches produce equivalent MCD spectra at the weak field limit.

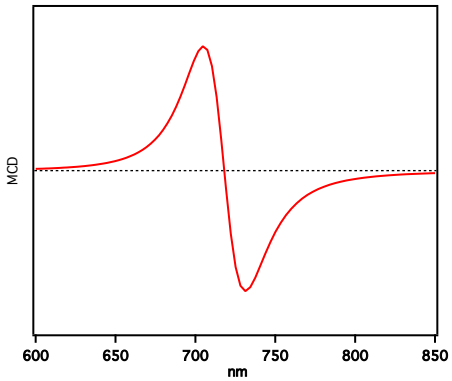

Figure 5.1. Simulated MCD spectra of Na^- $s \rightarrow p$ transitions in a 5×10^{-5} a.u. ($\sim$11.75 T) magnetic field. An arbitrary unit and spectral broadening with a damping factor of $\Gamma = 500$ a.u. are used.

5.4.2 Pyrimidine and Pyrazine

Pyrimidine and pyrazine are structural isomers of six-membered heterocyclic ring (Fig. 5.2). With UV/Vis absorption spectroscopy, these two isomers are not differentiable because they

(A) (B)

Figure 5.2. (A) Pyrimidine, (B) Pyrazine

have very similar linear absorption spectra. In this case, MCD can be a powerful experimental tool to analyze the photochemical properties of structural isomers due to the difference in their point group symmetry. In addition, since their $n \rightarrow \pi^*$ and $\pi \rightarrow \pi^*$ transitions give rise to alternating positive and negative MCD peaks, they are frequently used as benchmark systems for theoretical simulations. [13, 16, 70, 74, 75, 134]

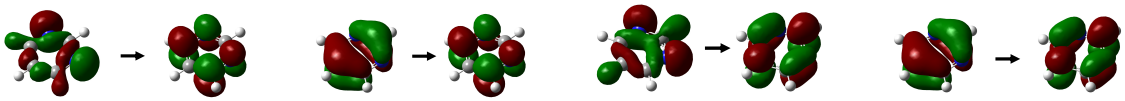

(A) (B) (C) (D)

Figure 5.3. Main molecular orbital contributions to optical excitations in pyrimidine.

In the C_{2v} point group, pyrimidine has several low-lying allowed optical transitions. The first peak at 3.5×10^4 cm^{-1} is the $n \rightarrow \pi^*$ transition, giving rise to the the $1B_1$ excited state, with correpsponding molecular orbitals shown in Fig. 5.3A. The next two excitations are associated with the $1B_2$ and $2B_1$ excited states, with the $\pi \rightarrow \pi^*$ (Fig. 5.3B) and $n \rightarrow \pi^*$ (Fig. 5.3C) characteristics, located at 4.7×10^4 cm^{-1} and 4.9×10^4 cm^{-1}, respectively. The last, and strongest, excitation in this simulated spectral range is the $\pi \rightarrow \pi^*$ excitation (Fig. 5.3D) from the ground state to the $1A_1$ state.

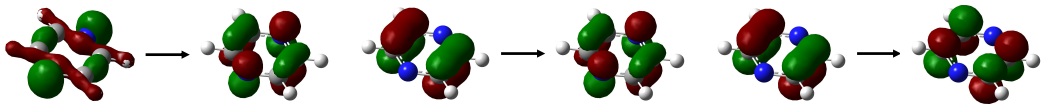

(A) (B) (C)

Figure 5.4. Main molecular orbital contributions to optical excitations in pyrazine.

The pyrazine molecule has the D_{2h} symmetry. The first peak at 3.1×10^4 cm^{-1} corresponds to the excitation from the ground state to the B_{3u} state. This transition is dominated by the $n \rightarrow \pi^*$ transition, where the electron in the lone pair orbital of N atom is excited to π^* orbital (Fig. 5.4A). The next two excitations in pyrazine both have the $\pi \rightarrow \pi^*$ character and give rise to the B_{2u} and B_{1u} states (Fig. 5.4B and Fig. 5.4C).

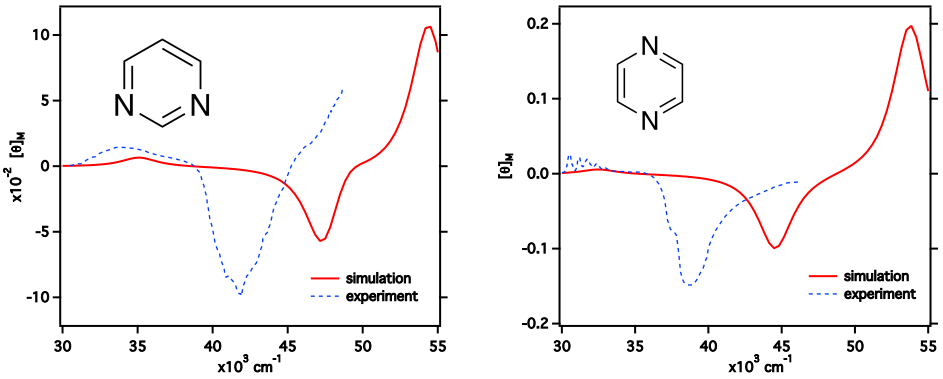

(A) (B)

Figure 5.5. Simulated MCD spectra of pyrimidine (Fig. 5.5A) and pyrazine (Fig. 5.5B) in a 2.238×10^{-5} a.u. ($\sim$5.26 T) magnetic field, with a damping factor of 150 a.u. Experimental MCD spectra from Ref. 70 are also plotted in dashed blue curves.

The MCD spectra of pyrimidine and pyrazine computed using the RT-TDDFT method introduced in this paper are shown in Fig. 5.5, compared to experiments. [13, 70] For these closed shell molecules, the excited states with singlet spins have no degeneracy. Therefore,

Pyrimidine	$\omega'_{0J}/\mathrm{cm}^{-1}$	$\omega_{0J}/\mathrm{cm}^{-1}$
$1B_1$	3.512×10^4	3.506×10^4
$1B_2$	4.732×10^4	4.734×10^4
$2B_1$	4.916×10^4	4.880×10^4
$1A_1$	5.452×10^4	5.440×10^4

Pyrazine	$\omega'_{0J}/\mathrm{cm}^{-1}$	$\omega_{0J}/\mathrm{cm}^{-1}$
B_{3u}	3.077×10^4	3.248×10^4
B_{2u}	4.448×10^4	4.454×10^4
B_{1u}	5.385×10^4	5.376×10^4

Table 5.1. Excitation energies of pyrimidine and pyrazine molecules in a 2.238×10^{-5} a.u. ($\sim$5.26 T) magnetic field. ω'_{0J} is the estimated excitation energy from the real-time spectra. ω_{0J} is the excitation energy computed using the linear response formalism of the corresponding TDDFT in the absence of the external magnetic field.

the MCD signals is driven by the $\mathscr{B}$ term, which is caused by the magnetic perturbation to the transition dipole. The estimated energies for these characteristic excitations (ω'_{0J}) from the real-time spectra are summarized in Tab. 5.1 and compared to absorption peaks (ω_{0J}) in the absence of the external magnetic field. The computed $n \to \pi^*$ transitions are in excellent agreement with experimental measurements. However, the $\pi \to \pi^*$ transitions in both molecules are blue-shifted by 0.6 eV, compared to experiments, although the computed signs and relative magnitudes of all transitions are in agreement with experiments. Compared to the absorption spectra of linearly polarized light, although the presence of an external magnetic field gives rise to a different spectral shape it only slightly shifts the spectral positions. This comparison suggests that the disagreement with experiments is likely due to the choice of functional. These results, computed using the time-dependent variational method, are also consistent with calculations using the excited state gradients. [75] Perturbative calculations overestimate the magnitude of the $1B_2$ state of pyrimidine and this work underestimated its intensity compared to the experiment.

5.4.3 1,4-Naphthoquinone

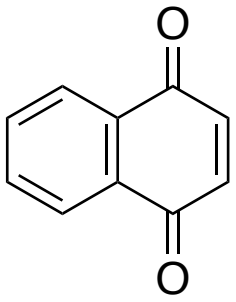

Figure 5.6. 1,4-naphthoquinone

The real-time approach is particularly convenient when simulating a broad spectral range with many excited states. Figure 5.7 plots the computed MCD spectrum of 1,4-naphthoquinone using the RT-TDDFT approach. Compared to the available experimental result [105] at the low energy range, the computed MCD spectrum are in good agreement with experiment. Figure 5.7B plots a broad energy range (0-30 eV) of the computed MCD spectrum. In contrast to solving for all excited states in a generalized eigenvalue problem, real-time approach can produce a broad band MCD spectrum with only three dynamic simulations.

5.5 Conclusion

In this paper, a real-time time-dependent density functional theory (RT-TDDFT) method, with a variational treatment of the static magnetic perturbation in London orbital basis, for simulating MCD spectra is developed and applied to several azaheterocycles. The MCD spectra can be obtained by the simulation of the linear response function. The Kohn-Sham formalism with finite magnetic field is extended to the time-dependent case at the level of hybrid functionals. Due to the use of London orbitals, the exchange-correlation energy and potentials are evaluated with complex atomic orbitals.

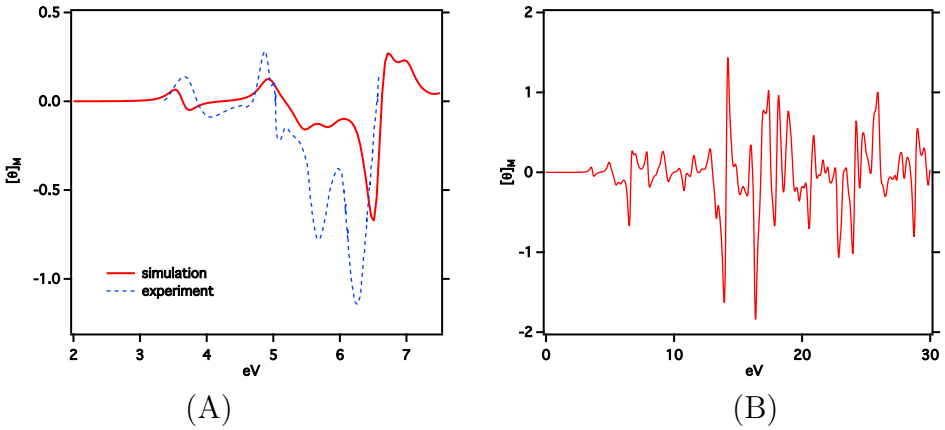

Figure 5.7. Simulated MCD spectrum of 1,4-naphthoquinone in a 2.238×10^{-5} a.u. ($\sim$5.26 T) magnetic field, with a damping factor of 150 a.u. Experimental MCD spectrum from Ref. 105 is also plotted in a dashed blue curve. Note that the experimental first ionization energy of 1,4-naphthoquinone is $\sim$9.4eV. [109] Spectral features above the first ionization threshold correspond to excitations of deeper valence electrons.

RT-TDDFT simulations of pyrimidine and pyrazine predict correct signs of MCD absorption peaks, although excitation energies of the $\pi \rightarrow \pi^*$ transitions are blue-shifted compared to experiment. This work also highlights a unique advantage of the RT-TDDFT approach through the computation of a broad MCD spectrum of 1,4-Naphthoquinone using six dynamic simulations.

The scope of the simulation is limited to the effective $\mathscr{A}$ and $\mathscr{B}$ terms in MCD. Future directions include the development to enable the simulation of open-shell system MCD spectra and the $\mathscr{C}$ term using the time-dependent variational approach.

Chapter 6

FOUR COMPONENT RELATIVISTIC FORMALISM WITH GAUGE INCLUDING ATOMIC ORBITALS

In this section, we briefly give the relativistic four component formalism with gauge-including atomic orbitals in the presence of external magentic field.

The one electron Dirac Hamiltonian is given in Eq. (4.1). In four component relativistic formalism, there are several choices for two component Hamiltonian, for example, Coulomb interaction, Gaunt interaction, Breit interaction. For simplicity, we discuss the Coulomb ($\frac{1}{r_{12}}$) and Gaunt ($\frac{1}{r_{12}} - \frac{\boldsymbol{\alpha}_1 \cdot \boldsymbol{\alpha}_2}{r_{12}}$) interactions.

6.1 Two Spinor Basis

Four component wave function are called four spinor. They can be expanded with two spinor basis. Define four spinor

$$\psi = \begin{pmatrix} \psi^L \\ \psi^S \end{pmatrix} \tag{6.1}$$

where the two spinors are expanded by two spinor basis as

$$\psi^L = \sum_{\mu=1}^{2NB} a_\mu^L \tilde{\chi}_\mu^L, \quad \psi^S = \sum_{\mu=1}^{2NB} a_\mu^S \tilde{\chi}_\mu^S \tag{6.2}$$

where NB is the number of spatial basis function. $\tilde{\chi}^X$ is the two spinor basis.

$$\tilde{\chi}_\mu^L = \begin{pmatrix} \tilde{\chi}_\mu \\ 0 \end{pmatrix} \quad \text{when } 0 < \mu \leq NB, \qquad \tilde{\chi}_\mu^L = \begin{pmatrix} 0 \\ \tilde{\chi}_{\mu-NB} \end{pmatrix} \quad \text{when } NB < \mu \leq 2NB \tag{6.3}$$

$\tilde{\chi}_\mu$ is the spatial basis function. In this context, it is gauge including atomic orbital

(GIAO). Here, $X = L, S$. $1 \leq \mu \leq NB$. In the presence of magnetic field, restricted magnetic balance is applied for the large and small component spinor basis.

6.2 Restricted Magnetic Balance

The relationship between the large and small component two spinor basis is

$$\tilde{\chi}_\mu^S = \frac{1}{2mc}[\sigma \cdot (\mathbf{p} + \mathbf{A})]\tilde{\chi}_\mu^L = \frac{1}{2mc}\sigma \cdot (-i\nabla + \frac{1}{2}\mathbf{B} \times \mathbf{r})\tilde{\chi}_\mu^L \tag{6.4}$$

this relation ensures that in the non-relativistic limit, where the speed of light becomes infinity, the Dirac equation becomes Pauli equation like in Eq. (4.8).

6.3 Restricted Magnetic Balance in Detail

In Eq. (6.4), the Pauli matrices are defined as

$$\sigma_x = \begin{pmatrix} 0 & 1 \\ 1 & 0 \end{pmatrix}, \quad \sigma_y = \begin{pmatrix} 0 & -i \\ i & 0 \end{pmatrix}, \quad \sigma_z = \begin{pmatrix} 1 & 0 \\ 0 & -1 \end{pmatrix}, \tag{6.5}$$

so

$$\begin{aligned} \sigma \cdot \nabla &= \begin{pmatrix} 0 & \nabla_x \\ \nabla_x & 0 \end{pmatrix} + \begin{pmatrix} 0 & -i\nabla_y \\ i\nabla_y & 0 \end{pmatrix} + \begin{pmatrix} \nabla_z & 0 \\ 0 & -\nabla_z \end{pmatrix} \\ &= \begin{pmatrix} \nabla_z & \nabla_x - i\nabla_y \\ \nabla_x + i\nabla_y & -\nabla_z \end{pmatrix} \end{aligned} \tag{6.6}$$

For α spinor basis $\tilde{\chi}_\mu^L = \begin{pmatrix} \tilde{\chi}_\mu \\ 0 \end{pmatrix}$ $(\mu <= NB)$,

$$\sigma \cdot \nabla \tilde{\chi}_\mu^L = \begin{pmatrix} \nabla_z & \nabla_x - i\nabla_y \\ \nabla_x + i\nabla_y & -\nabla_z \end{pmatrix} \begin{pmatrix} \tilde{\chi}_\mu \\ 0 \end{pmatrix} = \begin{pmatrix} \partial_z \tilde{\chi}_\mu \\ (\partial_x + i\partial_y)\tilde{\chi}_\mu \end{pmatrix} \tag{6.7}$$

and the α spinor basis for small component

$$\tilde{\chi}_\mu^S = \frac{-i}{2c}\begin{pmatrix} \partial_z\tilde{\chi}_\mu \\ (\partial_x + i\partial_y)\tilde{\chi}_\mu \end{pmatrix} + \frac{\sigma\cdot(\mathbf{B}\times\mathbf{r})}{4c}\tilde{\chi}_\mu^S \tag{6.8}$$

Now we take a look at the second term on the right hand side

$$\begin{aligned}\frac{\sigma\cdot(\mathbf{B}\times\mathbf{r})}{4c} =& \frac{1}{4c}[(\mathbf{B}\times\mathbf{r})_x\sigma_x + (\mathbf{B}\times\mathbf{r})_y\sigma_y + (\mathbf{B}\times\mathbf{r})_z\sigma_z] \\ =& \frac{1}{4c}\begin{pmatrix} (\mathbf{B}\times\mathbf{r})_z & (\mathbf{B}\times\mathbf{r})_x - i(\mathbf{B}\times\mathbf{r})_y \\ (\mathbf{B}\times\mathbf{r})_x + i(\mathbf{B}\times\mathbf{r})_y & -(\mathbf{B}\times\mathbf{r})_z \end{pmatrix} \\ =& \frac{1}{4c}\begin{pmatrix} B_x r_y - B_y r_x & B_y r_z - B_z r_y - i(B_z y_x - B_x y_z) \\ B_y r_z - B_z r_y + i(B_z r_x - B_x r_z) & -(B_x r_y - B_y r_x) \end{pmatrix}\end{aligned} \tag{6.9}$$

thus

$$\frac{\sigma\cdot(\mathbf{B}\times\mathbf{r})}{4c}\tilde{\chi}_\mu^L = \frac{1}{4c}\begin{pmatrix} (B_x r_y - B_y r_x)\tilde{\chi}_\mu \\ [(B_y r_z - B_z r_y) + i(B_z r_x - B_x r_z)]\tilde{\chi}_\mu \end{pmatrix} \tag{6.10}$$

In summary, for α small component spinor, we have

$$\tilde{\chi}_\mu^S = \frac{-i}{2c}\begin{pmatrix} \partial_z\tilde{\chi}_\mu \\ (\partial_x + i\partial_y)\tilde{\chi}_\mu \end{pmatrix} + \frac{1}{4c}\begin{pmatrix} (B_x r_y - B_y r_x)\tilde{\chi}_\mu \\ [(B_y r_z - B_z r_y) + i(B_z r_x - B_x r_z)]\tilde{\chi}_\mu \end{pmatrix} \tag{6.11}$$

For β spinor basis $\tilde{\chi}_\mu^L = \begin{pmatrix} 0 \\ \tilde{\chi}_\mu \end{pmatrix}$ $(NB < \mu <= 2NB)$, For β spinor basis of small component,

$$\sigma\cdot\nabla\tilde{\chi}_\mu^L = \begin{pmatrix} (\partial_x - i\partial_y)\tilde{\chi}_{\mu-NB} \\ -\partial_z\tilde{\chi}_{\mu-NB} \end{pmatrix} \tag{6.12}$$

and

$$\frac{\sigma\cdot(\mathbf{B}\times\mathbf{r})}{4c}\tilde{\chi}_\mu^L=\frac{\sigma\cdot(\mathbf{B}\times\mathbf{r})}{4c}\begin{pmatrix}0\\ \tilde{\chi}_{\mu-NB}\end{pmatrix}=\frac{1}{4c}\begin{pmatrix}\left[(B_yr_z-B_zr_y)-i(B_zr_x-B_xr_z)\right]\tilde{\chi}_{\mu-NB}\\ (-B_xr_y-B_yr_x)\tilde{\chi}_{\mu-NB}\end{pmatrix} \tag{6.13}$$

so in summary, for β small component spinors,

$$\tilde{\chi}_\mu^S=\begin{pmatrix}(\partial_x-i\partial_y)\tilde{\chi}_{\mu-NB}\\ -\partial_z\tilde{\chi}_{\mu-NB}\end{pmatrix}+\frac{1}{4c}\begin{pmatrix}(B_yr_z-B_zr_y)-i(B_zr_x-B_xr_z)\tilde{\chi}_{\mu-NB}\\ (-B_xr_y-B_yr_x)\tilde{\chi}_{\mu-NB}\end{pmatrix} \tag{6.14}$$

If χ_μ^L is in Cartesian Gaussian gauge including atomic orbital, we have

$$\partial_i\tilde{\chi}_\mu(\mathbf{a})=-2\zeta\tilde{\chi}(\mathbf{a}+\mathbf{1}_i)+N_i(\mathbf{a})\tilde{\chi}(\mathbf{a}-\mathbf{1}_i)+ik_{ai}\tilde{\chi}(\mathbf{a}) \tag{6.15}$$

where $\mathbf{a}=(a_x,a_y,a_z)$ is the orbital angular momentum of $\tilde{\chi}_\mu$. $\tilde{\chi}(\mathbf{a})$ stands for Gauge including Cartesian Gaussian orbital with angular momentum $\mathbf{a}$.

The only missing piece now in Eq. (6.11) and Eq. (6.14) are $r_i\tilde{\chi}_\mu$, we have

$$r_i\tilde{\chi}_\mu(\mathbf{a})=(r_i-A_i+A_i)\tilde{\chi}_\mu(\mathbf{a})=\tilde{\chi}_\mu(\mathbf{a}+\mathbf{1}_i)+A_i\tilde{\chi}_\mu(\mathbf{a}) \tag{6.16}$$

6.4 Two Electron Integrals in Molecular Orbital

The coulomb integral of four spinors are

$$(pq|rs)=\int d\mathbf{r}_1\int d\mathbf{r}_2\begin{pmatrix}\psi_p^L(1)\\ \psi_p^S(1)\end{pmatrix}^\dagger\begin{pmatrix}\psi_q^L(1)\\ \psi_q^S(1)\end{pmatrix}\frac{1}{r_{12}}\begin{pmatrix}\psi_r^L(2)\\ \psi_r^S(2)\end{pmatrix}^\dagger\begin{pmatrix}\psi_s^L(2)\\ \psi_s^S(2)\end{pmatrix} \tag{6.17}$$

$$=(p^Lq^L|r^Ls^L)+(p^Lq^L|r^Ss^S)+(p^Sq^S|r^Ls^L)+(p^Sq^S|r^Ss^S) \tag{6.18}$$

For Gaunt interaction, since we have

$$\psi_p^\dagger \alpha \psi_q = \begin{pmatrix} \psi_p^{L\dagger} & \psi_p^{S\dagger} \end{pmatrix} \begin{pmatrix} 0 & \sigma \\ \sigma & 0 \end{pmatrix} \begin{pmatrix} \psi_q^L \\ \psi_q^S \end{pmatrix} = \psi_p^{S\dagger} \sigma \psi_q^L + \psi_p^{L\dagger} \sigma \psi_q^S \tag{6.19}$$

So

$$(p\alpha q|r\alpha s) = (p^L \sigma q^S|r^L \sigma s^S) + (p^L \sigma q^S|r^S \sigma s^L) + (p^S \sigma q^L|r^L \sigma s^S) + (p^S \sigma q^L|r^S \sigma s^L) \tag{6.20}$$

6.5 Fock Matrix

The Fock matrix elements are defined in Ref.25. However, there are many typos in the definition in Ref.25, which will affect the implementation. We decide to list the corrected definition of Fock matrix here to avoid confusion.

For a Dirac-Coulomb-Gaunt Hamiltonian, the Fock matrix in four spinor MO is (by Slater-Condon rule)

$$f_{pq} = h_{pq} + \sum_{i=1}^{N} [(pq|ii) - (pi|iq)] - \sum_{i=1}^{N} [(p\alpha q|i\alpha i) - (p\alpha i|i\alpha q)] \tag{6.21}$$

where N is the number of occupied electron.

In two spinor,

$$\begin{aligned} f_{pq}^{LL} = h_{pq}^{LL} + \sum_{i=1}^{N} [(p^L q^L|i^L i^L) + (p^L q^L|i^S i^S) - (p^L i^L|i^L q^L)] \\ - \sum_{i=1}^{N} [-(p^L \sigma i^S|i^S \sigma q^L)] \end{aligned} \tag{6.22}$$

$$f_{pq}^{SS} = h_{pq}^{SS} + \sum_{i=1}^{N}[(p^S q^S|i^L i^L) + (p^S q^S|i^S i^S) - (p^S i^S|i^S q^S)] - \sum_{i=1}^{N}[-(p^S \sigma i^L|i^L \sigma q^S)] \tag{6.23}$$

$$f_{pq}^{LS} = h_{pq}^{LS} + \sum_{i=1}^{N}[-(p^L i^L|i^S q^S)] - \sum_{i=1}^{N}[(p^L \sigma q^S|i^L \sigma i^S) + (p^L \sigma q^S|i^S \sigma i^L) - (p^L \sigma i^S|i^L \sigma q^S)]$$

$$f_{pq}^{SL} = h_{pq}^{SL} + \sum_{i=1}^{N}[-(p^S i^S|i^L q^L)] - \sum_{i=1}^{N}[(p^S \sigma q^L|i^L \sigma i^S) + (p^S \sigma q^L|i^S \sigma i^L) - (p^S \sigma i^L|i^S \sigma q^L)]$$

Expand the two spinors in AO basis

$$\psi_p^{X\dagger} = \sum_{\mu=1}^{2NB} a_{\mu p}^{X*} \tilde{\chi}_\mu^{X\dagger} \tag{6.24}$$

$$\psi_q^{X} = \sum_{\mu=1}^{2NB} a_{\nu q}^{X} \tilde{\chi}_\nu^{X} \tag{6.25}$$

$$\psi_r^{X\dagger} = \sum_{\mu=1}^{2NB} a_{\kappa r}^{X*} \tilde{\chi}_\kappa^{X\dagger} \tag{6.26}$$

$$\psi_s^{X} = \sum_{\lambda=1}^{2NB} a_{\lambda s}^{X} \tilde{\chi}_\lambda^{X} \tag{6.27}$$

Then Fock matrix elements in 2 spinor AO basis are

$$f_{\mu\nu}^{LL} = h_{\mu\nu}^{LL} + \sum_{i=1}^{N}[a_{\kappa i}^{L*} a_{\lambda i}^{L} 5(\mu^L\nu^L|\kappa^L\lambda^L) + a_{\kappa i}^{S*} a_{\lambda i}^{S}(\mu^L\nu^L|\kappa^S\lambda^S) - a_{\kappa i}^{L*} a_{\lambda i}^{L}(\mu^L\lambda^L|\kappa^L\nu^L)]$$
$$- \sum_{i=1}^{N}[-a_{\kappa i}^{S*} a_{\lambda i}^{S}(\mu^L\sigma\lambda^S|\kappa^S\sigma\nu^L)] \tag{6.28}$$
$$= h_{\mu\nu}^{LL} + D_{\lambda\kappa}^{LL}[(\mu^L\nu^L|\kappa^L\lambda^L) - (\mu^L\lambda^L|\kappa^L\nu^L)]$$
$$+ D_{\lambda\kappa}^{SS}[(\mu^L\nu^L|\kappa^S\lambda^S) + (\mu^L\sigma\lambda^S|\kappa^S\sigma\nu^L)] \tag{6.29}$$

Where the definition of two component density matrix is

$$D_{\mu\nu}^{XY} = \sum_{i=1}^{N} a_{\mu i}^{X} a_{\nu i}^{Y*} \quad X, Y = \{L, S\} \tag{6.30}$$

And we have the Fock matrix for other blocks

$$f_{\mu\nu}^{SS} = h_{\mu\nu}^{SS} + \sum_{i=1}^{N}[a_{\kappa i}^{L*} a_{\lambda i}^{L}(\mu^S\nu^S|\kappa^L\lambda^L) + a_{\kappa i}^{S*} a_{\lambda i}^{S}(\mu^S\nu^S|\kappa^S\lambda^S) - a_{\kappa i}^{S*} a_{\lambda i}^{S}(\mu^S\lambda^S|\kappa^S\nu^S)]$$
$$- \sum_{i=1}^{N}[-a_{\kappa i}^{L*} a_{\lambda i}^{L}(\mu^S\sigma\lambda^L|\kappa^L\sigma\nu^S)] \tag{6.31}$$
$$= h_{\mu\nu}^{SS} + D_{\lambda\kappa}^{LL}[(\mu^S\nu^S|\kappa^L\lambda^L) + (\mu^S\sigma\lambda^L|\kappa^L\sigma\nu^S)]$$
$$+ D_{\lambda\kappa}^{SS}[(\mu^S\nu^S|\kappa^S\lambda^S) - (\mu^S\lambda^S|\kappa^S\nu^S)] \tag{6.32}$$

$$
\begin{aligned}
f^{LS}_{\mu\nu} &= h^{LS}_{\mu\nu} + \sum_{i=1}^{N}[-a^{S*}_{\kappa i}a^{L}_{\lambda i}(\mu^{L}\lambda^{L}|\kappa^{S}\nu^{S})] \\
&\quad - \sum_{i=1}^{N}[a^{L*}_{\kappa i}a^{S}_{\lambda i}(\mu^{L}\sigma\nu^{S}|\kappa^{L}\sigma\lambda^{S}) + a^{S*}_{\kappa i}a^{L}_{\lambda i}(\mu^{L}\sigma\nu^{S}|\kappa^{S}\sigma\nu^{L}) - a^{L*}_{\kappa i}a^{S}_{\lambda i}(\mu^{L}\sigma\lambda^{S}|\kappa^{L}\sigma\nu^{S})] \\
&= h^{LS}_{\mu\nu} + D^{LS}_{\lambda\kappa}[-(\mu^{L}\lambda^{L}|\kappa^{S}\nu^{S}) - (\mu^{L}\sigma\nu^{S}|\kappa^{S}\sigma\nu^{L})] \\
&\quad - D^{SL}_{\lambda\kappa}[(\mu^{L}\sigma\nu^{S}|\kappa^{L}\sigma\lambda^{S}) - (\mu^{L}\sigma\lambda^{S}|\kappa^{L}\sigma\nu^{S})]
\end{aligned} \tag{6.33}
$$

$$
\begin{aligned}
f^{SL}_{\mu\nu} &= h^{SL}_{\mu\nu} + \sum_{i=1}^{N}[-a^{L*}_{\kappa i}a^{S}_{\lambda i}(\mu^{S}\lambda^{S}|\kappa^{L}\nu^{L})] \\
&\quad - \sum_{i=1}^{N}[a^{L*}_{\kappa i}a^{S}_{\lambda i}(\mu^{S}\sigma\nu^{L}|\kappa^{L}\sigma\lambda^{S}) + a^{S*}_{\kappa i}a^{L}_{\lambda i}(\mu^{S}\sigma\nu^{L}|\kappa^{S}\sigma\lambda^{L}) - a^{S*}_{\kappa i}a^{L}_{\lambda i}(\mu^{S}\sigma\lambda^{L}|\kappa^{S}\sigma\nu^{L})] \\
&= h^{SL}_{\mu\nu} + D^{SL}_{\lambda\kappa}[-(\mu^{S}\lambda^{S}|\kappa^{L}\nu^{L}) - (\mu^{S}\sigma\nu^{L}|\kappa^{L}\sigma\lambda^{S})] \\
&\quad - D^{LS}_{\lambda\kappa}[(\mu^{S}\sigma\nu^{L}|\kappa^{S}\sigma\lambda^{L}) - (\mu^{S}\sigma\lambda^{L}|\kappa^{S}\sigma\nu^{L})]
\end{aligned} \tag{6.34}
$$

The next thing to do is to write two-spinor integral in the form of spatial orbital integral. The large component two spinor basis is defined in Eq. (6.3), the details of small component two spinor basis is given in Eq. (6.11) and Eq. (6.14).

BIBLIOGRAPHY

[1] O-A Al-Hujaj and P Schmelcher. Helium in Superstrong Magnetic Fields. *Phys. Rev. A*, 67(2):023403, 2003.

[2] Philip Warren Anderson. *Basic Notions of Condensed Matter Physics*. Benjamin-Cummings, 1984.

[3] G. A. Aucar, T. Saue, L. Visscher, and H. J. Aa. Jensen. On the Origin and Contribution of the Diamagnetic Term in Four-Component Relativistic Calculations of Magnetic Properties. *J. Chem. Phys.*, 110(13):6208–6218, 1999.

[4] Jochen Autschbach. Analyzing NMR Shielding Tensors Calculated with Two-Component Relativistic Methods Using Spin-Free Localized Molecular Orbitals. *J. Chem. Phys.*, 128(16):164112, 2008.

[5] Jochen Autschbach. Relativistic Effects on Electron–Nucleus Hyperfine Coupling Studied with an Exact 2-Component (X2C) Hamiltonian. *J. Chem. Theory Comput.*, 13(2):710–718, 2017.

[6] Laurence D Barron. *Molecular Light Scattering and Optical Activity*. Cambridge University Press, 2009.

[7] Gunter Barth, Edward Bunnenberg, Carl Djerassi, Danny Elder, and Ruth Records. Magnetic Circular Dichroism Studies. Part 10. Investigations of Some Carbonyl Compounds. In *Symposia of the Faraday Society*, volume 3, pages 49–60. Royal Society of Chemistry, 1969.

[8] A. D. Becke. A Multicenter Numerical Integration Scheme for Polyatomic Molecules. *J. Chem. Phys.*, 88(4):2547–2553, 1988.

[9] Axel D Becke. Density-Functional Thermochemistry. III. The Role of Exact Exchange. *J. Chem. Phys.*, 98(7):5648–5652, 1993.

[10] R Bouten, EJ Baerends, E Van Lenthe, L Visscher, G Schreckenbach, and T Ziegler. Relativistic Effects for NMR Shielding Constants in Transition Metal Oxides Using the Zeroth-Order Regular Approximation. *J. Phys. Chem. A*, 104(23):5600–5611, 2000.

[11] AD Buckingham and PJ Stephens. Magnetic Optical Activity. *Annu. Rev. Phys. Chem.*, 17(1):399–432, 1966.

[12] K. Capelle and G. Vignale. Nonuniqueness and Derivative Discontinuities in Density-Functional Theories for Current-Carrying and Superconducting systems. *Phys. Rev. B*, 65:113106, Feb 2002.

[13] Alain Castellan and Josef Michl. Magnetic circular dichroism of cyclic .pi.-electron systems. 4. aza analogs of benzene. *J. Am. Chem. Soc.*, 100(22):6824–6827, 1978.

[14] Lan Cheng, Yunlong Xiao, and Wenjian Liu. Four-Component Relativistic Theory for Nuclear Magnetic Shielding: Magnetically Balanced Gauge-Including Atomic Orbitals. *J. Chem. Phys.*, 131(24):244113, 2009.

[15] Christine M. Isborn and Xiaosong Li and John C. Tully. Tddft ehrenfest dynamics: Collisions between atomic oxygen and graphite clusters. *J. Chem. Phys.*, 126:134307, 2007.

[16] Sonia Coriani, Christof Hättig, Poul Jørgensen, and Trygve Helgaker. Gauge-Origin Independent Magneto-Optical Activity within Coupled Cluster Response Theory. *J. Chem. Phys.*, 113(9):3561–3572, 2000.

[17] Sonia Coriani, Poul Jørgensen, Antonio Rizzo, Kenneth Ruud, and Jeppe Olsen. Ab initio Determinations of Magnetic Circular Dichroism. *Chem. Phys. Lett.*, 300(1-2):61–68, 1999.

[18] Silvio Decurtins and Hans U Guedel. Superexchange in Bis(μ-hydroxo)-Bridged Chromium(III) Dimers. Optical Spectroscopic Study of Singly Excited $^2E_g{}^4A_{2g}$ pair states. *Inorg. Chem.*, 21(10):3598–3606, 1982.

[19] Silvio Decurtins, Hans U Guedel, and Andreas Pfeuti. Optical Spectroscopy of $[(NH_3)_4Cr(OH)_2Cr(NH3)_4]^{4+}$ and $[(en)_2Cr(OH)_2Cr(en)_2]^{4+}$. *Inorg. Chem.*, 21(3):1101–1106, 1982.

[20] Feizhi Ding, Joshua J. Goings, Michael J. Frisch, and Xiaosong Li. Ab Initio Non-Relativistic Spin Dynamics. *J. Chem. Phys.*, 141(21):214111, 2014.

[21] Feizhi Ding, Joshua J. Goings, Hongbin Liu, David B. Lingerfelt, and Xiaosong Li. Ab Initio Two-Component Ehrenfest Dynamics. *J. Chem. Phys.*, 143:114105, 2015.

[22] Feizhi Ding, Wenkel Liang, Craig T. Chapman, Christine M. Isborn, and Xiaosong Li. On the Gauge Invariance of Nonperturbative Electronic Dynamics Using the Time-Dependent Hartree-Fock and Time-Dependent Kohn-Sham. *J. Chem. Phys.*, 135(16):164101, 2011.

[23] R. Ditchfield. Molecular Orbital Theory of Magnetic Shielding and Magnetic Susceptibility. *J. Chem. Phys.*, 56(11):5688–5691, 1972.

[24] Thom H Dunning Jr. Gaussian Basis Sets for Use in Correlated Molecular Calculations. I. The Atoms Boron through Neon and Hydrogen. *J. Chem. Phys.*, 90(2):1007–1023, 1989.

[25] Kenneth G Dyall and Knut Fægri Jr. *Introduction to Relativistic Quantum Chemistry*. Oxford University Press, 2007.

[26] Eleftherios N Economou. *Green's Functions in Quantum Physics*. Springer, 2006.

[27] Franco Egidi, Joshua J. Goings, Michael J. Frisch, and Xiaosong Li. Direct Atomic-Orbital-Based Relativistic Two-Component Linear Response Method for Calculating Excited-State Fine Structures. *J. Chem. Theory Comput.*, 12(8):3711–3718, 2016.

[28] Franco Egidi, Shichao Sun, Joshua J. Goings, Giovanni Scalmani, Michael J. Frisch, and Xiaosong Li. Two-Component Non-Collinear Time-Dependent Spin Density Functional Theory for Excited State Calculations. *J. Chem. Theory Comput.*, 13(6):2591–2603, 2017.

[29] Saul T Epstein. Gauge Invariance of the Hartree-Fock Approximation. *J. Chem. Phys.*, 42(8):2897–2898, 1965.

[30] ST Epstein. Gauge Invariance, Current Conservation, and GIAO's. *J. Chem. Phys.*, 58(4):1592–1595, 1973.

[31] Michelle M Francl, William J Pietro, Warren J Hehre, J Stephen Binkley, Mark S Gordon, Douglas J DeFrees, and John A Pople. Self-consistent molecular orbital methods. xxiii. a polarization-type basis set for second-row elements. *J. Chem. Phys.*, 77(7):3654–3665, 1982.

[32] M. J. Frisch, G. W. Trucks, H. B. Schlegel, G. E. Scuseria, M. A. Robb, J. R. Cheeseman, G. Scalmani, V. Barone, G. A. Petersson, H. Nakatsuji, X. Li, M. Caricato, A. V. Marenich, J. Bloino, B. G. Janesko, R. Gomperts, B. Mennucci, H. P. Hratchian, J. V. Ortiz, A. F. Izmaylov, J. L. Sonnenberg, D. Williams-Young, F. Ding, F. Lipparini,

F. Egidi, J. Goings, B. Peng, A. Petrone, T. Henderson, D. Ranasinghe, V. G. Zakrzewski, J. Gao, N. Rega, G. Zheng, W. Liang, M. Hada, M. Ehara, K. Toyota, R. Fukuda, J. Hasegawa, M. Ishida, T. Nakajima, Y. Honda, O. Kitao, H. Nakai, T. Vreven, K. Throssell, J. A. Montgomery, Jr., J. E. Peralta, F. Ogliaro, M. J. Bearpark, J. J. Heyd, E. N. Brothers, K. N. Kudin, V. N. Staroverov, T. A. Keith, R. Kobayashi, J. Normand, K. Raghavachari, A. P. Rendell, J. C. Burant, S. S. Iyengar, J. Tomasi, M. Cossi, J. M. Millam, M. Klene, C. Adamo, R. Cammi, J. W. Ochterski, R. L. Martin, K. Morokuma, O. Farkas, J. B. Foresman, and D. J. Fox. Gaussian 16 Revision A.03. Gaussian Inc. Wallingford CT 2016.

[33] M. J. Frisch, G. W. Trucks, H. B. Schlegel, G. E. Scuseria, M. A. Robb, J. R. Cheeseman, G. Scalmani, V. Barone, G. A. Petersson, H. Nakatsuji, X. Li, M. Caricato, A. V. Marenich, J. Bloino, B. G. Janesko, R. Gomperts, B. Mennucci, H. P. Hratchian, J. V. Ortiz, A. F. Izmaylov, J. L. Sonnenberg, D. Williams-Young, F. Ding, F. Lipparini, F. Egidi, J. Goings, B. Peng, A. Petrone, T. Henderson, D. Ranasinghe, V. G. Zakrzewski, J. Gao, N. Rega, G. Zheng, W. Liang, M. Hada, M. Ehara, K. Toyota, R. Fukuda, J. Hasegawa, M. Ishida, T. Nakajima, Y. Honda, O. Kitao, H. Nakai, T. Vreven, K. Throssell, J. A. Montgomery, Jr., J. E. Peralta, F. Ogliaro, M. J. Bearpark, J. J. Heyd, E. N. Brothers, K. N. Kudin, V. N. Staroverov, T. A. Keith, R. Kobayashi, J. Normand, K. Raghavachari, A. P. Rendell, J. C. Burant, S. S. Iyengar, J. Tomasi, M. Cossi, J. M. Millam, M. Klene, C. Adamo, R. Cammi, J. W. Ochterski, R. L. Martin, K. Morokuma, O. Farkas, J. B. Foresman, and D. J. Fox. Gaussian16 Revision B.01, 2016. Gaussian Inc. Wallingford CT.

[34] Hideo Fukutome. Unrestricted Hartree–Fock Theory and its Applications to Molecules and Chemical Reactions. *Int. J. Quant. Chem.*, 20(5):955–1065, 1981.

[35] James W Furness, Ulf Ekström, Trygve Helgaker, and Andrew M Teale. Electron Localisation Function in Current-Density-Functional Theory. *Mol. Phys.*, 114(7-8):1415–1422, 2016.

[36] James W Furness, Joachim Verbeke, Erik I Tellgren, Stella Stopkowicz, Ulf Ekström, Trygve Helgaker, and Andrew M Teale. Current Density Functional Theory Using Meta-Generalized Gradient Exchange-Correlation Functionals. *J. Chem. Theory Comput.*, 11(9):4169–4181, 2015.

[37] Dmitry Ganyushin and Frank Neese. First-Principles Calculations of Magnetic Circular Dichroism Spectra. *J. Chem. Phys.*, 128(11):114117, 2008.

[38] Jurgen Gauss and John F Stanton. Electron-Correlated Approaches for the Calculation of NMR Chemical Shifts. *Adv. Chem. Phys.*, 123:355–422, 2002.

[39] Frédéric Gendron, Valerie E Fleischauer, Thomas J Duignan, Brian L Scott, Matthias W Löble, Samantha K Cary, Stosh A Kozimor, Hélène Bolvin, Michael L Neidig, and Jochen Autschbach. Magnetic Circular Dichroism of UCl^{6-} in the Ligand-to-Metal Charge-Transfer Spectral Region. *Phys. Chem. Chem. Phys.*, 19(26):17300–17313, 2017.

[40] J. J. Goings, F. Egidi, and X Li. Current Development of Non-collinear Electronic Structure Theory. *Int. J. Quant. Chem.*, 118:e25398, 2018.

[41] Joshua J. Goings, Feizhi Ding, Ernest R. Davidson, and Xiaosong Li. Approximate Singly Excited States from a Two-Component Hartree Fock Reference. *J. Chem. Phys.*, 143:144106, 2015.

[42] Joshua J. Goings, Joseph M. Kasper, Franco Egidi, Shichao Sun, and Xiaosong Li. Real Time Propagation of the Exact Two Component Time-Dependent Density Functional Theory. *J. Chem. Phys.*, 145(10):104107, 2016.

[43] Joshua J. Goings, Patrick J. Lestrange, and Xiaosong Li. Real-Time Time-Dependent Electronic Structure Theory. *WIREs Comput. Mol. Sci.*, 8(1):e1341, 2018.

[44] Joshua J. Goings and Xiaosong Li. An Atomic Orbital Based Real-Time Time-Dependent Density Functional Theory for Computing Electronic Circular Dichroism Band Spectra. *J. Chem. Phys.*, 144(23):234102, 2016.

[45] Goings, Joshua J and Ding, Feizhi and Frisch, Michael J and Li, Xiaosong. Stability of the Complex Generalized Hartree-Fock Equations. *J. Chem. Phys.*, 142(15):154109, 2015.

[46] JB Goodenough. *Magnetism and the Chemical Bond*. John Wiley & Sons, 1963.

[47] O. Götze, D.J.J. Farnell, R.F. Bishop, P.H.Y. Li, and J. Richter. Heisenberg Antiferromagnet on the Kagomé Lattice With Arbitrary Spin: A Higher-order Coupled Cluster Treatment. *Phys. Rev. B*, 84(22):224428, 2011.

[48] Christopher J. Grayce and Robert A. Harris. Magnetic-Field Density-Functional Theory. *Phys. Rev. A*, 50:3089–3095, Oct 1994.

[49] HF Hameka. Calculation of Magnetic Susceptibilities of Diatomic Molecules: I. General Theory. *Physica*, 28(9):908–916, 1962.

[50] HF Hameka. On Pople's Molecular-Orbital Theory of Diamagnetism. *J. Chem. Phys.*, 37(12):3008–3009, 1962.

[51] Florian Hampe and Stella Stopkowicz. Equation-of-Motion Coupled-Cluster Methods for Atoms and Molecules in Strong Magnetic Fields. *J. Chem. Phys.*, 146(15):154105, 2017.

[52] Praveen C Hariharan and John A Pople. The Influence of Polarization Functions on Molecular Orbital Hydrogenation Energies. *Theor. Chem. Acc.*, 28(3):213–222, 1973.

[53] Masao Hayami, Junji Seino, and Hiromi Nakai. Gauge-Origin Independent Formalism of Two-Component Relativistic Framework Based on Unitary Transformation in Nuclear Magnetic Shielding Constant. *J. Chem. Phys.*, 148(11):114109, 2018.

[54] Martin Head-Gordon and John A Pople. A Method for Two-Electron Gaussian Integral and Integral Derivative Evaluation Using Recurrence Relations. *J. Chem. Phys.*, 89(9):5777–5786, 1988.

[55] Yonaton N. Heit, Dumitru-Claudiu Sergentu, and Jochen Autschbach. Magnetic Circular Dichroism Spectra of Transition Metal Complexes Calculated from Restricted Active Space Wavefunctions. *Phys. Chem. Chem. Phys.*, 21:5586–5597, 2019.

[56] Trygve Helgaker, Sonia Coriani, Poul Jørgensen, Kasper Kristensen, Jeppe Olsen, and Kenneth Ruud. Recent Advances in Wave Function-Based Methods of Molecular-Property Calculations. *Chem. Rev.*, 112(1):543–631, 2012.

[57] Trygve Helgaker, Michał Jaszuński, and Kenneth Ruud. Ab Initio Methods for the Calculation of NMR Shielding and Indirect Spin-Spin Coupling Constants. *Chem. Rev.*, 99(1):293–352, 1999.

[58] Trygve Helgaker and Poul Jørgensen. An Electronic Hamiltonian for Origin Independent Calculations of Magnetic Properties. *J. Chem. Phys.*, 95(4):2595–2601, 1991.

[59] Trygve Helgaker and Peter R. Taylor. Gaussian basis sets and molecular integrals. In David R. Yarkony, editor, *Modern Electronic Structure Theory*, chapter 12, pages 725–856. World Scientific Publishing Co. Pte. Ltd., Singapore, 1995.

[60] Masaru Honda, Kikue Sato, and Shigeru Obara. Formulation of Molecular Integrals over Gaussian Functions Treatable by both the Laplace and Fourier Transforms of Spatial Operators by Using Derivative of Fourier-Kernel Multiplied Gaussians. *J. Chem. Phys.*, 94(5):3790–3804, 1991.

[61] Y Honda, M Hada, M Ehara, H Nakatsuji, J Downing, and J Michl. Relativistic Effects on Magnetic Circular Dichroism Studied by GUHF/SECI Method. *Chem. Phys. Lett.*, 355(3-4):219–225, 2002.

[62] Y Honda, M Hada, M Ehara, H Nakatsuji, and J Michl. Theoretical Studies on Magnetic Circular Dichroism by the Finite Perturbation Method with Relativistic Corrections. *J. Chem. Phys.*, 123(16):164113, 2005.

[63] Hang Hu, Andrew J. Jenkins, Hongbin Liu, Joseph M. Kasper, Michael J. Frisch, and Xiaosong Li. Relativistic Two-Component Multireference Configuration Interaction Method with Tunable Correlation Space. *J. Chem. Theory Comput.*, 16(5):2975–2984, 2020.

[64] Miroslaŵ Ilias and Trond Saue. An Infinite-Order Relativistic Hamiltonian by a Simple One-Step Transformation. *J. Chem. Phys.*, 126:064102, 2007.

[65] Tom JP Irons, Jan Zemen, and Andrew M Teale. Efficient Calculation of Molecular Integrals over London Atomic Orbitals. *J. Chem. Theory Comput.*, 13(8):3636–3649, 2017.

[66] Huseyin Isci and W. Roy Mason. Ligand-to-Metal Charge-Transfer Spectra of Tetrahaloaurate(III) and Trans-Dicyanodihaloaurate(III) Ions. *Inorg. Chem.*, 22(16):2266–2272, 1983.

[67] Huseyin Isci and W. Roy Mason. Electronic Absorption and MCD Spectra for Octacyanometallate Complexes $M(CN)_8^{n-}$, M=Mo(IV), W(IV), n=4 and Mo(V), W(V), n=3. *Inorg. Chim. Acta*, 357(14):4065 – 4072, 2004.

[68] Hyseyin. Isci and W. Roy. Mason. Electronic Structure and Spectra of Square-Planar Cyano and Cyanoamine Complexes of Platinum(II). *Inorg. Chem.*, 14(4):905–912, 1975.

[69] Andrew J. Jenkins, Hongbin Liu, Joseph M. Kasper, Michael J. Frisch, and Xiaosong Li. Variational Relativistic Complete Active Space Self-Consistent Field Method. *J. Chem. Theory Comput.*, 15:2974–2982, 2019.

[70] Akira Kaito, Masahiro Hatano, and Akio Tajiri. CNDO Treatment for Faraday B Terms of Some Azaheterocycles. *J. Am. Chem. Soc.*, 99(16):5241–5246, 1977.

[71] U Kappes and P Schmelcher. Electronic Bond Structure of the H_2^+ Ion in a Strong Magnetic Field: A Study of the Parallel Configuration. *Phys. Rev. A*, 51(6):4542, 1995.

[72] Sarah Karbalaei Khani, Rasmus Faber, Fabrizio Santoro, Christof Hättig, and Sonia Coriani. UV Absorption and Magnetic Circular Dichroism Spectra of Purine, Adenine, and Guanine: A Coupled Cluster Study in Vacuo and in Aqueous Solution. *J. Chem. Theory Comput.*, 15(2):1242–1254, 2019.

[73] Thomas Kjærgaard, Sonia Coriani, and Kenneth Ruud. Ab initio Calculation of Magnetic Circular Dichroism. *WIREs Comput. Mol. Sci.*, 2(3):443–455, 2012.

[74] Thomas Kjærgaard, Branislav Jansík, Poul Jørgensen, Sonia Coriani, and Josef Michl. Gauge-Origin-Independent Coupled Cluster Singles and Doubles Calculation of Magnetic Circular Dichroism of Azabenzenes and Phosphabenzene Using London Orbitals. *J. Phys. Chem. A*, 111(44):11278–11286, 2007.

[75] Thomas Kjærgaard, Poul Jørgensen, Andreas J Thorvaldsen, Paweł Sałek, and Sonia Coriani. Gauge-Origin Independent Formulation and Implementation of Magneto-Optical Activity within Atomic-Orbital-Density Based Hartree- Fock and Kohn- Sham Response Theories. *J. Chem. Theory Comput.*, 5(8):1997–2020, 2009.

[76] Stanislav Komorovsky, Peter J. Cherry, and Michal Repisky. Four-Component Relativistic Time-Dependent Density-Functional Theory Using a Stable Noncollinear DFT Ansatz Applicable to both Closed- and Open-Shell Systems. *J. Chem. Phys.*, 151(18):184111, 2019.

[77] Stanislav Komorovský, Michal Repiský, Olga L. Malkina, and Vladimir G. Malkin. Fully Relativistic Calculations of NMR Shielding Tensors Using Restricted Magnetically Balanced Basis and Gauge Including Atomic Orbitals. *J. Chem. Phys.*, 132(15):154101, 2010.

[78] Stanislav Komorovský, Michal Repiský, Olga L. Malkina, Vladimir G. Malkin, Irina Malkin Ondík, and Martin Kaupp. A Fully Relativistic Method for Calculation of Nuclear Magnetic Shielding Tensors with a Restricted Magnetically Balanced Basis in the Framework of the Matrix Dirac-Kohn-Sham Equation. *J. Chem. Phys.*, 128(10):104101, 2008.

[79] Lukas Konecny, Marius Kadek, Stanislav Komorovsky, Olga L. Malkina, Kenneth Ruud, and Michal Repisky. Acceleration of Relativistic Electron Dynamics by Means of X2C Transformation: Application to the Calculation of Nonlinear Optical Properties. *J. Chem. Theory Comput.*, 12(12):5823–5833, Dec 2016.

[80] Mykhaylo Krykunov and Jochen Autschbach. Calculation of Origin-Independent Optical Rotation Tensor Components in Approximate Time-Dependent Density Functional Theory. *J. Chem. Phys.*, 125(3):034102, 2006.

[81] Mykhaylo Krykunov, Arup Banerjee, Tom Ziegler, and Jochen Autschbach. Calculation of Verdet Constants with Time-Dependent Density Functional Theory: Implementation and Results for Small Molecules. *J. Chem. Phys.*, 122(7):074105, 2005.

[82] Mykhaylo Krykunov, Michael Seth, Tom Ziegler, and Jochen Autschbach. Calculation of the Magnetic Circular Dichroism B Term from the Imaginary Part of the Verdet Constant Using Damped Time-Dependent Density Functional Theory. *J. Chem. Phys.*, 127(24):244102, 2007.

[83] Atsushi Kubo. The Hydrogen Molecule in Strong Magnetic Fields: Optimizations of Anisotropic Gaussian Basis Sets. *J. Phys. Chem. A*, 111(25):5572–5581, 2007.

[84] W Kutzelnigg. Theory of Magnetic Susceptibilities and NMR Chemical Shifts in Terms of Localized Quantities. *Israel J. Chem.*, 19(1-4):193–200, 1980.

[85] Werner Kutzelnigg. Diamagnetism in Relativistic Theory. *Phys. Rev. A*, 67:032109, Mar 2003.

[86] Werner Kutzelnigg and Wenjian Liu. Quasirelativistic Theory Equivalent to Fully Relativistic Theory. *J. Chem. Phys.*, 123:241102, 2005.

[87] Kai K Lange, Erik I Tellgren, MR Hoffmann, and T Helgaker. A Paramagnetic Bonding Mechanism for Diatomics in Strong Magnetic Fields. *Science*, 337(6092):327–331, 2012.

[88] Chengteh Lee, Weitao Yang, and Robert G Parr. Development of the Colle-Salvetti Correlation-Energy Formula into a Functional of the Electron Density. *Phys. Rev. B*, 37(2):785, 1988.

[89] K-M Lee, K Yabana, and GF Bertsch. Magnetic Circular Dichroism in Real-Time Time-Fependent Density Functional Theory. *J. Chem. Phys.*, 134(14):144106, 2011.

[90] Patrick J. Lestrange, Franco Egidi, and Xiaosong Li. The Consequences of Improperly Describing Oscillator Strengths Beyond the Electric Dipole Approximation. *J. Chem. Phys.*, 143:234103, 2015.

[91] Xiaosong Li and Michael J. Frisch. Energy-Represented Direct Inversion in the Iterative Subspace within a Hybrid Geometry Optimization Method. *J. Chem. Theory Comput.*, 2(3):835–839, 2006.

[92] Xiaosong Li, Stanley M. Smith, Alexei N. Markevitch, Dmitri A. Romanov, Robert J. Levis, and H. Bernhard Schlegel. A Time-Dependent Hartree-Fock Approach for Studying the Electronic Optical Response of Molecules in Intense Fields. *Phys. Chem. Chem. Phys.*, 7:233–239, 2005.

[93] Xiaosong Li, John C. Tully, H. Bernhard Schlegel, and Michael J. Frisch. Ab Initio Ehrenfest Dynamics. *J. Chem. Phys.*, 123(8):084106, 2005.

[94] Xiaosong Li, David Williams-Young, Edward F. Valeev, Alessio Petrone, Shichao Sun, Torin Stetina, and Joesph Kasper. Chronus Quantum, Beta 2 Version, 2018. http://www.chronusquantum.org.

[95] Zhendong Li, Yunlong Xiao, and Wenjian Liu. On the Spin Separation of Algebraic Two-Component Relativistic Hamiltonians. *J. Chem. Phys.*, 137:154114, 2012.

[96] Zhendong Li, Yunlong Xiao, and Wenjian Liu. On the Spin Separation of Algebraic Two-Component Relativistic Hamiltonians: Molecular Properties. *J. Chem. Phys.*, 141(5):054111, 2014.

[97] Wenkel Liang, Craig T. Chapman, and Xiaosong Li. Efficient First-Principles Electronic Dynamics. *J. Chem. Phys.*, 134(18):184102, 2011.

[98] W. Liu and D. Peng. Exact Two-component Hamiltonians Revisited. *J. Chem. Phys.*, 131(3):031104, 2009.

[99] Wenjian Liu. Ideas of Relativistic Quantum Chemistry. *Mol. Phys.*, 108:1679–1706, 2010.

[100] Wenjian Liu and Daoling Peng. Infinite-Order Quasirelativistic Density Functional Method Based on the Exact Matrix Quasirelativistic Theory. *J. Chem. Phys.*, 125:044102, 2006.

[101] Fritz London. Théorie quantique des courants interatomiques dans les combinaisons aromatiques. *J. phys. radium*, 8(10):397–409, 1937.

[102] Per-Olov Löwdin and Istvan Mayer. Some Studies of the General Hartree-Fock Method. *Adv. Quantum Chem.*, 24:79–114, 1992.

[103] W. Roy Mason. *A Practical Guide to Magnetic Circular Dichroism Spectroscopy.* John Wiley & Sons, Inc, Hoboken, New Jersey, 2006.

[104] W. Roy Mason and Harry B. Gray. Electronic Structures of Square-Planar Complexes. *J. Am. Chem. Soc.*, 90(21):5721–5729, 1968.

[105] Alfred A Meier and Georges H Wagnière. The Long-Wavelength MCD of Some Quinones and its Interpretation by Semi-empirical MO Methods. *Chem. Phys.*, 113(2):287–307, 1987.

[106] L. Messio, B. Bernu, and C. Lhuillier. Kagomé Antiferromagnet: A Chiral Topological Spin Liquid? *Phys. Rev. Lett.*, 108(20):207204, 2012.

[107] B. Miehlich, A. Savin, H. Stoll, and H. Preuss. Results Obtained with the Correlation Energy Density Functionals of Becke and Lee, Yang and Parr. *Chem. Phys. Lett.*, 157(3):200–206, 1989.

[108] A. Mielke. Exact Ground States for the Hubbard Model on the Kagomé Lattice. *J. Phys. A: Math. Gen.*, 25(16):4335–4345, 1992.

[109] S Millefiori, A Gulino, and M Casarin. UV Photoelectron Spectra, Reduction Potentials and MO Calculations of Intramolecularly Hydrogen-Bonded Naphtoquinones. *J. Chim. Phys.*, 87:317–330, 1990.

[110] Takeshi Noro, Masahiro Sekiya, and Toshikatsu Koga. Segmented contracted basis sets for atoms H through Xe: Sapporo-(DK)-nZP sets (n = D, T, Q). *Theor. Chem. Acc.*, 131(2):1124, Feb 2012.

[111] Takeshi Noro, Masahiro Sekiya, and Toshikatsu Koga. Sapporo-(DKH3)-nZP (n = D, T, Q) sets for the sixth period s-, d-, and p-block atoms. *Theor. Chem. Acc.*, 132(5):1363, Apr 2013.

[112] Jens Oddershede, Poul Jørgensen, and Danny L. Yeager. Polarization Propagator Methods in Atomic and Molecular Calculations. *Comput. Phys. Rep.*, 2(2):33 – 92, 1984.

[113] Małgorzata Olejniczak, Radovan Bast, Trond Saue, and Magdalena Pecul. A Simple Scheme for Magnetic Balance in Four-Component Relativistic Kohn-Sham Calculations of Nuclear Magnetic Resonance Shielding Constants in a Gaussian Basis. *J. Chem. Phys.*, 136(1):014108, 2012.

[114] Jeppe Olsen and Poul Jørgensen. Linear and Nonlinear Response Functions for an Exact State and for an MCSCF State. *J. Chem. Phys.*, 82(7):3235–3264, 1985.

[115] Magdalena Pecul, Trond Saue, Kenneth Ruud, and Antonio Rizzo. Electric Field Effects on the Shielding Constants of Noble Gases: A Four-Component Relativistic Hartree-Fock Study. *J. Chem. Phys.*, 121(7):3051–3057, 2004.

[116] Daoling Peng, Wenjian Liu, Yunlong Xiao, and Lan Cheng. Making Four- and Two-Component Relativistic Density Functional Methods Fully Equivalent Based on the Idea of From Atoms to Molecule. *J. Chem. Phys.*, 127:104106, 2007.

[117] Daoling Peng, Nils Middendorf, Florian Weigend, and Markus Reiher. An Efficient Implementation of Two-Component Relativistic Exact-Decoupling Methods for Large Molecules. *J. Chem. Phys.*, 138:184105, 2013.

[118] Alessio Petrone, David B. Williams-Young, Shichao Sun, Torin F. Stetina, and Xiaosong Li. An Efficient Implementation of Two-Component Relativistic Density Functional Theory with Torque-Free Auxiliary Variables. *Euro. Phys. J. B*, 91(7):169, 2018.

[119] Susan B Piepho and Paul N Schatz. *Group Theory in Spectroscopy: with Applications to Magnetic Circular Dichroism*. Wiley-Interscience, 1983.

[120] JA Pople. Molecular-Orbital Theory of Diamagnetism. I. An Approximate LCAO Scheme. *J. Chem. Phys.*, 37(1):53–59, 1962.

[121] JA Pople. Reply to Letter by HF Hameka. *J. Chem. Phys.*, 37(12):3009–3010, 1962.

[122] Sarah Reimann, Alex Borgoo, Jon Austad, Erik I Tellgren, Andrew M Teale, Trygve Helgaker, and Stella Stopkowicz. Kohn–Sham Energy Decomposition for Molecules in a Magnetic Field. *Mol. Phys.*, 117(1):97–109, 2019.

[123] Sarah Reimann, Alex Borgoo, Erik I. Tellgren, Andrew M. Teale, and Trygve Helgaker. Magnetic-Field Density-Functional Theory (BDFT): Lessons from the Adiabatic Connection. *J. Chem. Theory Comput.*, 13(9):4089–4100, 2017. PMID: 28768100.

[124] Ryan D Reynolds and Toru Shiozaki. Fully Relativistic Self-Consistent Field under a Magnetic Field. *Phys. Chem. Chem. Phys.*, 17(22):14280–14283, 2015.

[125] M. Rigol and R. R. P. Singh. Kagomé Lattice Antiferromagnets and Dzyaloshinsky-Moriya Interactions. *Phys. Rev. B*, 76(18):184403, 2007.

[126] Trond Saue. Relativistic Hamiltonians for Chemistry: A Primer. *ChemPhysChem*, 12:3077–3094, 2011.

[127] Michael Schindler and Werner Kutzelnigg. Theory of Magnetic Susceptibilities and NMR Chemical Shifts in Terms of Localized Quantities. II. Application to Some Simple Molecules. *J. Chem. Phys.*, 76(4):1919–1933, 1982.

[128] Lloyd Seamans and Jan Linderberg. Magneto-Pptical Activity: Gauge-Invariant Calculations in the Random-Phase Approximation. *Mol. Phys.*, 24(6):1393–1405, 1972.

[129] R. Seeger and J. A. Pople. Self-Consistent Molecular Orbital Methods. XVIII. Constraints and Stability in Hartree-Fock Theory. *J. Chem. Phys.*, 66(7):3045–3050, 1977.

[130] Sangita Sen, Kai K. Lange, and Erik I. Tellgren. Excited States of Molecules in Strong Uniform and Nonuniform Magnetic Fields. *J. Chem. Theory Comput.*, 15(7):3974–3990, 2019. PMID: 31117478.

[131] Sangita Sen and Erik I Tellgren. Non-Perturbative Calculation of Orbital and Spin Effects in Molecules Subject to Non-Uniform Magnetic Fields. *J. Chem. Phys.*, 148(18):184112, 2018.

[132] Michael Seth, Jochen Autschbach, and Tom Ziegler. Calculation of the Term of Magnetic Circular Dichroism. a Time-Dependent Density Functional Theory Approach. *J. Chem. Theory Comput.*, 3(2):434–447, 2007.

[133] Michael Seth, Mykhaylo Krykunov, Tom Ziegler, and Jochen Autschbach. Application of Magnetically Perturbed Time-Dependent Density Functional Theory to Magnetic Circular Dichroism. II. Calculation of A Terms. *J. Chem. Phys.*, 128(23):234102, 2008.

[134] Michael Seth, Mykhaylo Krykunov, Tom Ziegler, Jochen Autschbach, and Arup Banerjee. Application of Magnetically Perturbed Time-Dependent Density Functional Theory to Magnetic Circular Dichroism: Calculation of B Terms. *J. Chem. Phys.*, 128(14):144105, 2008.

[135] Michael Seth and Tom Ziegler. Calculation of Excitation Energies of Open-Shell Molecules with Spatially Degenerate Ground States. I. Transformed Reference via an Intermediate Configuration Kohn-Sham Density-Functional Theory and Applications to d1 and d2 Systems with Octahedral and Tetrahedral Symmetries. *J. Chem. Phys.*, 123(14):144105, 2005.

[136] Michael Seth and Tom Ziegler. Calculation of Excitation Energies of Open-Shell Molecules with Spatially Degenerate Ground States. II. Transformed Reference via Intermediate Configuration Kohn-Sham Time Dependent Density Functional Theory Oscillator Strengths and Magnetic Circular Dichroism C Terms. *J. Chem. Phys.*, 124(14):144105, 2006.

[137] Michael Seth and Tom Ziegler. Formulation of Magnetically Perturbed Time-Dependent Density Functional Theory. *J. Chem. Phys.*, 127(13):134108, 2007.

[138] Michael Seth, Tom Ziegler, and Jochen Autschbach. Application of Magnetically Perturbed Time-Dependent Density Functional Theory to Magnetic Circular Dichroism. III. Temperature-Dependent Magnetic Circular Dichroism Induced by Spin-Orbit Coupling. *J. Chem. Phys.*, 129(10):104105, 2008.

[139] D Smith, BE Williamson, and PN Schatz. Identification of the Alkalide, Na-, in Na/NH3 Matrices using MCD. *Chem. Phys. Lett.*, 131(6):457–462, 1986.

[140] Harald Solheim, Luca Frediani, Kenneth Ruud, and Sonia Coriani. An IEF-PCM Study of Solvent Effects on the Faraday $\mathcal{B}$ Term of MCD. *Theor. Chem. Acc.*, 119(1-3):231–244, 2008.

[141] Harald Solheim, Kenneth Ruud, Sonia Coriani, and Patrick Norman. Complex Polarization Propagator Calculations of Magnetic Circular Dichroism Spectra. *J. Chem. Phys.*, 128(9):094103, 2008.

[142] Harald Solheim, Kenneth Ruud, Sonia Coriani, and Patrick Norman. The A and B Terms of Magnetic Circular Dichroism Revisited. *J. Phys. Chem. A*, 112(40):9615–9618, 2008.

[143] EI Solomon, ML Neidig, and G Schenk. *Magnetic Circular Dichroism of Paramagnetic Species*, chapter 2.26, pages 339–349. Elsevier Pergamon, Amsterdam, 2003.

[144] PJ Stephens, FJ Devlin, CFN Chabalowski, and Michael J Frisch. Ab Initio Calculation of Vibrational Absorption and Circular Dichroism Spectra Using Density Functional Force Fields. *J. Phys. Chem.*, 98(45):11623–11627, 1994.

[145] Torin Stetina, Shichao Sun, David B Williams-Yong, and Xiaosong Li. Modeling Magneto-Photoabsorption Using Time-Dependent Complex Generalized Hartree-Fock. *ChemPhotoChem*, 3:739–746, 2019.

[146] Stella Stopkowicz, Jürgen Gauss, Kai K Lange, Erik I Tellgren, and Trygve Helgaker. Coupled-Cluster Theory for Atoms and Molecules in Strong Magnetic Fields. *J. Chem. Phys.*, 143(7):074110, 2015.

[147] R.Eric Stratmann, Gustavo E. Scuseria, and Michael J. Frisch. Achieving Linear Scaling in Exchange-Correlation Density Functional Quadratures. *Chem. Phys. Lett.*, 257(3):213 – 223, 1996.

[148] J. L. Stuber and J. Paldus. Symmetry breaking in the independent particle model. In E. J. Brändas and E. S. Kryachko, editors, *Fundamental World of Quantum Chemistry: A Tribute Volume to the Memory of Per-Olov Löwdin*, pages 67–139. Kluwer Academic Publishers, 2003.

[149] Qiming Sun, Wenjian Liu, Yunlong Xiao, and Lan Cheng. Exact Two-Tomponent Relativistic Theory for Nuclear Magnetic Resonance Parameters. *J. Chem. Phys.*, 131(8):081101, 2009.

[150] Qiming Sun, Yunlong Xiao, and Wenjian Liu. Exact Two-Component Relativistic Theory for NMR Parameters: General Formulation and Pilot Application. *J. Chem. Phys.*, 137(17):174105, 2012.

[151] S. Sun, R. Beck, D. B. Williams-Young, and X. Li. Simulating Magnetic Circular Dichroism Spectra with Real-Time Time-Dependent Density Functional Theory in Gauge Including Atomic Orbitals. *J. Chem. Theory Comput.*, 15:6824–6831, 2019.

[152] Shichao Sun, David Williams-Young, and Xiaosong Li. An Ab Initio Linear Response Method for Computing Magnetic Circular Dichroism Spectra with Nonperturbative Treatment of Magnetic Field. *J. Chem. Theory Comput.*, 15:3162–3169, 2019. PMID: 30933558.

[153] Shichao Sun, David Williams-Young, Torin F. Stetina, and Xiaosong Li. Generalized Hartree-Fock with Non-perturbative Treatment of Strong Magnetic Field: Application to Molecular Spin Phase Transition. *J. Chem. Theory Comput.*, 15:348–356, 2019.

[154] Patrick K. Tamukong, Mark R. Hoffmann, Zhendong Li, and Wenjian Liu. Relativistic GVVPT2 Multireference Perturbation Theory Description of the Electronic States of Y_2 and Tc_2. *J. Phys. Chem. A*, 118(8):1489–1501, 2014.

[155] Erik I Tellgren, Trygve Helgaker, and Alessandro Soncini. Non-Perturbative Magnetic Phenomena in Closed-Shell Paramagnetic Molecules. *Phys. Chem. Chem. Phys.*, 11(26):5489–5498, 2009.

[156] Erik I Tellgren, Alessandro Soncini, and Trygve Helgaker. Nonperturbative ab initio Calculations in Strong Magnetic Fields Using London Orbitals. *J. Chem. Phys.*, 129(15):154114, 2008.

[157] Erik I Tellgren, Andrew M Teale, James W Furness, KK Lange, Ulf Ekström, and Trygve Helgaker. Non-Perturbative Calculation of Molecular Magnetic Properties within Current-Density Functional Theory. *J. Chem. Phys.*, 140(3):034101, 2014.

[158] G. Vignale and Mark Rasolt. Density-Functional Theory in Strong Magnetic Fields. *Phys. Rev. Lett.*, 59:2360–2363, Nov 1987.

[159] G. Vignale and Mark Rasolt. Current- and Spin-Density-Functional Theory for Inhomogeneous Electronic Systems in Strong Magnetic Fields. *Phys. Rev. B*, 37:10685–10696, Jun 1988.

[160] G. Vignale and Mark Rasolt. Density-Functional Theory in Strong Magnetic Fields. *Phys. Rev. Lett.*, 62:115–115, Jan 1989.

[161] G. Vignale and Mark Rasolt. Erratum: Current- and Spin-Density-Functional Theory for Inhomogeneous Electronic Systems in Strong Magnetic Fields. *Phys. Rev. B*, 39:5475–5475, Mar 1989.

[162] L. Visscher and K.G. Dyall. Dirac-Fock Atomic Electronic Structure Calculations using Different Nuclear Charge Distributions. *Atomic Data and Nuclear Data Tables*, 67(2):207 – 224, 1997.

[163] Seymour H Vosko, Leslie Wilk, and Marwan Nusair. Accurate Spin-Dependent Electron Liquid Correlation Energies for Local Spin Density Calculations: A Critical Analysis. *Can. J. Phys.*, 58(8):1200–1211, 1980.

[164] David Williams-Young, Franco Egidi, and Xiaosong Li. Relativistic Two-Component Particle-Particle Tamm-Dancoff Approximation. *J. Chem. Theory Comput.*, 12(11):5379–5384, 2016.

[165] David B Williams-Young, Alessio Petrone, Shichao Sun, Torin F Stetina, Patrick Lestrange, Chad E Hoyer, Daniel R Nascimento, Lauren Koulias, Andrew Wildman, Joseph Kasper, Joshua J. Goings, Feizhi Ding, A. Eugene DePrince III, Edward F. Valeev, and Xiaosong Li. The chronus quantum (chronusq) software package. *WIREs Comput. Mol. Sci.*, page e1436, 2019.

[166] Artur Wodyński and Martin Kaupp. Density Functional Calculations of Electron Paramagnetic Resonance g- and Hyperfine-Coupling Tensors Using the Exact Two-Component (X2C) Transformation and Efficient Approximations to the Two-Electron Spin–Orbit Terms. *J. Phys. Chem. A*, 123(26):5660–5672, 2019.

[167] Krzysztof Wolinski, James F. Hinton, and Peter Pulay. Efficient Implementation of the Gauge-Independent Atomic Orbital Method for NMR Chemical Shift Calculations. *J. Am. Chem. Soc.*, 112(23):8251–8260, 1990.

[168] K. Yabana and G. F. Bertsch. Application of the Time-Dependent Local Density Approximation to Optical Activity. *Phys. Rev. A*, 60:1271–1279, Aug 1999.

[169] D. Yamaki, Y. Shigeta, S. Yamanaka, H. Nagao, and K. Yamaguchi. MP2, Tamm-Dancoff, and RPA Methods Based on the Generalized HF Solution. *Int. J. Quant. Chem.*, 80:701–707, 2000.

[170] Terutaka Yoshizawa and Masahiko Hada. Calculations of Nuclear Magnetic Shielding Constants Based on the Exact Two-Component Relativistic Method. *J. Chem. Phys.*, 147(15):154104, 2017.

[171] Terutaka Yoshizawa, Wenli Zou, and Dieter Cremer. Calculations of Atomic Magnetic Nuclear Shielding Constants Based on the Two-Component Normalized Elimination of the Small Component Method. *J. Chem. Phys.*, 146(13):134109, 2017.

Appendix A

INTEGRAL EVALUATION

A London orbital is defined as

$$\tilde{\chi}(\mathbf{r}, \mathbf{k}_A) = \chi(\mathbf{r} - \mathbf{R}_A) e^{i\mathbf{k}_A \cdot (\mathbf{r} - \mathbf{R}_A)} \tag{A.1}$$

where $\{\chi\}$ are primary atom-centered Gaussian type orbitals,

$$\chi_a = (x - A_x)^{a_x} (y - A_y)^{a_y} (z - A_z)^{a_z} e^{-\zeta_a |\mathbf{r} - \mathbf{A}|} \tag{A.2}$$

$$|\mathbf{r} - \mathbf{A}| = \sqrt{(x - A_x)^2 + (y - A_y)^2 + (z - A_z)^2} \tag{A.3}$$

$\mathbf{A} = \{A_x, A_y, A_z\}$ is the coordinate of the atom center and $\mathbf{a} = \{a_x, a_y, a_z\}$ is the angular momentum. ζ_a is the exponent of primary Gaussian type orbitals.

The London orbital defined in Eq. (A.1) has the following identity,

$$\tilde{\chi}^*_\mu(\mathbf{r}, \mathbf{k}_A) = \tilde{\chi}_\mu(\mathbf{r}, -\mathbf{k}_A) \tag{A.4}$$

The one-electron integral for any one-electron operator $\hat{O}_1$ can be defined as

$$(\mathbf{a}|\hat{O}_1|\mathbf{b}) = \int \mathrm{d}^3\mathbf{r} \tilde{\chi}^*(\mathbf{r}, \mathbf{k}_A)\, \hat{O}_1\, \tilde{\chi}(\mathbf{r}, \mathbf{k}_B) = \int \mathrm{d}^3\mathbf{r} \tilde{\chi}(\mathbf{r}, -\mathbf{k}_A)\, \hat{O}_1\, \tilde{\chi}(\mathbf{r}, \mathbf{k}_B) \tag{A.5}$$

and, for a two-electron operator $\hat{O}_2$, the integral is defined as

$$\begin{aligned}(\mathbf{ab}|\hat{O}_2|\mathbf{cd}) &= \int \mathrm{d}^3\mathbf{r}_1 \int \mathrm{d}^3\mathbf{r}_2\, \tilde{\chi}^*(\mathbf{r}_1, \mathbf{k}_A) \tilde{\chi}(\mathbf{r}_1, \mathbf{k}_B)\, \hat{O}_2\, \tilde{\chi}^*(\mathbf{r}_2, \mathbf{k}_C) \tilde{\chi}(\mathbf{r}_2, \mathbf{k}_D) \\ &= \int \mathrm{d}^3\mathbf{r}_1 \int \mathrm{d}^3\mathbf{r}_2\, \tilde{\chi}(\mathbf{r}_1, -\mathbf{k}_A) \tilde{\chi}(\mathbf{r}_1, \mathbf{k}_B)\, \hat{O}_2\, \tilde{\chi}(\mathbf{r}_2, -\mathbf{k}_C) \tilde{\chi}(\mathbf{r}_2, \mathbf{k}_D)\end{aligned} \tag{A.6}$$

General recursion relationships for one- and two-electron integrals using mixed plane-wave/Gaussian type orbitals were presented by Obara and coworkers, [60] and the application to London orbitals was developed by Helgaker and Teale. [65, 156] In this work, we use a modified Obara-Saika algorithm to calculate one- and two-electron integrals using London orbitals. As the derivations are similar to those in references 60 and 156, we only present the working equations used in this work without going through the detailed mathematics. Note that recursive algorithms presented herein can be used for evaluating integrals of mixed plane-wave/Gaussian orbitals with an arbitrary wave vector.

The following intermediate quantities are defined for integral recursion relationships used in this work,

$$\zeta = \zeta_a + \zeta_b \tag{A.7}$$

$$\eta = \zeta_c + \zeta_d \tag{A.8}$$

$$\xi = \frac{\zeta_a \zeta_b}{\zeta_a + \zeta_b} \tag{A.9}$$

$$\rho = \frac{\zeta \eta}{\zeta + \eta} \tag{A.10}$$

$$\mathbf{P} = \frac{\zeta_a A + \zeta_b B}{\zeta_a + \zeta_b} \tag{A.11}$$

$$\mathbf{Q} = \frac{\zeta_c C + \zeta_d D}{\zeta_c + \zeta_d} \tag{A.12}$$

$$\mathbf{W} = \frac{\zeta P + \eta Q}{\zeta + \eta} \tag{A.13}$$

$$\mathbf{k}_p = -\mathbf{k}_a + \mathbf{k}_b \tag{A.14}$$

$$\mathbf{k}_q = -\mathbf{k}_c + \mathbf{k}_d \tag{A.15}$$

A.1 Overlap Integral

The recursion for the overlap integral is

$$(\mathbf{a}+\mathbf{1}_\mu||\mathbf{b}) = \left(\mathbf{P}+\frac{i(-\mathbf{k}_A+\mathbf{k}_B)}{2\zeta}-\mathbf{A}\right)_\mu(\mathbf{a}||\mathbf{b}) + \frac{1}{2\zeta}\Big\{N_\mu(\mathbf{a})(\mathbf{a}-\mathbf{1}_\mu||\mathbf{b}) + N_\mu(\mathbf{b})(\mathbf{a}||\mathbf{b}-\mathbf{1}_\mu)\Big\} \tag{A.16}$$

$$(\mathbf{0}_A||\mathbf{0}_B) = \left(\frac{\pi}{\zeta}\right)^{3/2} e^{-\xi(\mathbf{A}-\mathbf{B})^2} e^{-\frac{(-\mathbf{k}_a+\mathbf{k}_b)^2}{4\zeta}} e^{i\{(-\mathbf{k}_a)\cdot(\mathbf{P}-\mathbf{A})+\mathbf{k}_b\cdot(\mathbf{P}-\mathbf{B})\}} \tag{A.17}$$

where $N_\mu(\mathbf{a})$ is the μ component of the angular momentum $\mathbf{a}$. $\mathbf{a}\pm\mathbf{1}_\mu$ means that the μ component of the angular momentum $\mathbf{a}$ is raised/lowered by one.

A.2 Kinetic Energy Integral

Kinetic integral is the second derivatives of overlap integrals,

$$(\mathbf{a}|\mathscr{T}|\mathbf{b}) = -\frac{1}{2}\sum_{\nu=x,y,z}(\mathbf{a}||\partial_\nu^2\mathbf{b}) \tag{A.18}$$

The recursion relationship for the kinetic energy integral is

$$\begin{aligned}-\frac{1}{2}(\mathbf{a}||\partial_\nu^2\mathbf{b}) =& -2{\zeta_b}^2(\mathbf{a}||\mathbf{b}+\mathbf{2}_\nu) + 2i\zeta_b k_{b\mu}(\mathbf{a}||\mathbf{b}+\mathbf{1}_\nu) + \left(2\zeta_b N_\nu(\mathbf{b})\zeta_b + \frac{1}{2}\mathbf{k}_{b\nu}^2\right)(\mathbf{a}||\mathbf{b}) \\ & - iN_\nu(\mathbf{b})k_{b\nu}(\mathbf{a}||\mathbf{b}-\mathbf{1}_\nu) - \frac{1}{2}N_\nu(\mathbf{b})(N_\nu(\mathbf{b})-1)(\mathbf{a}||\mathbf{b}-\mathbf{2}_\nu)\end{aligned} \tag{A.19}$$

where $k_{b\mu}$ is the μ component of the wave vector $\mathbf{k}_b$.

A.0.1 Angular Momentum Integral

Angular momentum integral is defined as

$$\begin{aligned}(\mathbf{a}|\mathbf{r}\times\boldsymbol{\nabla}|\mathbf{b}) &= \hat{\mathbf{x}}\,(\mathbf{a}|r_y\partial_z - r_z\partial_y|\mathbf{b}) + \hat{\mathbf{y}}\,(\mathbf{a}|r_z\partial_x - r_x\partial_z|\mathbf{b}) + \hat{\mathbf{z}}\,(\mathbf{a}|r_x\partial_y - r_y\partial_x|\mathbf{b}) \\ &= -\hat{\mathbf{x}}\,(\mathbf{a}|r_y\partial_{B_z} - r_z\partial_{B_y}|\mathbf{b}) - \hat{\mathbf{y}}\,(\mathbf{a}|r_z\partial_{B_x} - r_x\partial_{B_z}|\mathbf{b}) - \hat{\mathbf{z}}\,(\mathbf{a}|r_x\partial_{B_y} - r_y\partial_{B_x}|\mathbf{b})\end{aligned} \tag{A.20}$$

where $\hat{\mathbf{x}}, \hat{\mathbf{y}}, \hat{\mathbf{z}}$ are unit vectors in the x, y, z directions. ∂_{B_μ} is the partial derivative with respect to nuclear coordinates at atom center B. The integral of the type $(\mathbf{a}|r_\mu\partial_\nu|\mathbf{b})$ where $\mu, \nu = x, y, z$ can be evaluated as linear combinations of overlap integrals:

$$\begin{aligned}(\mathbf{a}|r_\mu\partial_\nu|\mathbf{b}) = &-\big\{2\zeta_b(\mathbf{a}+\mathbf{1}_\mu||\mathbf{b}+\mathbf{1}_\nu) - N_\nu(\mathbf{b})(\mathbf{a}+\mathbf{1}_\mu||\mathbf{b}-\mathbf{1}_\nu) - ik_{b\nu}(\mathbf{a}+\mathbf{1}_\mu||\mathbf{b})\big\} \\ &- A_\mu\big\{2\zeta_b(\mathbf{a}||\mathbf{b}+\mathbf{1}\nu) - N_\nu(\mathbf{b})(\mathbf{a}||\mathbf{b}-\mathbf{1}_\nu) - ik_{b\nu}(\mathbf{a}||\mathbf{b})\big\}\end{aligned} \tag{A.21}$$

A.3 Electric Quadrupole Integral

The recursion relationship for the electric quadrupole integral is

$$(\mathbf{a}|r_\mu r_\nu|\mathbf{b}) = (\mathbf{a}+\mathbf{1}_\mu||\mathbf{b}+\mathbf{1}_\nu) + A_\mu(\mathbf{a}||\mathbf{b}+\mathbf{1}_\nu) + B_\nu(\mathbf{a}+\mathbf{1}_\mu||\mathbf{b}) + A_\mu B_\nu(\mathbf{a}||\mathbf{b}) \tag{A.22}$$

A.4 Nuclear Attraction Integral

Define the operator

$$V = \frac{1}{|\mathbf{r}-\mathbf{C}|} \tag{A.23}$$

where $\mathbf{C}$ is the nuclear coordinate. The recursion for nuclear attraction integral is

$$\begin{aligned}(\mathbf{a}+\mathbf{1}_\mu|V|\mathbf{b})^{(m)} =&(\mathbf{P}+\frac{i\mathbf{k}_{p\mu}}{2\zeta}-\mathbf{A})_\mu(\mathbf{a}|V|\mathbf{b})^{(m)}-(\mathbf{P}+\frac{i\mathbf{k}_{p\mu}}{2\zeta}-\mathbf{C})_\mu(\mathbf{a}|V|\mathbf{b})^{(m+1)}\\ &+\frac{1}{2\zeta}N_\mu(\mathbf{a})\Big\{(\mathbf{a}-\mathbf{1}_\mu|V|\mathbf{b})^{(m)}-(\mathbf{a}-\mathbf{1}_\mu|V|\mathbf{b})^{(m+1)}\Big\}\\ &+\frac{1}{2\zeta}N_\mu(\mathbf{b})\Big\{(\mathbf{a}|V|\mathbf{b}-\mathbf{1}_\mu)^{(m)}-(\mathbf{a}|V|\mathbf{b}-\mathbf{1}_\mu)^{(m+1)}\Big\} \qquad \text{(A.24)}\end{aligned}$$

$$(\mathbf{0}_A|V|\mathbf{0}_B)^{(m)} =2\left(\frac{\zeta}{\pi}\right)^{1/2}(\mathbf{0}_A||\mathbf{0}_B)\ F_m(T) \qquad \text{(A.25)}$$

$$T =\zeta\left(\mathbf{P}-\mathbf{C}+i\frac{-\mathbf{k}_a+\mathbf{k}_b}{2\zeta}\right)^2 \qquad \text{(A.26)}$$

where $F_m(T)$ is the Boys function.

A.5 Electron Repulsion Integral

The recursion for electron repulsion integral is

$$\begin{aligned}((\mathbf{a}+\mathbf{1}_\mu)\mathbf{b}|\mathbf{cd})^{(m)} =&\left(\mathbf{P}-\mathbf{A}+\frac{i\mathbf{k}_{p\mu}}{2\zeta}\right)_\mu(\mathbf{ab}|\mathbf{cd})^{(m)}\\ &+\left(\mathbf{W}-\mathbf{P}-\frac{i\rho(\mathbf{k}_a+\mathbf{k}_b)_\mu}{2\zeta^2}+\frac{i(\mathbf{k}_c+\mathbf{k}_d)_\mu}{2(\zeta+\eta)}\right)_\mu(\mathbf{ab}|\mathbf{cd})^{(m+1)}\\ &+\frac{1}{2\zeta}N_\mu(\mathbf{a})\Big\{((\mathbf{a}-\mathbf{1}_\mu)\mathbf{b}|\mathbf{cd})^{(m)}-\frac{\rho}{\zeta}((\mathbf{a}-\mathbf{1}_\mu)\mathbf{b}|\mathbf{cd})^{(m+1)}\Big\}\\ &+\frac{1}{2\zeta}N_\mu(\mathbf{b})\Big\{(\mathbf{a}(\mathbf{b}-\mathbf{1}_\mu)|\mathbf{cd})^{(m)}-\frac{\rho}{\zeta}(\mathbf{a}(\mathbf{b}-\mathbf{1}_\mu)|\mathbf{cd})^{(m+1)}\Big\}\\ &+\frac{1}{2(\zeta+\eta)}\Big\{N_\mu(\mathbf{c})(\mathbf{ab}|(\mathbf{c}-\mathbf{1}_\mu)\mathbf{d})^{(m+1)}+N_\mu(\mathbf{d})(\mathbf{ab}|\mathbf{c}(\mathbf{d}-\mathbf{1}_\mu))^{(m+1)}\Big\}\end{aligned} \qquad \text{(A.27)}$$

$$(\mathbf{00}|\mathbf{00})^{(m)} =2\left(\frac{\rho}{\pi}\right)^{1/2}(\mathbf{0}_A||\mathbf{0}_B)(\mathbf{0}_C||\mathbf{0}_D)\ F_m(T) \qquad \text{(A.28)}$$

$$T =\rho\left[\left(\mathbf{P}+i\frac{\mathbf{k}_p}{2\zeta}\right)-\left(\mathbf{Q}+i\frac{\mathbf{k}_q}{2\eta}\right)\right]^2 \qquad \text{(A.29)}$$

where F_m is the Boys function. The horizontal recursion can be derived from Eq. (A.27)

easily. [54]

$$(\mathbf{a}(\mathbf{b}+\mathbf{1}_{\mu})|\mathbf{cd})^{(m)} = ((\mathbf{a}+\mathbf{1}_{\mu})\mathbf{b}|\mathbf{cd})^{(m)} + (\mathbf{A}-\mathbf{B})_{\nu}(\mathbf{ab}|\mathbf{cd})^{(m)} \tag{A.30}$$

Appendix B

MCD PEAK BROADENING

We use two peaks close in energy with opposite sign as an example to illustrate the derivative peak profile in an MCD measurement. For example, when p orbitals of different M_L quantum numbers split due to the orbital Zeeman term, two excitations with opposite sign appear in the MCD measurement (Fig. 3.1). The discussion herein can be extended to other types of Zeeman splitting as well.

The separation of energy is $2\Delta\omega$, which is usually on the order of meV. Assuming a Gaussian broadening, the band shape function of these two peaks can be written as

$$f(x) = Ce^{-\left[\frac{(x+\Delta\omega)}{\sigma}\right]^2} - Ce^{-\left[\frac{(x-\Delta\omega)}{\sigma}\right]^2} \tag{B.1}$$

where C is normalization constant. The peak positions are the stationary points of function $f(x)$, where the first derivative of the band is zero:

$$\frac{df}{dx} = \frac{2C}{\sigma^2}\left((x-\Delta\omega)e^{-\left[\frac{(x-\Delta\omega)}{\sigma}\right]^2} - (x+\Delta\omega)e^{-\left[\frac{(x+\Delta\omega)}{\sigma}\right]^2}\right) = 0 \tag{B.2}$$

The solution of Eq. (B.2) can be obtained by locating the intersects of the two functions in the following equation, shown in Eq. (B.3),

$$-\frac{4x\Delta\omega}{\sigma^2} = \ln\frac{x-\Delta\omega}{x+\Delta\omega} \tag{B.3}$$

Equation (B.3) shows that the separation between two stationary points are greater than separation between the two excitations ($2\Delta\omega$). A larger Gaussian width σ gives rise to a larger peak separation and a broader profile.

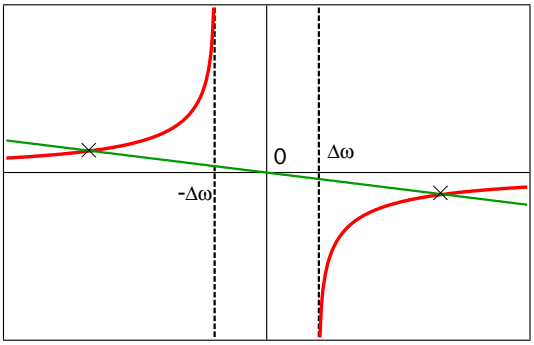

Figure B.1. Green and red curves are $y = -\frac{4x\Delta\omega}{\sigma^2}$ and $y = \ln\frac{x-\Delta\omega}{x+\Delta\omega}$. Dotted lines are located at $x = +\Delta\omega$ and $x = -\Delta\omega$. Positions where $-\frac{4x\Delta\omega}{\sigma^2}$ intersects, $\ln\frac{x-\Delta\omega}{x+\Delta\omega}$, are marked with an $\times$.

Appendix C

EVALUATION OF THE ONE-ELECTRON RELATIVISTIC GIAO INTEGRALS

We only discuss about the spatial integral. The spinor form can be easily obtained once the spatial orbital integrals are evaluated.

Evaluation of One-Electron Relativistic Integrals

The one electron relativistic integrals can be categorized into several types. 1) The spin-free integral $(\tilde{\mathbf{a}}|\mathbf{p}V\cdot\mathbf{p}|\tilde{\mathbf{b}})$ and spin-orbit integral $(\tilde{\mathbf{a}}|\mathbf{p}V\times\mathbf{p}|\tilde{\mathbf{b}})$ have two derivative operator and one nuclear potential operator. The tilde shows that it is GIAO integral, and $\mathbf{a},\mathbf{b}$ denote the angular momentum of the basis function. 2) The $(\tilde{\mathbf{a}}|\nabla_\beta V r_\alpha|\tilde{\mathbf{b}})$ and $(\tilde{\mathbf{a}}|r_\alpha V\nabla_\beta|\tilde{\mathbf{b}})$ in Eqs. (4.11) and (4.12) have one derivative operator, one cartesian coordinate operator and a nuclear potential operator. 3) $(\tilde{\mathbf{a}}|\mathbf{A}V\cdot\mathbf{A}|\tilde{\mathbf{b}})$ have two coordinate operator and a nuclear potential operator. We will discuss their evaluation separately.

The way to treat the derivative operator is to transform it into the derivative with respect to the nuclear coordinate

$$\begin{aligned}
&\frac{\partial}{\partial r_j}\tilde{\chi}_\mu(\mathbf{r}-\mathbf{R}_A;\mathbf{k}_A;\mathbf{a};\zeta_\alpha)\\
&=-\frac{\partial}{\partial R_{A,j}}\tilde{\chi}_\mu(\mathbf{r}-\mathbf{R}_A;\mathbf{k}_A;\mathbf{a};\zeta_\alpha)\\
&=-2\zeta_\alpha\tilde{\chi}_\mu(\mathbf{r}-\mathbf{R}_A;\mathbf{k}_A;\mathbf{a}+\mathbf{1}_j;\zeta_\alpha)+a_j\tilde{\chi}_\mu(\mathbf{r}-\mathbf{R}_A;\mathbf{k}_A;\mathbf{a}-\mathbf{1}_j;\zeta_\alpha)\\
&\quad+i(k_A)_j\tilde{\chi}_\mu(\mathbf{r}-\mathbf{R}_A;\mathbf{k}_A;\mathbf{a};\zeta_\alpha)
\end{aligned}\tag{C.1}$$

with that, we can treat the first type of integrals.

1) For spin-free integral and spin-orbit integral, we can rewrite them as the second deriva-

tive of nuclear attraction integral with respect to nuclear coordinates,

$$(\tilde{\mathbf{a}}|\mathbf{p}V\cdot\mathbf{p}|\tilde{\mathbf{b}}) = -(\tilde{\mathbf{a}}|\nabla V\cdot\nabla|\tilde{\mathbf{b}}) = (\nabla\tilde{\mathbf{a}}|V\cdot|\nabla\tilde{\mathbf{b}}) = \sum_{\alpha=x,y,z}\partial_{A_\alpha}\partial_{B_\alpha}(\tilde{\mathbf{a}}|V|\tilde{\mathbf{b}}) \tag{C.2}$$

$$(\tilde{\mathbf{a}}|\mathbf{p}V\times\mathbf{p}|\tilde{\mathbf{b}}) = -(\tilde{\mathbf{a}}|\nabla V\times\nabla|\tilde{\mathbf{b}}) = (\nabla\tilde{\mathbf{a}}|V\times|\nabla\tilde{\mathbf{b}}) = \varepsilon_{\alpha\beta\gamma}\,\partial_{A_\alpha}\partial_{B_\beta}(\tilde{\mathbf{a}}|V|\tilde{\mathbf{b}})\,\hat{i}_\gamma \tag{C.3}$$

according to Eq. (C.1), the second derivative can be evaluated as

$$\begin{aligned}\partial_{A_\alpha}\partial_{B_\beta}(\tilde{\mathbf{a}}|V|\tilde{\mathbf{b}}) =& 2\zeta_a\{2\zeta_b(\tilde{\mathbf{a}}+\mathbf{1}_\mu|V|\tilde{\mathbf{b}}+\mathbf{1}_\nu) - N_\nu(b)(\tilde{\mathbf{a}}+\mathbf{1}_\mu|V|\tilde{\mathbf{b}}-\mathbf{1}_\nu) - ik_{b\nu}(\tilde{\mathbf{a}}+\mathbf{1}_\mu|V|\mathbf{b})\}\\ &- N_\mu(a)\{2\zeta_b(\tilde{\mathbf{a}}-\mathbf{1}_\mu|V|\tilde{\mathbf{b}}+\mathbf{1}_\nu) - N_\nu(b)(\tilde{\mathbf{a}}-\mathbf{1}_\mu|V|\tilde{\mathbf{b}}-\mathbf{1}_\nu)\\ &- ik_{b\nu}(\tilde{\mathbf{a}}-\mathbf{1}_\mu|V|\tilde{\mathbf{b}})\}\\ &- ik_{a\mu}\{2\zeta_b(\tilde{\mathbf{a}}|V|\tilde{\mathbf{b}}+\mathbf{1}_\nu) - N_\nu(b)(\tilde{\mathbf{a}}|V|\tilde{\mathbf{b}}-\mathbf{1}_\nu) - ik_{b\nu}(\tilde{\mathbf{a}}|V|\tilde{\mathbf{b}})\}\end{aligned} \tag{C.4}$$

2) For $(\tilde{\mathbf{a}}|\nabla_\alpha V r_\beta|\tilde{\mathbf{b}})$, the r_β can be decomposed into $(r-B)_\beta + B_\beta$, and the derivative can be treated with Eq. (C.1)

$$\begin{aligned}(\tilde{\mathbf{a}}|\nabla_\alpha V r_\beta|\tilde{\mathbf{b}}) =& -(\nabla_\alpha\tilde{\mathbf{a}}|Vr_\beta|\tilde{\mathbf{b}}) = (\nabla_{A_\alpha}\tilde{\mathbf{a}}|Vr_\beta|\tilde{\mathbf{b}})\\ =& 2\zeta_a(\tilde{\mathbf{a}}+\mathbf{1}_\alpha|V|\tilde{\mathbf{b}}+\mathbf{1}_\beta) + B_\beta(\tilde{\mathbf{a}}+\mathbf{1}_\alpha|V|\tilde{\mathbf{b}})]\\ &- N_\alpha(\mathbf{a})[(\tilde{\mathbf{a}}-\mathbf{1}_\alpha|V|\tilde{\mathbf{b}}+\mathbf{1}_\beta) + B_\beta(\tilde{\mathbf{a}}-\mathbf{1}_\alpha|V|\tilde{\mathbf{b}})]\\ &- ik_{a\alpha}[(\tilde{\mathbf{a}}|V|\tilde{\mathbf{b}}+\mathbf{1}_\beta) + B_\beta(\tilde{\mathbf{a}}|V|\tilde{\mathbf{b}})]\end{aligned} \tag{C.5}$$

Similarly, we have

$$\begin{aligned}(\tilde{\mathbf{a}}|r_\beta V\nabla_\alpha|\tilde{\mathbf{b}}) =& -\partial_{B\alpha}(\tilde{\mathbf{a}}|r_\beta V|\tilde{\mathbf{b}})\\ =& -[2\zeta_b(\tilde{\mathbf{a}}+\mathbf{1}_\beta|V|\tilde{\mathbf{b}}+\mathbf{1}_\alpha) - N_\alpha(\mathbf{b})(\tilde{\mathbf{a}}+\mathbf{1}_\beta|V|\tilde{\mathbf{b}}-\mathbf{1}_\alpha) - ik_{b\alpha}(\tilde{\mathbf{a}}+\mathbf{1}_\beta|V|\tilde{\mathbf{b}})]\\ &- A_\beta[2\zeta_b(\tilde{\mathbf{a}}|V|\tilde{\mathbf{b}}+\mathbf{1}_\alpha) - N_\alpha(\mathbf{b})(\tilde{\mathbf{a}}|V|\tilde{\mathbf{b}}-\mathbf{1}_\alpha) - ik_{b\alpha}(\tilde{\mathbf{a}}|V|\tilde{\mathbf{b}})]\end{aligned} \tag{C.6}$$

Notice that either $(\tilde{\mathbf{a}}|\nabla_\alpha V r_\beta|\tilde{\mathbf{b}})$ or $(\tilde{\mathbf{a}}|r_\beta V \nabla_\alpha|\tilde{\mathbf{b}})$ are not hermitian or anti-hermitian. Their linear combination $\nabla_\beta V r_\alpha - r_\alpha V \nabla_\beta$ is Hermitian, and $r_\alpha V \nabla_\beta + \nabla_\beta V r_\alpha$ is anti-Hermitian.

3) Operator $\mathbf{A}V \cdot \mathbf{A}$ can be expanded as

$$\begin{aligned}
\mathbf{A}V \cdot \mathbf{A} =& \mathbf{B}^2 \mathbf{r} V \cdot \mathbf{r} - (\mathbf{B} \cdot \mathbf{r}) V (\mathbf{B} \cdot \mathbf{r}) \\
=& (B_x^2 + B_y^2 + B_z^2)(xVx + yVy + zVz) \\
& - (B_x x + B_y y + B_z z) V (B_x x + B_y y + B_z z) \\
=& xVx(B_y^2 + B_z^2) + yVy(B_x^2 + B_z^2) + zVz(B_x^2 + B_y^2) \\
& - xVy 2B_x B y - yVz 2B_y B_z - 2xVz B_x B_z
\end{aligned} \tag{C.7}$$

where the integral of the type $(\tilde{\mathbf{a}}|r_\alpha V r_\beta|\tilde{\mathbf{b}})$ can be evaluated as

$$\begin{aligned}
(\tilde{\mathbf{a}}|r_\alpha V r_\beta|\tilde{\mathbf{b}}) &= (\tilde{\mathbf{a}}|[(r-A)_\alpha + A_\alpha] V [(r-B)_\beta + B_\beta]|\tilde{\mathbf{b}}) \\
&= (\tilde{\mathbf{a}} + \mathbf{1}_\alpha|V|\tilde{\mathbf{b}} + \mathbf{1}_\beta) + B_\beta(\tilde{\mathbf{a}} + \mathbf{1}_\alpha|V|\tilde{\mathbf{b}}) + A_\alpha(\tilde{\mathbf{a}}|V|\tilde{\mathbf{b}} + \mathbf{1}_\beta) + A_\alpha B_\beta(\tilde{\mathbf{a}}|V|\tilde{\mathbf{b}})
\end{aligned} \tag{C.8}$$

Evaluation of Nuclear Attraction Integral with Finite Width Nuclei

We assume gaussian charge distribution of the nuclei, [162] the nuclear potential is

$$V(\mathbf{r}) = -\int d^3\mathbf{R} \quad \frac{e^{-\zeta_C(\mathbf{R}-\mathbf{C})^2}}{|\mathbf{r}-\mathbf{R}|} \tag{C.9}$$

Where $e^{-\zeta_C(\mathbf{R}-\mathbf{C})^2}$ is the gaussian distribution of the charge with the nucleus located at $\mathbf{C}$, ζ_C is the exponential parameter, which decide how diffused the nucleus is.

The nuclear attraction integral can be viewed as a special case of electron repulsion

integral,

$$(\tilde{\mathbf{a}}|V(\mathbf{r})|\tilde{\mathbf{b}}) = \iint d\mathbf{R}d\mathbf{r}\tilde{\chi}_a(\mathbf{r})\tilde{\chi}_b(\mathbf{r})\frac{e^{-\zeta_C(\mathbf{R}-\mathbf{C})^2}}{|\mathbf{r}-\mathbf{R}|}$$
$$= \iint d\mathbf{R}d\mathbf{r}\tilde{\chi}_a(\mathbf{r})\tilde{\chi}_b(\mathbf{r})\frac{1}{|\mathbf{r}-\mathbf{R}|}\chi_c(\mathbf{R})\chi_d(\mathbf{R}) \tag{C.10}$$

where

$$\chi_c = N_C e^{-g(\mathbf{R}-\mathbf{C})^2}, \qquad \chi_d = 1 = e^0 \tag{C.11}$$

with normalization condition

$$\int d^3\mathbf{R}\, N_C e^{\zeta_C(\mathbf{R}-\mathbf{C})^3} = Z_C \tag{C.12}$$

where Z_C is the nuclear charge. χ_c and χ_d are gaussian orbital instead of London orbitals. We define

$$\zeta = \zeta_a + \zeta_b, \tag{C.13}$$
$$\rho = \frac{\zeta\zeta_C}{\zeta+\zeta_C} = \frac{\zeta\zeta_C}{\zeta+\zeta_C} \tag{C.14}$$
$$\mathbf{P} = \frac{\zeta_a\mathbf{A}+\zeta_b\mathbf{B}}{\zeta} \tag{C.15}$$
$$\mathbf{k}_p = -\mathbf{k}_a + \mathbf{k}_b \tag{C.16}$$
$$\mathbf{k}_q = \mathbf{0} \tag{C.17}$$

then, we have

$$\mathbf{W} = \frac{\zeta\mathbf{P}+\zeta_C\mathbf{C}}{\zeta+\zeta_c} \tag{C.18}$$

substitute these quantities in the the recursion of electron repulsion integral in Ref. 153, we

get the same recursion of nuclear attraction integral

$$\begin{aligned}((\tilde{\mathbf{a}}+\mathbf{1}_\mu)|V|\tilde{\mathbf{b}})^{(m)} =&(P_\mu+\frac{ik_{p\mu}}{2\zeta}-A_\mu)(\tilde{\mathbf{a}}|V|\tilde{\mathbf{b}})^{(m)}-(P_\mu+\frac{ik_{p\mu}}{2\zeta}-C_\mu)(\tilde{\mathbf{a}}|V|\tilde{\mathbf{b}})^{(m+1)}\\ &+\frac{1}{2\zeta}N_i(\mathbf{a})\big\{((\tilde{\mathbf{a}}-\mathbf{1}_i)|V|\tilde{\mathbf{b}})^{(m)}-((\tilde{\mathbf{a}}-\mathbf{1}_i)|V|\tilde{\mathbf{b}})^{(m+1)}\big\}\\ &+\frac{1}{2\zeta}N_i(\mathbf{b})\big\{(\tilde{\mathbf{a}}|V|(\tilde{\mathbf{b}}-\mathbf{1}_i))^{(m)}-(\tilde{\mathbf{b}}|V|(\tilde{\mathbf{a}}-\mathbf{1}_i))^{(m+1)}\big\}\end{aligned} \tag{C.19}$$

with a different definition of the auxiliary integrals

$$(\tilde{\mathbf{0}}_A|V|\tilde{\mathbf{0}}_B)^{(m)}=Z_C(\tilde{\mathbf{0}}_A||\tilde{\mathbf{0}}_B)\left(\frac{\zeta_C}{\zeta+\zeta_C}\right)^m 2\left(\frac{\rho}{\pi}\right)^{1/2}F_m(T) \tag{C.20}$$

where T in the Boys function have a different definition

$$T=\rho\left(\mathbf{P}-\mathbf{C}+i\frac{\mathbf{k}_p}{2\zeta}\right)^2 \tag{C.21}$$

Appendix D

DETAILS OF GIAO DFT AND TDDFT

D.1 Outline of the evaluation of exchange-correlation potential integrals with Complex Atomic Orbitals

In order to ensure the gauge origin invariance, the 1-e molecular orbitals $\{\psi_p(\mathbf{r})\}$ are expanded in terms of a set of contracted complex London orbitals $\{\tilde{\chi}_\mu(\mathbf{r}-\mathbf{R}_A;\mathbf{k}_A;\mathbf{a})\}$,

$$\psi_p(\mathbf{r}) = \sum_\mu C_{\mu p}\tilde{\chi}_\mu(\mathbf{r}-\mathbf{R}_A;\mathbf{k}_A;\mathbf{a}) \tag{D.1}$$

$$\tilde{\chi}_\mu(\mathbf{r}-\mathbf{R}_A;\mathbf{k}_A;\mathbf{a}) = \chi_\mu(\mathbf{r}-\mathbf{R}_A;\mathbf{a})e^{i\mathbf{k}_A\cdot(\mathbf{r}-\mathbf{R}_A)} \tag{D.2}$$

where $\{\chi_\mu(\mathbf{r}-\mathbf{R}_A;\mathbf{a})\}$ are real contracted Gaussian type atomic orbital (AO) basis functions centered at $\mathbf{R}_A$, and $\mathbf{R}_A$ is the nuclear coordinate of atomic orbital μ.

$$\chi_\mu(\mathbf{r}-\mathbf{R}_A;\mathbf{a}) = \sum_\alpha \Phi_\mu(\mathbf{r}-\mathbf{R}_A;\mathbf{a};\zeta_\alpha) \tag{D.3}$$

where we define primitive London atomic orbitals

$$\tilde{\Phi}_\mu(\mathbf{r}-\mathbf{R}_A;\mathbf{k}_A;\mathbf{a};\zeta_\alpha) = \Phi_\mu(\mathbf{r}-\mathbf{R}_A;\mathbf{a};\zeta_\alpha)e^{i\mathbf{k}_A\cdot(\mathbf{r}-\mathbf{R}_A)} \tag{D.4}$$

When the atomic orbitals are complex valued, the complex arithmetic is required. The formalism is consistent with [118]. Up to GGA level of functional, the exchange correlation functional is defined as a function of auxiliary variable $\{U_I\}$,

$$E_{xc} = \int d\mathbf{r}\, f(n^+, n^-, \gamma^{++}, \gamma^{--}, \gamma^{+-}) \tag{D.5}$$

where the variables are consistent with the definition in Ref. 28 and Ref. 118

$$
\begin{aligned}
n^{\pm} &= \frac{1}{2}\rho^{S} \pm \frac{1}{2}\sqrt{\sum_{\alpha=x,y,z} m_\alpha m_\alpha} \\
\gamma^{\pm\pm} &= \frac{1}{4}\nabla n \cdot \nabla n + \frac{1}{4}\sum_{\alpha=x,y,z} \nabla m_\alpha \cdot \nabla m_\alpha \pm \frac{f_\nabla}{2}\sqrt{\sum_{\alpha=x,y,z} \nabla n \cdot \nabla m_\alpha \nabla n \cdot \nabla m_\alpha} \\
\gamma^{+-} &= \frac{1}{4}\nabla n \cdot \nabla n - \frac{1}{4}\sum_{\alpha=x,y,z} \nabla m_\alpha \nabla m_\alpha \\
f_\nabla &= \mathrm{sgn}(\nabla n \cdot \sum_{\alpha=x,y,z} (\nabla m_\alpha)\, m_\alpha)
\end{aligned}
\tag{D.6}
$$

where sgn is the sign function. Although the variables are constructed from complex atomic basis, they are real valued.

The exchange-correlation energy of hybrid functional is defined as

$$
E_{\mathrm{xc}}[\rho] = E_{\mathrm{xc}}^{\mathrm{GGA}}[\rho, \nabla\rho] + c_{\mathrm{x}} E_{\mathrm{x}}^{\mathrm{HF}}[\rho] \tag{D.7}
$$

and the exchange correlation potential

$$
V^{\mathrm{xc}}(\mathbf{r}) = \frac{\delta E_{\mathrm{xc}}}{\delta\rho(\mathbf{r})} \tag{D.8}
$$

The details about the implementation of GKS with finite field gauge including atomic orbital is presented in the earlier works [151].

In order to calculate the exchange correlation integral, $V_{\mu\nu}^{\mathrm{xc}}(\mathbf{r})$, we define the auxiliary variables $\{U_I\}$ and $\{V_I\}$. Where the exchange-correlation kernel is defined as a functional of $\{U_I\}$, and $\{U_I\}$ are the function of $\{V_I\}$, where $\{V_I\}$ are linear with density matrices.

$$
\rho(\mathbf{r}) = \sum_{\mu\nu} P_{\mu\nu}^{S} \tilde{\chi}_\mu(\mathbf{r}) \tilde{\chi}_\nu^{*}(\mathbf{r}) \tag{D.9}
$$

In the KS formalism and real time dynamics, since the density matrix is always Hermitian,

the density function is always real.

$$(\rho(\mathbf{r}))^* = \sum_{\mu\nu} P^{S,*}_{\mu\nu} \tilde{\chi}^*_\mu(\mathbf{r})\tilde{\chi}_\nu(\mathbf{r}) = \sum_{\mu\nu} P^{S}_{\nu\mu} \tilde{\chi}^*_\mu(\mathbf{r})\tilde{\chi}_\nu(\mathbf{r}) = \rho(\mathbf{r}) \tag{D.10}$$

And similarly the gradient of the density is also real

$$\nabla\rho(\mathbf{r}) = \sum_{\mu\nu} P^{S}_{\mu\nu} [(\nabla\tilde{\chi}_\mu(\mathbf{r}))\tilde{\chi}^*_\nu(\mathbf{r}) + \tilde{\chi}_\mu(\mathbf{r})(\nabla\tilde{\chi}^*_\nu(\mathbf{r}))] \tag{D.11}$$

$$\begin{aligned} V^{\mathrm{xc},\Gamma}_{\mu\nu} &= \sum_I \sum_J \frac{\partial E_{\mathrm{xc}}}{\partial U_I} \frac{\partial U_I}{\partial V_J} \frac{\partial V_J}{\partial P^\Gamma_{\nu\mu}} \\ &= \sum_i \sum_I \sum_J w_i \frac{\partial f}{\partial U_I(\mathbf{r}_i)} \frac{\partial U_I(\mathbf{r}_i)}{\partial V_J(\mathbf{r}_i)} \frac{\partial V_J(\mathbf{r}_i)}{\partial P^\Gamma_{\nu\mu}} \end{aligned} \tag{D.12}$$

where $\Gamma = S, x, y, z$ which label the spin components. In the RKS case, only S is required.

The summation can be decomposed into two parts, one is the density parts, with $V_J = n^\Gamma$. We have

$$\frac{\partial V_J(\mathbf{r}_i)}{\partial P^\Gamma_{\nu\mu}} = \tilde{\chi}^*_\mu(\mathbf{r}_i)\tilde{\chi}_\nu(\mathbf{r}_i) \tag{D.13}$$

The other is gradient part, where $V_J = \nabla n^\Gamma$. We have

$$\frac{\partial V_J(\mathbf{r}_i)}{\partial P^\Gamma_{\nu\mu}} = (\nabla\tilde{\chi}_\mu(\mathbf{r}_i))\tilde{\chi}^*_\nu(\mathbf{r}_i) + \tilde{\chi}_\mu(\mathbf{r}_i)(\nabla\tilde{\chi}^*_\nu(\mathbf{r}_i)) \tag{D.14}$$

We can calculate the exchange correlation potential integral with the complex valued atomic orbitals as

$$V^{\mathrm{GGA},\Gamma}_{\mu\nu} = \sum_i [Z^\Gamma_\mu(\mathbf{r}_i)]^* \tilde{\chi}_\nu(\mathbf{r}_i) + Z^\Gamma_\nu(\mathbf{r}_i)[\tilde{\chi}_\nu(\mathbf{r}_i)]^* \tag{D.15}$$

i runs over all the grid points.

$$Z_\mu(\mathbf{r}_i) = w(\mathbf{r}_i)\left(\frac{1}{2}\mathcal{Z}_\rho^\Gamma(\mathbf{r}_i)\tilde{\chi}_\mu(\mathbf{r}_i) + \sum_{k=x,y,z}\mathcal{Z}_{\nabla,k}^\Gamma(\mathbf{r}_i)(\nabla_k\tilde{\chi}_\mu(\mathbf{r}_i))\right) \tag{D.16}$$

where $k = x, y, z$ is Cartesian coordinate. and

$$\mathcal{Z}_\rho^\Gamma(\mathbf{r}_i) = \sum_I \frac{\partial f}{\partial U_I(\mathbf{r}_i)}\frac{\partial U_I(\mathbf{r}_i)}{\partial \rho^\Gamma(\mathbf{r}_i)} \tag{D.17}$$

$$\mathcal{Z}_{\nabla,k}^\Gamma(\mathbf{r}_i) = \sum_I \frac{\partial f}{\partial U_I(\mathbf{r}_i)}\frac{\partial U_I(\mathbf{r}_i)}{\partial \nabla_\xi \rho^\Gamma(\mathbf{r}_i)} \tag{D.18}$$

Since the value of $f, \{U_I(\mathbf{r}_i)\}, \{V_I(\mathbf{r}_i)\}$ are real, the quantities $\mathcal{Z}_\rho^\Gamma(\mathbf{r}_i), \mathcal{Z}_{\nabla,\xi}^\Gamma(\mathbf{r}_i)$ are also real valued. The explicit form of $\mathcal{Z}_\rho^\Gamma(\mathbf{r}_i), \mathcal{Z}_{\nabla,\xi}^\Gamma(\mathbf{r}_i)$ is given in Ref. 118:

$$\mathcal{Z}_\rho^\Gamma = \frac{\partial f}{\partial \rho^\Gamma} = \frac{1}{2}\begin{cases}\left(\dfrac{\partial f}{\partial n^+} + \dfrac{\partial f}{\partial n^-}\right) & \Gamma = S \\ \left(\dfrac{\partial f}{\partial n^+} - \dfrac{\partial f}{\partial n^-}\right) K^\Gamma & \Gamma \neq S\end{cases} \tag{D.19a}$$

$$\mathcal{Z}_{\nabla,k}^\Gamma = \frac{\partial f}{\partial \nabla_k \rho^\Gamma} = \frac{1}{2}\begin{cases}\nabla_k\rho^S\left(\dfrac{\partial f}{\partial \gamma^{++}} + \dfrac{\partial f}{\partial \gamma^{+-}} + \dfrac{\partial f}{\partial \gamma^{--}}\right) & \\ \quad + \sum_{\kappa=x,y,z}\nabla_k\rho^\kappa H^\kappa\left(\dfrac{\partial f}{\partial \gamma^{++}} - \dfrac{\partial f}{\partial \gamma^{--}}\right) & \Gamma = S \\ \nabla_k\rho^S H^\Gamma\left(\dfrac{\partial f}{\partial \gamma^{++}} - \dfrac{\partial f}{\partial \gamma^{--}}\right) & \\ \quad + \nabla_k\rho^\Gamma\left(\dfrac{\partial f}{\partial \gamma^{++}} - \dfrac{\partial f}{\partial \gamma^{+-}} + \dfrac{\partial f}{\partial \gamma^{--}}\right) & \Gamma \neq S\end{cases} \tag{D.20a}$$

we use the convention for the index, such that capitalized Greek letter (like Γ) are spin component index running over S, x, y, z. Lower case Greek letter (γ, κ) are spin component index running over x, y, z only. Lower case English letter k are Cartesian coordinate index, running over x, y, z. When we limit $\Gamma = x, y, z$, the K^Γ, H^Γ are defined for significant $\mathbf{m}$

($|\mathbf{m}| \geq 10^{-12}$) and small $\mathbf{m}$ ($|\mathbf{m}| < 10^{-12}$)

$$K^{\Gamma} = \begin{cases} \dfrac{\rho^{\Gamma}}{|\mathbf{m}|} & \text{(Significant } \mathbf{m}\text{)} \\ \dfrac{1}{3} & \text{(Small } \mathbf{m}\text{)} \end{cases} \tag{D.21a}$$

$$H^{\Gamma} = \begin{cases} \dfrac{f_{\nabla} \nabla n \cdot \nabla \rho^{\Gamma}}{\sqrt{\nabla n \cdot \nabla \mathbf{m} \circ \nabla \mathbf{m} \cdot \nabla n}} & \text{(Significant } \mathbf{m}\text{)} \\ \dfrac{f_{\nabla}}{3} & \text{(Small } \mathbf{m}\text{)} \end{cases} \tag{D.21b}$$

For closed shell systems and some regions in the open shell system with insignificant magnetization, the definition of K^I, H^I for the small $\mathbf{m}$ ($|\mathbf{m}| < 10^{-12}$) makes the GKS result consistent with RKS and UKS. This definition ensures the numerical stability of V_{xc} of non-collinear DFT.

We also define that

$$\rho^{\Gamma} = \begin{cases} \rho^S = \rho & \text{when } \Gamma = S \\ \rho^{\Gamma} = m^{\Gamma} & \text{when } \Gamma = x, y, Z \end{cases} \tag{D.22}$$

D.2 Brief Overview of the Linear Response TDDFT in MO basis

In this derivation, we assume the orbitals are complex. For DFT, the Fock matrix in molecular orbitals is

$$F_{pq} = \sum_{rs} \frac{\partial F_{pq}}{\partial P_{rs}} P_{rs} = \sum_{rs} [(pq|sr) - c_x(pr|sq) + f_{xc,pq,sr}] P_{rs} \tag{D.23}$$

where

$$f_{xc,pq,rs} = \frac{\partial V^{\mathrm{xc}}_{pq}}{\partial P_{rs}} \tag{D.24}$$

If we apply the perturbation V_a with frequency ω_a, by expanding the Liouville-von Neumann equation by orders of magnitude of frequencies, the first order gives us the linear response equation of motion,

$$\omega_a P^{(a)} - [F^{(0)}, P^{(a)}] - [F^{(1)}[P^{(a)}], P^{(0)}] = [V^a, P^{(0)}] \tag{D.25}$$

where the unperturbed matrices are

$$F^{(0)} = \begin{pmatrix} \epsilon_o & 0 \\ 0 & \epsilon_v \end{pmatrix}, \quad P^{(0)} = \begin{pmatrix} I_o & 0 \\ 0 & 0 \end{pmatrix} \tag{D.26}$$

and the perturbed Fock matrix $F^{(1)}[P^{(a)}]$ is the kernel $\frac{\partial F_{pq}}{\partial P_{rs}}$ contracted with perturbed density matrix $P^{(a)}$:

$$F^{(1)}[P^{(a)}] = \sum_{rs} \frac{\partial F_{pq}}{\partial P_{rs}}\bigg|_{P^{(0)}} P^{(a)}_{rs} = \sum_{rs} [(pq|sr) - c_x(pr|sq) + f_{xc,pq,sr}] P^{(a)}_{rs} \tag{D.27}$$

which means the kernel is evaluated with unperturbed density matrix $P^{(0)}$, and then contracted with perturbed density matrix $P^{(a)}$.

we get equation of elements for vo and ov blocks

$$\left[\frac{\partial F_{ai}}{\partial P_{bj}} + \delta_{ab}\delta_{ij}(\epsilon_a - \epsilon_i)\right] P^{(a)}_{bj} + \frac{\partial F_{ai}}{\partial P_{jb}} P^{(a)}_{jb} - \omega_a P^{(a)}_{ai} = -v^a_{ai} \tag{D.28}$$

$$\left[\frac{\partial F_{ia}}{\partial P_{jb}} + \delta_{ab}\delta_{ij}(\epsilon_a - \epsilon_i)\right] P^{(a)}_{jb} + \frac{\partial F_{ia}}{\partial P_{bj}} P^{(a)}_{bj} + \omega_a P^{(a)}_{ia} = -v^a_{ia} \tag{D.29}$$

Define

$$B_{ai,bj} = \frac{\partial F_{ai}}{\partial P_{jb}}, \quad A_{ai,bj} = \frac{\partial F_{ai}}{\partial P_{bj}} + \delta_{ab}\delta_{ij}(\epsilon_a - \epsilon_i) \tag{D.30}$$

in DFT, $B_{ai,bj} = [(ai|bj) - c_x(aj|bi) + f_{xc,ai,bj}]$, and $A_{ai,bj} = [(ai|jb) - c_x(ab|ji) + f_{xc,ai,jb}] + \delta_{ab}\delta_{ij}(\epsilon_a - \epsilon_i)$.

Then the linear response equation becomes

$$A_{ai,bj}P^{(a)}_{bj} + B_{ai,bj}P^{(a)}_{jb} - \omega_a P^{(a)}_{ai} = -v^a_{ai} \tag{D.31}$$

$$A^*_{ai,bj}P^{(a)}_{jb} + B^*_{ai,bj}P^{(a)}_{bj} + \omega_a P^{(a)}_{ia} = -v^a_{ia} \tag{D.32}$$

since we only want the poles and transition density matrices in this work, we need to solve the homogeneous equations (generalized eigen value problems)

$$\begin{aligned} A_{ai,bj}X^{(n)}_{bj} + B_{ai,bj}Y^{(n)}_{bj} - \omega_n X^{(n)}_{ai} &= 0 \\ A^*_{ai,bj}Y^{(n)}_{bj} + B^*_{ai,bj}X^{(n)}_{bj} + \omega_n Y^{(n)}_{ai} &= 0 \end{aligned} \tag{D.33}$$

where ω_n are the pole of excited state n, and $X^{(n)}_{bj} = P^{(n)}_{bj}$, $Y^{(n)}_{bj} = P^{(n)}_{jb}$ are the transition density matrices of excited state n.

D.3 Implementation of the complex orbital linear response TDDFT

Define transition density matrix in molecular orbitals

$$T_{ai} = X_{ai}, \quad T_{ia} = Y_{ai} \tag{D.34}$$

where we omit the superscript J for simplicity. $\{i, j\}$ are index for occupied orbitals, $\{a, b\}$ are index for unoccupied orbitals, $\{p, q\}$ are index for general spin orbitals.

Transform the transition density matrix into atomic orbital basis, we have

$$T_{\mu\nu} = \sum_{pq} C_{\mu p} T_{pq} C^*_{\nu q} \tag{D.35}$$

The transition density and the gradient of transition density can be evaluated as

$$T(\mathbf{r}) = \sum_{\mu\nu} \tilde{\phi}_\mu(\mathbf{r}) T_{\mu\nu} \tilde{\phi}^*_\nu(\mathbf{r}) \tag{D.36}$$

$$\nabla T(\mathbf{r}) = \sum_{\mu\nu} T_{\mu\nu}[(\nabla\tilde{\phi}_\mu(\mathbf{r}))\tilde{\phi}^*_\nu(\mathbf{r}) + \tilde{\phi}_\mu(\mathbf{r})(\nabla\tilde{\phi}^*_\nu(\mathbf{r}))] \tag{D.37}$$

since $T_{\mu\nu}$ is not a Hermitian matrix, the transition density $T(\mathbf{r})$ and its gradient $\nabla T(\mathbf{r})$ is a complex function of coordinate $\mathbf{r}$.

We can transform the contractions in the left hand side of Eq. (D.33) of this type $\sum_{rs}[(pq|sr) - c_x(pr|sq) + f^{\mathrm{xc}}_{pq,sr}]T_{rs}$ from MO basis to atomic orbitals:

$$\begin{aligned}
&\sum_{rs}[(pq|sr) - c_x(pr|sq) + f^{\mathrm{xc}}_{pq,sr}]T_{rs} \\
&= \sum_{rs}\sum_{\mu\nu\kappa\lambda} C^*_{\mu p}C_{\nu q}C^*_{\kappa s}C_{\lambda r}[(\mu\nu|\kappa\lambda) - c_x(\mu\lambda|\kappa\nu) + f^{\mathrm{xc}}_{\mu\nu,\kappa\lambda}]T_{rs} \\
&= \sum_{\mu\nu} C^*_{\mu p}C_{\nu q}\sum_{\kappa\lambda}[(\mu\nu|\kappa\lambda) - c_x(\mu\lambda|\kappa\nu) + f^{\mathrm{xc}}_{\mu\nu,\kappa\lambda}]T_{\lambda\kappa}
\end{aligned} \tag{D.38}$$

The main task is to evaluate the contraction of second order derivative of the functional kernel with transition density matrix

$$f^{\mathrm{xc}}_{\mu\nu}[T] = \sum_{\kappa\lambda} f^{\mathrm{xc}}_{\mu\nu,\kappa\lambda}T_{\lambda\kappa} \tag{D.39}$$

Where the second order derivative of the exchange-correlation kernel is defined with U and V variable

$$f^{\mathrm{xc}}_{\mu\nu,\kappa\lambda} = \sum_{IJKL}\int\left(\frac{\partial^2 f}{\partial U_I\partial U_J}\frac{\partial U_I}{\partial V_K}\frac{\partial U_J}{\partial V_L} + \frac{\partial f}{\partial U_I}\frac{\partial^2 U_I}{\partial V_K\partial V_L}\right)\frac{\partial V_K}{\partial P_{\nu\mu}}\frac{\partial V_L}{\partial P_{\lambda\kappa}}d^3\mathbf{r} \tag{D.40}$$

The analytical expression of first and second order derivative of U variable with respect to V variable are provided in Ref. 28. Notice that the P and T in Eq. (D.40) are two spinor matrix

$$P = P^S \otimes I_2 + \sum_{\gamma=x,y,z} P^\gamma \otimes \sigma_\gamma \tag{D.41}$$

$$T = T^S \otimes I_2 + \sum_{\gamma=x,y,z} T^\gamma \otimes \sigma_\gamma \tag{D.42}$$

The basis $\{\tilde{\phi}_\mu, 0 < \mu \leq 2NB\}$ are two-spinor basis, and can be formed from the product of spin basis $\{\alpha, \beta\}$ and spatial basis $\{\tilde{\chi}_\mu, 0 < \mu \leq NB\}$, where NB is the number of spatial basis function

$$\tilde{\phi}_\mu = \begin{cases} \tilde{\chi}_\mu \otimes \alpha & \mu \leq NB \\ \tilde{\mu}_{\mu-NB} \otimes \beta & NB < \mu \end{cases} \tag{D.43}$$

In the two component formalism, the V variable are divided into Pauli components, $\Gamma = s, x, y, z$, which are defined in Eq. (D.13) and Eq. (D.14). Therefore, the contracted quantity $f^{\mathrm{xc}}_{\mu\nu}[T]$ can be divided into Pauli components,

$$f^{\mathrm{xc},\Gamma}_{\mu\nu}[T] = \sum_{\kappa\lambda} \sum_{\Gamma'=S,x,y,z} \sum_{IJKL} \int \left(\frac{\partial^2 f}{\partial U_I \partial U_J} \frac{\partial U_I}{\partial V_K} \frac{\partial U_J}{\partial V_L} + \frac{\partial f}{\partial U_I} \frac{\partial^2 U_I}{\partial V_K \partial V_L} \right) \frac{\partial V_K}{\partial P^{\Gamma}_{\nu\mu}} \frac{\partial V_L}{\partial P^{\Gamma'}_{\lambda\kappa}} T^{\Gamma'}_{\lambda\kappa} d^3\mathbf{r} \tag{D.44}$$

and the matrix vector product Eq. (D.38) can be calculated from Eq. (D.44) However, the definition of the auxiliary variable will cause numerical instability for closed shell systems, whose magnetization density is small. The analytical expression of derivative and second order derivative in Ref. 28 is ill defined in this case. It is also problem for open shell systems, since they have regions where the magnetization is not significant.

Thus in the region where the magnetization is not significant ($|\mathbf{m}| < 10^{-12}$), when $\Gamma = x, y, z$ (scalar doesn't need this treatment), instead of using the treatment for small

magnetization in Ref. 28, we make the followingchange to the derivative of the U variables

$$\frac{\partial n^+}{\partial m_\alpha} = \delta_{\alpha\Gamma} \tag{D.45}$$

$$\frac{\partial n^-}{\partial m_\alpha} = -\delta_{\alpha\Gamma} \tag{D.46}$$

$$\frac{\partial \gamma^{++}}{\partial(\nabla n)} = \frac{1}{2}\nabla n + \frac{1}{2}\nabla m_\Gamma \tag{D.47}$$

$$\frac{\partial \gamma^{++}}{\partial \nabla m_\alpha} = \frac{1}{2}\nabla m_\alpha + \delta_{\alpha\Gamma}\frac{1}{2}\nabla n \tag{D.48}$$

$$\frac{\partial \gamma^{--}}{\partial(\nabla n)} = \frac{1}{2}\nabla n - \frac{1}{2}\nabla m_\Gamma \tag{D.49}$$

$$\frac{\partial \gamma^{--}}{\partial \nabla m_\alpha} = \frac{1}{2}\nabla m_\alpha - \delta_{\alpha\Gamma}\frac{1}{2}\nabla n \tag{D.50}$$

Notice that in Eqs. (D.47) and (D.49), the component Γ is chosen the same as the component of $f_{\mu\nu}^{\mathrm{xc},\Gamma}[T]$. The derivatives of γ^{+-} are not changed.

The second derivative of n^+, n^- become 0. And the second derivatives of γ variables are derived from the modified first derivatives,

$$\frac{\partial^2 \gamma^{++}}{\partial(\partial_i n)\partial(\partial_j n)} = \frac{1}{2}\delta_{ij} \tag{D.51}$$

$$\frac{\partial^2 \gamma^{++}}{\partial(\partial_i n)\partial(\partial_j m_\alpha)} = \frac{1}{2}\delta_{ij}\delta_{\alpha\Gamma} \tag{D.52}$$

$$\frac{\partial^2 \gamma^{++}}{\partial(\partial_i m_\alpha)\partial(\partial_j m_\beta)} = \frac{1}{2}\delta_{ij}\delta_{\alpha\beta} \tag{D.53}$$

$$\frac{\partial^2 \gamma^{--}}{\partial(\partial_i n)\partial(\partial_j n)} = \frac{1}{2}\delta_{ij} \tag{D.54}$$

$$\frac{\partial^2 \gamma^{--}}{\partial(\partial_i n)\partial(\partial_j m_\alpha)} = -\frac{1}{2}\delta_{ij}\delta_{\alpha\Gamma} \tag{D.55}$$

$$\frac{\partial^2 \gamma^{--}}{\partial(\partial_i m_\alpha)\partial(\partial_j m_\beta)} = \frac{1}{2}\delta_{ij}\delta_{\alpha\beta} \tag{D.56}$$

The second derivatives of γ^{+-} are also not changed.

Such changes make the GKS-TDDFT result consistent with the RKS-TDDFT for closed

shell systems. For open shell system, these changes in the insignificant magnetization region ensure numerical stability.

For $f_{\mu\nu}^{xc,\Gamma}[T]$ with $\Gamma = S$ in Eq. (D.44), we still use the same definition of the insignificant magnetization case in Ref. 28.

The matrix element $f_{\mu\nu}^{xc,\Gamma}[T]$ can be evaluated with a numerical grid integration,

$$f_{\mu\nu}^{xc,\Gamma}[T] = \int d\,\mathbf{r}\omega(\mathbf{r})\left\{\mathcal{F}_{\rho}^{\Gamma}(\mathbf{r})\tilde{\chi}_{\mu}(\mathbf{r})\tilde{\chi}_{\nu}^{*}(\mathbf{r}) + \sum_{k=x,y,z}\mathcal{F}_{\nabla,k}^{\Gamma}(\mathbf{r})[(\nabla_k\tilde{\chi}_{\mu}(\mathbf{r}))\tilde{\chi}_{\nu}^{*}(\mathbf{r}) + \tilde{\chi}_{\mu}(\mathbf{r})\nabla_k\tilde{\chi}_{\nu}^{*}(\mathbf{r})]\right\} \tag{D.57}$$

where ξ is cartesian coordinate x, y, z, and ω is the weight factor.

If we define

$$\Lambda^{\Gamma\Gamma'}(\mathbf{r}) = \nabla\rho^{\Gamma}(\mathbf{r})\cdot\nabla T^{\Gamma'}(\mathbf{r}) \tag{D.58}$$

we have

$$\begin{aligned}
\mathcal{F}_{\rho}^{S} = &\left[\frac{\partial^2 f}{\partial n^+\partial n^+} + \frac{\partial^2 f}{\partial n^-\partial n^-} + 2\frac{\partial^2 f}{\partial n^+\partial n^-}\right]T^S + \left[\frac{\partial^2 f}{\partial n^+\partial n^+} - \frac{\partial^2 f}{\partial n^-\partial n^-}\right]\sum_{\gamma=x,y,z}K^{\gamma}T^{\gamma} + \\
&\Lambda^{SS}\left(\frac{\partial^2 f}{\partial n^+\partial\gamma^{++}} + \frac{\partial^2 f}{\partial n^-\partial\gamma^{++}} + \frac{\partial^2 f}{\partial n^+\partial\gamma^{+-}} + \frac{\partial^2 f}{\partial n^-\partial\gamma^{+-}} + \frac{\partial^2 f}{\partial n^+\partial\gamma^{--}} + \frac{\partial^2 f}{\partial n^-\partial\gamma^{--}}\right) + \\
&\left(\sum_{\gamma=x,y,z}\left(\Lambda^{\gamma S} + \Lambda^{S\gamma}\right)H^{\gamma}\right)\left(\frac{\partial^2 f}{\partial n^+\partial\gamma^{++}} + \frac{\partial^2 f}{\partial n^-\partial\gamma^{++}} - \frac{\partial^2 f}{\partial n^+\partial\gamma^{--}} - \frac{\partial^2 f}{\partial n^-\partial\gamma^{--}}\right) + \\
&\left(\sum_{\gamma=x,y,z}\Lambda^{\gamma\gamma}\right)\left(\frac{\partial^2 f}{\partial n^+\partial\gamma^{++}} + \frac{\partial^2 f}{\partial n^-\partial\gamma^{++}} - \frac{\partial^2 f}{\partial n^+\partial\gamma^{+-}} - \right. \\
&\left.\frac{\partial^2 f}{\partial n^-\partial\gamma^{+-}} + \frac{\partial^2 f}{\partial n^+\partial\gamma^{--}} + \frac{\partial^2 f}{\partial n^-\partial\gamma^{--}}\right)
\end{aligned} \tag{D.59}$$

$$\mathcal{F}_{\nabla}^{S} = \nabla\rho^{S}\left[\Lambda^{SS}\left(\frac{\partial^2 f}{\partial\gamma^{++}\partial\gamma^{++}} + \frac{\partial^2 f}{\partial\gamma^{+-}\partial\gamma^{+-}} + \frac{\partial^2 f}{\partial\gamma^{--}\partial\gamma^{--}} + 2\frac{\partial^2 f}{\partial\gamma^{++}\partial\gamma^{+-}} + 2\frac{\partial^2 f}{\partial\gamma^{++}\partial\gamma^{--}} + 2\frac{\partial^2 f}{\partial\gamma^{+-}\partial\gamma^{--}}\right) + \left(\sum_{\gamma=x,y,z}\left(\Lambda^{\gamma S} + \Lambda^{S\gamma}\right)H^{\gamma}\right)\left(\frac{\partial^2 f}{\partial\gamma^{++}\partial\gamma^{++}} + \frac{\partial^2 f}{\partial\gamma^{+-}\partial\gamma^{++}} - \frac{\partial^2 f}{\partial\gamma^{+-}\partial\gamma^{--}} - \frac{\partial^2 f}{\partial\gamma^{--}\partial\gamma^{--}}\right) + \left(\sum_{\gamma=x,y,z}\Lambda^{\gamma\gamma}\right)\left(\frac{\partial^2 f}{\partial\gamma^{++}\partial\gamma^{++}} - \frac{\partial^2 f}{\partial\gamma^{+-}\partial\gamma^{+-}} + \frac{\partial^2 f}{\partial\gamma^{--}\partial\gamma^{--}} + 2\frac{\partial^2 f}{\partial\gamma^{++}\partial\gamma^{--}}\right) + T^{S}\left(\frac{\partial^2 f}{\partial\gamma^{++}\partial n^{+}} + \frac{\partial^2 f}{\partial\gamma^{++}\partial n^{-}} + \frac{\partial^2 f}{\partial\gamma^{+-}\partial n^{+}} + \frac{\partial^2 f}{\partial\gamma^{+-}\partial n^{-}} + \frac{\partial^2 f}{\partial\gamma^{--}\partial n^{+}} + \frac{\partial^2 f}{\partial\gamma^{--}\partial n^{-}}\right) + \left(\sum_{\gamma=x,y,z}K^{\gamma}T^{\gamma}\right)\left(\frac{\partial^2 f}{\partial\gamma^{++}\partial n^{+}} - \frac{\partial^2 f}{\partial\gamma^{++}\partial n^{-}} + \frac{\partial^2 f}{\partial\gamma^{+-}\partial n^{+}} - \frac{\partial^2 f}{\partial\gamma^{+-}\partial n^{-}} + \frac{\partial^2 f}{\partial\gamma^{--}\partial n^{+}} - \frac{\partial^2 f}{\partial\gamma^{--}\partial n^{-}}\right)\right] +$$

$$\left(\sum_{\gamma=x,y,z}H^{\gamma}\nabla\rho^{\gamma}\right)\left[\Lambda^{SS}\left(\frac{\partial^2 f}{\partial\gamma^{++}\partial\gamma^{++}} - \frac{\partial^2 f}{\partial\gamma^{--}\partial\gamma^{--}} + \frac{\partial^2 f}{\partial\gamma^{++}\partial\gamma^{+-}} - \frac{\partial^2 f}{\partial\gamma^{+-}\partial\gamma^{--}}\right) + \left(\sum_{\gamma=x,y,z}\left(\Lambda^{\gamma S} + \Lambda^{S\gamma}\right)H^{\gamma}\right)\left(\frac{\partial^2 f}{\partial\gamma^{++}\partial\gamma^{++}} - 2\frac{\partial^2 f}{\partial\gamma^{++}\partial\gamma^{--}} + \frac{\partial^2 f}{\partial\gamma^{--}\partial\gamma^{--}}\right) + \left(\sum_{\gamma=x,y,z}\Lambda^{\gamma\gamma}\right)\left(\frac{\partial^2 f}{\partial\gamma^{++}\partial\gamma^{++}} - \frac{\partial^2 f}{\partial\gamma^{++}\partial\gamma^{+-}} + \frac{\partial^2 f}{\partial\gamma^{--}\partial\gamma^{+-}} - \frac{\partial^2 f}{\partial\gamma^{--}\partial\gamma^{--}}\right) + T^{S}\left(\frac{\partial^2 f}{\partial\gamma^{++}\partial n^{+}} + \frac{\partial^2 f}{\partial\gamma^{++}\partial n^{-}} - \frac{\partial^2 f}{\partial\gamma^{--}\partial n^{+}} - \frac{\partial^2 f}{\partial\gamma^{--}\partial n^{-}}\right) + \left(\sum_{\gamma=x,y,z}K^{\gamma}T^{\gamma}\right)\left(\frac{\partial^2 f}{\partial\gamma^{++}\partial n^{+}} - \frac{\partial^2 f}{\partial\gamma^{++}\partial n^{-}} - \frac{\partial^2 f}{\partial\gamma^{--}\partial n^{+}} + \frac{\partial^2 f}{\partial\gamma^{--}\partial n^{-}}\right)\right] +$$

$$2\nabla T^{S}\left[\frac{\partial f}{\partial\gamma^{++}} + \frac{\partial f}{\partial\gamma^{+-}} + \frac{\partial f}{\partial\gamma^{--}}\right] + 2\sum_{\gamma=x,y,z}H^{\gamma}\nabla T^{\gamma}\left[\frac{\partial f}{\partial\gamma^{++}} - \frac{\partial f}{\partial\gamma^{--}}\right] + 2\frac{f_{\nabla}}{|\nabla n\cdot\nabla\mathbf{m}|}\sum_{\gamma=x,y,z}\left[\nabla\rho^{\gamma}\sum_{\kappa=x,y,z}\left(\Lambda^{\kappa S} + \Lambda^{S\kappa}\right)\left(\delta_{\gamma\kappa} - H^{\gamma}H^{\kappa}\right)\right]\left[\frac{\partial f}{\partial\gamma^{++}} - \frac{\partial f}{\partial\gamma^{--}}\right] \quad \text{(D.60)}$$

where

$$|\nabla n \cdot \nabla \mathbf{m}| = \sqrt{\nabla n \cdot \nabla \mathbf{m} \circ \nabla \mathbf{m} \cdot \nabla n} \tag{D.61}$$

For other components $\Gamma = \gamma = x, y, z$,

$$\begin{aligned}
\mathcal{F}_{\rho}^{\gamma} = K^{\gamma} \Bigg\{ & \left[\frac{\partial^2 f}{\partial n^+ \partial n^+} - \frac{\partial^2 f}{\partial n^- \partial n^-} \right] T^S + \left[\frac{\partial^2 f}{\partial n^+ \partial n^+} + \frac{\partial^2 f}{\partial n^- \partial n^-} - 2 \frac{\partial^2 f}{\partial n^+ \partial n^-} \right] \sum_{\kappa=x,y,z} K^{\kappa} T^{\kappa} + \\
& \Lambda^{SS} \left(\frac{\partial^2 f}{\partial n^+ \partial \gamma^{++}} - \frac{\partial^2 f}{\partial n^- \partial \gamma^{++}} + \frac{\partial^2 f}{\partial n^+ \partial \gamma^{+-}} - \frac{\partial^2 f}{\partial n^- \partial \gamma^{+-}} + \frac{\partial^2 f}{\partial n^+ \partial \gamma^{--}} - \frac{\partial^2 f}{\partial n^- \partial \gamma^{--}} \right) + \\
& \left(\sum_{\kappa} \left(\Lambda^{\kappa S} + \Lambda^{S\kappa} \right) H^{\kappa} \right) \left(\frac{\partial^2 f}{\partial n^+ \partial \gamma^{++}} - \frac{\partial^2 f}{\partial n^- \partial \gamma^{++}} - \frac{\partial^2 f}{\partial n^+ \partial \gamma^{--}} + \frac{\partial^2 f}{\partial n^- \partial \gamma^{--}} \right) + \\
& \left(\sum_{\kappa=x,y,z} \Lambda^{\kappa\kappa} \right) \Bigg(\frac{\partial^2 f}{\partial n^+ \partial \gamma^{++}} - \frac{\partial^2 f}{\partial n^- \partial \gamma^{++}} - \frac{\partial^2 f}{\partial n^+ \partial \gamma^{+-}} + \\
& \qquad \frac{\partial^2 f}{\partial n^- \partial \gamma^{+-}} + \frac{\partial^2 f}{\partial n^+ \partial \gamma^{--}} - \frac{\partial^2 f}{\partial n^- \partial \gamma^{--}} \Bigg) \Bigg\} + \\
& \frac{2}{|\mathbf{m}|} \left(T^{\gamma} - K^{\gamma} \sum_{\kappa=x,y,z} K^{\kappa} T^{\kappa} \right) \left[\frac{\partial f}{\partial n^+} - \frac{\partial f}{\partial n^-} \right]
\end{aligned} \tag{D.62}$$

and for the gradient term

$$
\begin{aligned}
\mathcal{F}_{\nabla}^{\gamma} = \nabla\rho^{\gamma}\Bigg[& \Lambda^{SS}\left(\frac{\partial^2 f}{\partial\gamma^{++}\partial\gamma^{++}} - \frac{\partial^2 f}{\partial\gamma^{+-}\partial\gamma^{+-}} + \frac{\partial^2 f}{\partial\gamma^{--}\partial\gamma^{--}} + 2\frac{\partial^2 f}{\partial\gamma^{++}\partial\gamma^{--}}\right) + \\
& \left(\sum_{\kappa=x,y,z} H^{\kappa}\left(\Lambda^{\kappa S} + \Lambda^{S\kappa}\right)\right)\left(\frac{\partial^2 f}{\partial\gamma^{++}\partial\gamma^{++}} - \frac{\partial^2 f}{\partial\gamma^{+-}\partial\gamma^{++}} + \frac{\partial^2 f}{\partial\gamma^{+-}\partial\gamma^{--}} - \frac{\partial^2 f}{\partial\gamma^{--}\partial\gamma^{--}}\right) + \\
& \left(\sum_{\kappa=x,y,z} \Lambda^{\kappa\kappa}\right)\left(\frac{\partial^2 f}{\partial\gamma^{++}\partial\gamma^{++}} - 2\frac{\partial^2 f}{\partial\gamma^{++}\partial\gamma^{+-}} + 2\frac{\partial^2 f}{\partial\gamma^{++}\partial\gamma^{--}} + \right. \\
& \qquad \left. \frac{\partial^2 f}{\partial\gamma^{+-}\partial\gamma^{+-}} - 2\frac{\partial^2 f}{\partial\gamma^{+-}\partial\gamma^{--}} + \frac{\partial^2 f}{\partial\gamma^{--}\partial\gamma^{--}}\right) + \\
& T^{S}\left(\frac{\partial^2 f}{\partial\gamma^{++}\partial n^{+}} + \frac{\partial^2 f}{\partial\gamma^{++}\partial n^{-}} - \frac{\partial^2 f}{\partial\gamma^{+-}\partial n^{+}} - \frac{\partial^2 f}{\partial\gamma^{+-}\partial n^{-}} + \frac{\partial^2 f}{\partial\gamma^{--}\partial n^{+}} + \frac{\partial^2 f}{\partial\gamma^{--}\partial n^{-}}\right) + \\
& \left(\sum_{\kappa=x,y,z} K^{\kappa}T^{\kappa}\right)\left(\frac{\partial^2 f}{\partial\gamma^{++}\partial n^{+}} - \frac{\partial^2 f}{\partial\gamma^{++}\partial n^{-}} - \frac{\partial^2 f}{\partial\gamma^{+-}\partial n^{+}} + \right. \\
& \qquad \left. \frac{\partial^2 f}{\partial\gamma^{+-}\partial n^{-}} + \frac{\partial^2 f}{\partial\gamma^{--}\partial n^{+}} - \frac{\partial^2 f}{\partial\gamma^{--}\partial n^{-}}\right)\Bigg] + \\
& H^{\gamma}\nabla\rho^{S}\Bigg[\Lambda^{SS}\left(\frac{\partial^2 f}{\partial\gamma^{++}\partial\gamma^{++}} + \frac{\partial^2 f}{\partial\gamma^{++}\partial\gamma^{+-}} - \frac{\partial^2 f}{\partial\gamma^{--}\partial\gamma^{+-}} - \frac{\partial^2 f}{\partial\gamma^{--}\partial\gamma^{--}}\right) + \\
& \qquad \left(\sum_{\kappa=x,y,z} H^{\kappa}\left(\Lambda^{\kappa S} + \Lambda^{S\kappa}\right)\right)\left(\frac{\partial^2 f}{\partial\gamma^{++}\partial\gamma^{++}} - 2\frac{\partial^2 f}{\partial\gamma^{++}\partial\gamma^{--}} + \frac{\partial^2 f}{\partial\gamma^{--}\partial\gamma^{--}}\right) + \\
& \qquad \left(\sum_{\kappa=x,y,z} \Lambda^{\kappa\kappa}\right)\left(\frac{\partial^2 f}{\partial\gamma^{++}\partial\gamma^{++}} - \frac{\partial^2 f}{\partial\gamma^{++}\partial\gamma^{+-}} + \frac{\partial^2 f}{\partial\gamma^{--}\partial\gamma^{+-}} - \frac{\partial^2 f}{\partial\gamma^{--}\partial\gamma^{--}}\right) + \\
& \qquad T^{S}\left(\frac{\partial^2 f}{\partial\gamma^{++}\partial n^{+}} + \frac{\partial^2 f}{\partial\gamma^{++}\partial n^{-}} - \frac{\partial^2 f}{\partial\gamma^{--}\partial n^{+}} - \frac{\partial^2 f}{\partial\gamma^{--}\partial n^{-}}\right) + \\
& \qquad \left(\sum_{\kappa=x,y,z} K^{\kappa}T^{\kappa}\right)\left(\frac{\partial^2 f}{\partial\gamma^{++}\partial n^{+}} - \frac{\partial^2 f}{\partial\gamma^{++}\partial n^{-}} - \frac{\partial^2 f}{\partial\gamma^{--}\partial n^{+}} + \frac{\partial^2 f}{\partial\gamma^{--}\partial n^{-}}\right)\Bigg] + \\
& 2H^{\gamma}\nabla T^{S}\left[\frac{\partial f}{\partial\gamma^{++}} - \frac{\partial f}{\partial\gamma^{--}}\right] + 2\nabla T^{\gamma}\left[\frac{\partial f}{\partial\gamma^{++}} - \frac{\partial f}{\partial\gamma^{+-}} + \frac{\partial f}{\partial\gamma^{--}}\right] + \\
& f_{\nabla}\frac{2\nabla\rho^{S}}{|\nabla n\cdot\nabla\mathbf{m}|}\sum_{\kappa=x,y,z}\left(\Lambda^{\kappa S} + \Lambda^{S\kappa}\right)\left(\delta_{\kappa\gamma} - H^{\gamma}H^{\kappa}\right)\left[\frac{\partial f}{\partial\gamma^{++}} - \frac{\partial f}{\partial\gamma^{--}}\right] \qquad \text{(D.63)}
\end{aligned}
$$

For $\mathcal{F}_{\rho}^{\gamma}$ in Eq. (D.62) and $\mathcal{F}_{\nabla}^{\gamma}$ in Eq. (D.63), in the region where $|\mathbf{m}| < 10^{-12}$, the definition

in Eq. (D.56) requires that K^γ and H^γ of small $|\mathbf{m}|$ are defined as

$$K^\gamma = H^\gamma = \delta_{\gamma\Gamma} \quad \text{when } |\mathbf{m}| < 10^{-12} \tag{D.64}$$

Note that the form of $\mathcal{F}_\rho^\Gamma$ and $\mathcal{F}_\nabla^\Gamma$ are derived with the help of Dr. Alessio Petrone and Dr. David Williams-Young.